

MIGRATION OF BLOOD CELLS IN NON-UNIFORM SUSPENSION FOR A DIALYZER DESIGN

A Thesis
Presented to
The Academic Faculty

By

Jane Kang

In Partial Fulfillment
Of the Requirements for the Degree
Doctor of Philosophy in Mechanical Engineering

Georgia Institute of Technology

August 2015

Copyright 2015 by Jane Kang

MIGRATION OF BLOOD CELLS IN NON-UNIFORM SUSPENSION FOR A DIALYZER DESIGN

Approved by:

Dr. David W. Rosen, Co-chair
George W. Woodruff School of Mechanical Engineering
Georgia Institute of Technology

Dr. Cyrus K. Aidun, Co-chair
George W. Woodruff School of Mechanical Engineering
Georgia Institute of Technology

Dr. David N. Ku
George W. Woodruff School of Mechanical Engineering
Georgia Institute of Technology

Dr. Victor Breedveld
School of Chemical and Biomolecular Engineering
Georgia Institute of Technology

Dr. Richard W. Vuduc
School of Computer Science and Engineering
Georgia Institute of Technology

Date Approved: May 15, 2015

To my parents.

ACKNOWLEDGEMENTS

This work would not have been possible without the support of many great people and organizations.

I would like to sincerely thank my advisors, Dr. David Rosen and Dr. Cyrus Aidun. Dr. Rosen guided me with wise advice while allowing enormous freedom on the research direction and trained me to think of bigger picture. I learned how research should be conducted from his generous and patient support. Dr. Aidun encouraged me with his expertise to think through the basic principles. I will always remember their warm-hearted advice.

I would like to extend my appreciation to my reading committee members, Dr. David Ku, Dr. Victor Breedveld, and Dr. Richard Vuduc. Their advice and feedback was very important and helpful for the change in the research direction of the second part of my dissertation. This work owes a lot to their valuable comments.

I would also like to thank Dr. Aidun's group members for their support. Especially, Dr. Min Yun and Dr. Marmar Mehrabadi helped me to learn the code and taught me important concepts required for the first part of this research. I would like to acknowledge previous students and post-docs for the development of the direct numerical simulation code.

I would like to thank Dr. Rosen's lab members: Dr. Amit Jariwala, Dr. Wenchao Zhou, Namin Jeong, Sang-in Park, Xiayun Zhao, Chad Hume, Jonathan Holmes, Narumi Watanabe, Ying Zhang, Changxuan Zhao, Jason Nguyen, and Patrick Chang. They always encouraged me, and discussions with Amit and Sang-in especially helped me to move forward in each step. I was

lucky to share the office with such smart and warm-hearted friends, and I will miss the time we spent together.

I would like to thank Dr. Jeffrey Donnell for his thorough review of the dissertation. My deep appreciation also goes to Dr. Gy-young Han and Dr. Young-ae Han for their excellent care.

I would like to acknowledge the Carlos and Marguerite Mason Foundation for their financial support and the National Science Foundation's support through Extreme Science and Engineering Discovery Environment (XSEDE) on the access to the high performance computing system.

Finally, I would like to thank my parents, Mi Ryoung Song and Whoa Seug Kang, for devoting their endless love, support, and belief in me. My sincere appreciation also goes to my brother's couple, Sang-gu Kang and Min Sun Kwon, for their encouragement.

TABLE OF CONTENTS

| | |
|---|-------------|
| Acknowledgements | iv |
| List of Tables | ix |
| List of Figures | xi |
| List of Symbols and Abbreviations | xvii |
| Summary | xix |
| 1 Motivation and Problem Formulation | 1 |
| 1.1 Hemodialysis..... | 1 |
| 1.2 Proposed Configuration..... | 2 |
| 1.3 Research Questions and Hypothesis | 3 |
| 1.4 Summary..... | 5 |
| 2 Literature Review | 7 |
| 2.1 Blood Composition and Relevant Dimensionless Parameters in Blood Flow | 7 |
| 2.2 Uniform Suspension Flows | 9 |
| 2.3 Constitutive Models of Particle Migration in a Sheared-Suspension..... | 11 |
| 2.4 Blood Cell Migration Behaviors in Non-Uniform Suspension Flows | 13 |
| 2.4.1 Blood Cleansing Device for Sepsis Treatment | 14 |
| 2.4.2 Hemodialysis Filtration System | 15 |
| 2.4.3 Hydrodynamic Focusing | 17 |
| 2.5 Simulation Studies of Blood Flow..... | 18 |
| 2.6 Summary..... | 18 |
| 3 Lattice Boltzmann and Spectrin Link Method and Validation | 20 |
| 3.1 Fluid Simulation Method - Lattice Boltzmann Method..... | 20 |
| 3.2 Platelet Simulation Method | 23 |
| 3.3 Red Blood Cell Simulation Method – Spectrin-Link Method..... | 23 |
| 3.3.1 Helmholtz Energy Calculation | 24 |
| 3.3.2 Macroscopic Mechanical Properties Calculation | 26 |
| 3.3.3 Coarse Graining Method | 27 |
| 3.4 Fluid-Solid Coupling – Standard Bounce-back Method..... | 28 |

| | | |
|----------|--|-----------|
| 3.5 | Subgrid Modeling – Contact and Lubrication Model..... | 30 |
| 3.6 | Simulation Domain – Boundary Conditions | 31 |
| 3.7 | RBC Model Creation | 32 |
| 3.8 | Initial Seeding of Blood Cells in Dense Suspension Flow..... | 38 |
| 3.9 | Validation..... | 41 |
| 3.9.1 | Isolated RBC..... | 41 |
| 3.9.2 | Isolated Platelet..... | 42 |
| 3.9.3 | Domain Size | 45 |
| 3.9.4 | Subgrid Modeling – Effect of Contact and Lubrication Parameters..... | 48 |
| 3.9.5 | Cell Migration in Non-uniform Suspension Flows | 51 |
| 3.10 | Computational Performance | 62 |
| 3.11 | Summary..... | 65 |
| 4 | Migration of Cells in Non-uniform Suspension Flow | 67 |
| 4.1 | Relevant Variables and Parameters | 67 |
| 4.2 | Effect of Hematocrit and Re | 70 |
| 4.3 | Effect of Channel Dimensions and Geometry | 75 |
| 4.3.1 | Design of Experiments – Latin Hyper-Cube Method | 75 |
| 4.3.2 | Results | 77 |
| 4.4 | Meta-Model Creation..... | 90 |
| 4.5 | Summary..... | 97 |
| 5 | Design Space Exploration of a Dialyzer | 99 |
| 5.1 | Proposed Dialyzer Design | 99 |
| 5.2 | Comsol Model for the Study of Molecule Diffusion Behavior..... | 101 |
| 5.2.1 | Model Set-up | 102 |
| 5.2.2 | Relevant Variables and Parameters | 107 |
| 5.2.3 | Model Validation | 108 |
| 5.3 | Hemodialysis System Model..... | 113 |
| 5.3.1 | Overview..... | 114 |
| 5.3.2 | Waste Generation Rates..... | 116 |
| 5.4 | Design Requirements and Objective of the Proposed Dialyzer | 118 |
| 5.4.1 | Blood Cell Loss | 118 |
| 5.4.2 | Blood Flow Rate..... | 119 |
| 5.4.3 | Protein Loss | 120 |

| | | |
|----------|--|------------|
| 5.4.4 | Dialyzer Size | 120 |
| 5.4.5 | Fluid Usage | 121 |
| 5.4.6 | Waste Concentration..... | 121 |
| 5.5 | Design Model of the Proposed Dialyzer Design | 121 |
| 5.6 | Design Space Exploration Results..... | 126 |
| 5.6.1 | Design Space Exploration A – $D < 200\mu\text{m}$ | 126 |
| 5.6.2 | Design Space Exploration B – $D > 200\mu\text{m}$ | 129 |
| 5.7 | Summary and Conclusion | 136 |
| 5.8 | Future Design Space Exploration Strategy | 137 |
| 6 | Closure and Contributions..... | 140 |
| 6.1 | Answering the Research Questions..... | 140 |
| 6.1.1 | Research Question One | 140 |
| 6.1.2 | Research Question Two..... | 142 |
| 6.2 | Contributions..... | 143 |
| 6.2.1 | Validation for RBC Diffusivity in Non-uniform Suspension Flows | 143 |
| 6.2.2 | Parametric Study of Blood Cell Migration Behavior – Extraction Ratio | 144 |
| 6.2.3 | Dense Suspension Study with Improved RBC Properties | 144 |
| 6.2.4 | Feasibility Study of the Proposed Dialyzer Design | 145 |
| 6.3 | Scope and limitations | 146 |
| 6.4 | Future Work | 148 |
| 6.4.1 | Design Space Exploration for Larger Domain | 148 |
| 6.4.2 | Addition of Blood Cell Level Change to the Design Space Exploration Model | 149 |
| 6.4.3 | Experimental Proof of Concept | 149 |
| 6.4.4 | Segre Silberberg Effect for Rigid vs. Deformable RBCs..... | 150 |
| 6.4.5 | Particle Stress Analysis of Suspensions | 150 |
| 6.4.6 | LB-SL Method Based DNS for the Molecule Diffusion Behavior Study | 151 |
| | Appendix A: Tables | 152 |
| | Works Cited | 154 |

LIST OF TABLES

| | |
|---|----|
| Table 2-1. Relevant Dimensionless Parameters in Blood Flow | 8 |
| Table 2-2. Dimensions of Leonard’s micro-fluidic channel and currently used dialyzer tubule ... | 16 |
| Table 3-1. Equilibrium volume and area of the two RBCs..... | 37 |
| Table 3-2. Parameter values of the two RBCs | 37 |
| Table 3-3. Mechanical properties of the two RBCs | 38 |
| Table 3-4. Example growth plan for 2078 RBCs and 138 platelets with 40% HCT | 40 |
| Table 3-5. Initial seeding conditions of simulations | 53 |
| Table 3-6. Adjusted initial conditions of simulations for analysis | 56 |
| Table 3-7. Half-width along the channel for Case A ($w_0 = 40.75 \mu\text{m}$, $N_0 = 8.11 \mu\text{m}$) | 57 |
| Table 3-8. Half-width along the channel for Case B ($w_0 = 7.08 \mu\text{m}$, $N_0 = 2.69 \mu\text{m}$)..... | 57 |
| Table 3-9. Subdomain size of scaling simulations with 8715 RBCs in $(160\mu\text{m})^3$ domain | 63 |
| Table 3-10. Scaling simulation results for 100 LB time steps with 8715 RBCs in $(160\mu\text{m})^3$ domain | 64 |
| Table 4-1. Independent variables and parameters for the study of blood cell migration behavior | 68 |
| Table 4-2. Dimensionless parameters | 69 |
| Table 4-3. Details of each cases studied with circular channels | 77 |
| Table 4-4. Details of each cases studied with rectangular channels..... | 77 |
| Table 4-5. Resulting ER curve parameters of each cases studied with circular channels | 81 |
| Table 4-6. Resulting ER curve parameters of each cases studied with rectangular channels | 84 |
| Table 4-7. Constants of the meta-model of EReq | 91 |

| | |
|--|-----|
| Table 4-8. Constants of the meta-model of $L\tau$ | 92 |
| Table 5-1. Inward flux equations at the membrane boundaries | 106 |
| Table 5-2. Relevant variables and parameters for the study of waste diffusion behavior | 107 |
| Table 5-3. Validation cases studied for accuracy | 109 |
| Table 5-4. Validation cases studied for comparison to dialyzer FX60..... | 112 |
| Table 5-5. Comparisons of clearances [107] | 113 |
| Table 5-6. Relevant variables and parameters of hemodialysis system model | 115 |
| Table 5-7. Requirements of the proposed dialyzer design | 118 |
| Table 5-8. Resulting ER curve parameters of each cases studied with circular channels | 123 |
| Table 5-9. The minimum C_{b2m} values [mg/mL] for different cases..... | 130 |
| Table 6-1. Computational cost of LB-SL method based DNS studies | 147 |

LIST OF FIGURES

| | |
|---|----|
| Figure 1-1. A typical dialyzer (Gambro Training Manual)..... | 1 |
| Figure 1-2. a. Cross-section of a typical dialyzer and b. close-up view of proposed configuration | 3 |
| Figure 1-3. Scope of research questions | 4 |
| Figure 2-1.A. Overview of the system and B. flow configuration of the micro-fluidic channel for direct contact [42] | 15 |
| Figure 3-1. D3Q19 lattice..... | 21 |
| Figure 3-2. Discretization of fluid and solid phases [69] | 24 |
| Figure 3-3. Schematic of simulation domain (a) cross-section of a rectangular channel (b) cross-section of a circular channel (c) front-view..... | 32 |
| Figure 3-4. The shape change of RBC model during the deflation process | 34 |
| Figure 3-5. Side view of RBC models (red) in comparison to analytical RBC shape (blue)..... | 35 |
| Figure 3-6. Helmholtz energy, volume, and area change during RBC creation process | 36 |
| Figure 3-7. Initial random location generation: (a) flow direction view of the whole channel (b) cross-section view of RBCs (c) cross-section view of platelets | 39 |
| Figure 3-8. Deformation index vs. Capillary number for a RBC flowing through a 9.3 μm pipe ... | 41 |
| Figure 3-9. Tweezer simulation results and a stretched RBC..... | 42 |
| Figure 3-10. New platelet model with the new RBC B in 2.5 $\text{lu}/\mu\text{m}$ resolution | 43 |
| Figure 3-11. A ellipsoid aligned with the vorticity direction and immersed in simple shear flow | 43 |
| Figure 3-12. Angle and angular velocity of the platelet over time in comparison to Jeffery's solution..... | 44 |

| | |
|---|----|
| Figure 3-13. Angle and angular velocity of the platelet over time in comparison to Jeffery's solution (close-up view) | 45 |
| Figure 3-14. Simulation domains with two different domain lengths in the flow direction..... | 46 |
| Figure 3-15. Blood cell migration behavior results with two different domain lengths | 47 |
| Figure 3-16. Blood cell migration behavior flowing in 120 μm diameter channel with the initial blood stream diameter of 84.7 μm for three different contact and lubrication parameter values | 49 |
| Figure 3-17. Average trajectory of blood cells flowing in 120 μm diameter channel with the initial blood stream diameter of 84.7 μm for three different contact and lubrication parameter values | 50 |
| Figure 3-18. RBC diffusion in a flat channel with 15% hematocrit blood stream and PBS solution [40] | 51 |
| Figure 3-19. (a) Concentration profile in four sections of a flat channel, (b) Clouds half-width w along the channel for several different conditions and for two different thicknesses (empty symbols: $2h=53\mu\text{m}$, full symbols: $2h=101\mu\text{m}$) [40] | 52 |
| Figure 3-20. Initial concentration profile of the two simulation cases | 54 |
| Figure 3-21. Fitted parabolic curves (thin solid lines) of the initial concentration profile (dotted line) with concentration data used for the fitting shown in thick solid line | 55 |
| Figure 3-22. Concentration profile in several sections along the channel (dotted line: data, thin solid line: fitted parabolic curve, thick solid line: data used for fitting)..... | 56 |
| Figure 3-23. Log-log plot of w vs. flow distance x (stars: data, solid line: fitted linear line)..... | 58 |
| Figure 3-24. $wx^3 - w_0^3$ along the channel for several different conditions with simulations (stars: data, solid line: fitted linear line) | 59 |

Figure 3-25. Cross-section view of the channel for case A ($w_0=40.75 \mu\text{m}$, $N_0 = 8.11 \mu\text{m}$) 60

Figure 3-26. Cross-section view of the channel for case B ($w_0=7.08 \mu\text{m}$, $N_0 = 2.69 \mu\text{m}$) 60

Figure 3-27. Concentration profile (depth direction) in several sections along the channel 61

Figure 3-28. Screenshot of 8715 RBCs in $(160\mu\text{m})^3$ domain 63

Figure 3-29. Scaling simulation results for 100 LB time steps with 8715 RBCs in $160\mu\text{m}^3$ domain
..... 64

Figure 4-1. Cross-section of rectangular channels (a, b) and circular channel (c) with blood and sheath stream. (a. with fluid velocity field): flow direction is into the page 68

Figure 4-2. Screenshots of (a) 40%, (b) 30%, and (c) 20% hematocrit cases in $40 \mu\text{m}$ height channel with $32 \mu\text{m}$ initial blood stream height 71

Figure 4-3. Extraction ratios of RBCs (a, b, c) and platelets (d, e, f) with 40% (a,d), 30% (b, e), and 20% (c, f)..... 72

Figure 4-4. Extraction ratios of RBCs with 40% (a), 30% (b), and 20% (c) 72

Figure 4-5. Blood cell migration behavior flowing in $40 \mu\text{m}$ diameter channel with the initial blood stream diameter of $32 \mu\text{m}$ for three different flow velocities with 40% HCT 74

Figure 4-6. Simulation Study Space 76

Figure 4-7. RBC extraction ratio vs. flow distance fitted to an exponential curve..... 78

Figure 4-8. Extraction ratio of blood cells over flow distance for the 8 circular channel cases.... 80

Figure 4-9. Close-up view of extraction ratio of blood cells over flow distance for 3 circular channel cases..... 81

Figure 4-10. Extraction ratio of blood cells over flow distance for rectangular channel cases 1-6
..... 82

| | |
|--|-----|
| Figure 4-11. Extraction ratio of blood cells over flow distance for rectangular channel cases 7-13 | 83 |
| Figure 4-12. Close-up view of extraction ratio of blood cells over flow distance for 3 rectangular channel cases..... | 84 |
| Figure 4-13. RBC ER_{eq} vs. area ratio of sheath to channel..... | 85 |
| Figure 4-14. RBC scaled length constant L_{ra2D3} vs. channel size and area ratio of sheath to channel..... | 87 |
| Figure 4-15. RBC length constant L_r vs. channel size..... | 88 |
| Figure 4-16. The relations of length constant L_r vs. channel size and the area ratio of sheath to channel..... | 89 |
| Figure 4-17. Outline of research question 1..... | 90 |
| Figure 4-18. Meta-model of RBC L_{ra2H3} as a function of channel height and area ratio of sheath to channel..... | 92 |
| Figure 4-19. Meta-model of RBC L_r in function of channel height and area ratio of sheath to channel for rectangular channels..... | 93 |
| Figure 4-20. Meta-models of RBC L(ER = 0.05) as functions of channel size and sheath stream thickness for rectangular channels (top) and circular channels (bottom)..... | 94 |
| Figure 4-21. RBC L(ER = 0.05) vs. channel size and area ratio of sheath to channel..... | 95 |
| Figure 4-22. L(ER = 0.05) vs. channel size..... | 96 |
| Figure 5-1. A typical dialyzer (Gambro Training Manual)..... | 99 |
| Figure 5-2. a. Cross-section of a typical dialyzer and b. close-up view of proposed configuration | 100 |
| Figure 5-3. Clearance (filtration rate) vs. molecular mass for different filtration methods [97] | 101 |

| | |
|--|-----|
| Figure 5-4. Comsol model in 2D and 3D with concentration field and flow velocity (arrow)..... | 103 |
| Figure 5-5. Hexagonal-shaped unit cell of the fiber assembly (Comsol Document - model ID: 258. Separation through dialysis)..... | 104 |
| Figure 5-6. Comsol model in 2D and 3D with concentration field and flow velocity (arrow) for dialyzer validation | 111 |
| Figure 5-7. Clearance vs. partition coefficient and porosity coefficient | 112 |
| Figure 5-8. Waste level change for several cycles of treatment (solid line) and connections of maximum waste level for each cycle (dashed line – peak waste decay curve) [109] | 114 |
| Figure 5-9. Overview of the design space exploration | 122 |
| Figure 5-10. For-loop for waste diffusion study using Comsol tubule model | 124 |
| Figure 5-11. For-loop for dialyzer performance study using hemodialysis system model | 125 |
| Figure 5-12. Steady state concentration values of β_2 -microglobulin vs. v_i and L for cases 5 (red), 6 (blue), 9 (green) | 127 |
| Figure 5-13. Steady state concentration values of Albumin and β_2 -microglobulin vs. clearances and clearance ratios for cases 5 (red), 6 (blue), 9 (green) | 128 |
| Figure 5-14. Cb2m over v_i for different channel sizes | 130 |
| Figure 5-15. The effect of design variables on Calb, Cb2m, Curea for D = 500 μm (green), 600 μm (blue), 700 μm (red) | 131 |
| Figure 5-16. The effect of clearances and clearance ratio on Calb and Cb2m for D = 500 μm (green), 600 μm (blue), 700 μm (red)..... | 133 |
| Figure 5-17. Cb2m vs. dialyzer size and total fluid usage for D = 500 μm (green), 600 μm (blue), 700 μm (red)..... | 134 |

Figure 5-18. The effect of design variables on the total fluid usage for $D = 500 \mu\text{m}$ (green), $600 \mu\text{m}$ (blue), $700 \mu\text{m}$ (red) 135

Figure 5-19. An example variation of the proposed dialyzer design..... 138

LIST OF SYMBOLS AND ABBREVIATIONS

| | | |
|------------------------|--|--------------------|
| RBC | Red Blood Cell | |
| ER | Extraction Ratio | |
| LB-SL | Lattice Boltzmann and Spectrin Link | |
| DNS | Direct Numerical Simulation | |
| Re | Reynolds Number | |
| Re _p | Particle Reynolds Number | |
| HCT | Hematocrit or Volume Fraction of RBCs | |
| <i>Ca</i> | Capillary Number | |
| ν | Kinematic Viscosity | m ² /s |
| $\dot{\gamma}$ | Shear Rate | /s |
| <i>G</i> | RBC Membrane Shear Modulus | μN/m |
| <i>l</i> ₀ | Equilibrium Length of RBC Model | |
| lu | Lattice Unit | |
| D | Channel or Membrane Tubule Inside Diameter | μm |
| δ | Sheath Stream Thickness | μm |
| L | Flow Distance or Dialyzer Tubule Length | mm |
| ER _{eq} | Equilibrium Extraction Ratio | |
| L _τ | Length Constant | mm |
| L _(ER=0.05) | Length When the ER Reaches 5% | mm |
| tD | Dialysate Stream Thickness | μm |
| D0 | Stagnant Diffusivity | m ² /s |
| C0 | Initial Concentration | Mol/m ³ |

| | | |
|-------------|----------------------------|--------|
| v_i | Blood Maximum Velocity | mm/s |
| v_d | Dialysate Maximum Velocity | mm/s |
| K | Partition Coefficient | |
| P | Porosity Coefficient | |
| K^d | Clearance, | mL/min |
| Q_B | Blood Flow Rate | mL/min |
| Q_D | Dialysate Flow Rate | mL/min |
| C | Steady State Waste Level | mg/mL |
| K_0A | Dialyzer Property | mL/min |
| t_{treat} | Treatment Length | hr |
| t_{total} | Treatment Cycle Length | hr |

SUMMARY

Hemodialysis is a renal replacement therapy that removes waste solutes from the blood stream using concentration gradients across a membrane. In order to overcome several shortcomings and increase the waste removal rate, a new dialyzer (filter) design is proposed in this study. In the new dialyzer design, the blood concurrently flows with a sheath fluid in a micro-fluidic channel. Because the blood stream directly contacts the sheath stream, it is important to prevent blood cell migration from the blood stream to the sheath stream while providing enough time for the waste solutes to diffuse into the sheath stream. This research was intended to understand the migration behavior of red blood cells (RBC) and platelets in non-uniform suspension flow, where the blood and sheath flows in direct contact, and apply the results to identify the feasible design space of the proposed dialyzer.

The effect of different flow conditions and channel geometry on the blood cell extraction ratios (ER), the ratio of cells lost into the sheath stream, in non-uniform suspension flows was parametrically studied using Lattice Boltzmann and Spectrin Link (LB-SL) method based direct numerical simulation (DNS). Analyzing ER over the flow distance showed that the channel size and the area ratio of sheath to channel are the main variables that affect the ER. Based on the relationship found, a meta-model of RBC ER was created, although platelet ERs showed only a general trend. Based on the study, feasible conditions that will retain blood cells in the blood stream were identified.

Then, the DNS results of blood cell ER were used with a molecule diffusion model and a hemodialysis system model to study the feasibility of the proposed dialyzer design that

maximizes middle molecule filtration with limited blood cell and protein loss. No feasible design was found in the studied range suggesting that relying purely on the diffusion based on the direct contact for the removal of middle molecules is not a feasible solution with the small channel size ($\sim 700 \mu\text{m}$) due to the loss of protein. It suggested that in order to increase the middle molecule removal while maintain the protein level, clearance ratio of middle molecule to protein should be increased using large channel size, small sheath stream thickness, long tubule length, and slow blood flow velocity.

The intellectual merit of this research lies in understanding the migration behavior of blood cells in a non-uniform suspension. This knowledge helped to establish the feasibility of the proposed dialyzer design and can be applied in a variety of applications for the manipulation of cells in a micro-fluidic channel.

CHAPTER ONE

MOTIVATION AND PROBLEM FORMULATION

This chapter briefly explains the motivation for this thesis and introduces the research questions and hypotheses to be answered.

1.1 Hemodialysis

Nearly half a million Americans suffering from kidney failure undergo hemodialysis treatment to stay alive. Traditional hemodialysis has existed in relatively the same form for the last five decades even with side effects coming from the way of utilizing membranes.

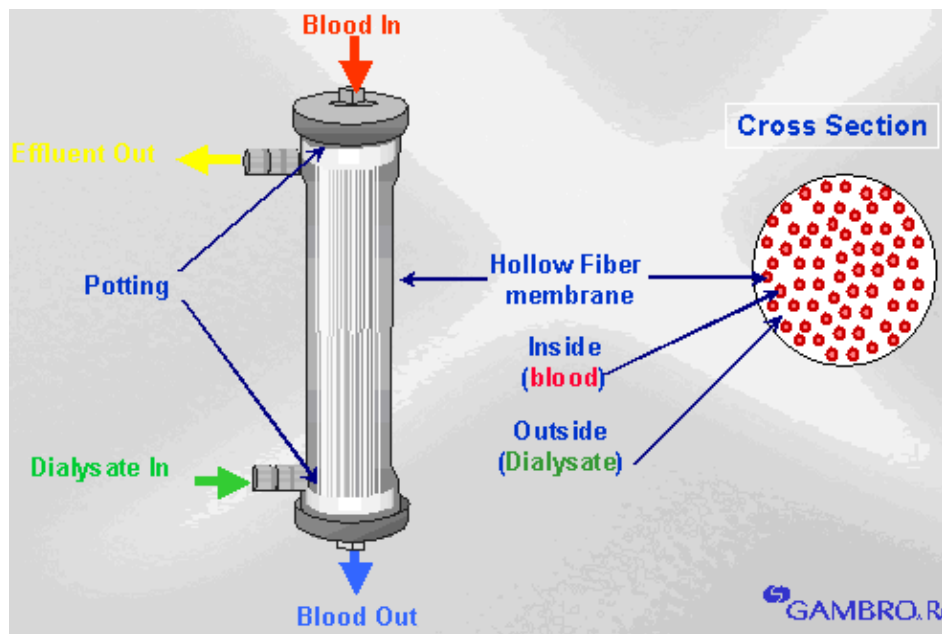


Figure 1-1. A typical dialyzer (Gambro Training Manual)

In a typical hemodialysis system, the blood leaves a patient's body and flows through a dialyzer, a filter. Typical dialyzers take the shape of long cylinders, typically 16 to 25 cm in length and 3 to 5 cm in diameter. They house 7,000 to 15,000 porous hollow fiber tubules, with

spacing between the tubules. The blood flows through the tubules while the dialysate, the cleaning fluid, flows countercurrent in the spacing between the tubules. The fiber tubules are made of a semi-permeable membrane. Due to the concentration gradient between the blood and dialysate, waste in the blood diffuses into the dialysate across the semi-permeable membrane. Then, the cleaned blood returns to the body, and used dialysate is disposed.

Current dialyzers suffer from several drawbacks, such as bioincompatibility issues including inflammatory reactions due to the blood directly contacting a foreign surface (membrane) [1]. Inefficient waste removal rate is another huge problem. Current dialyzers are efficient in removal of small molecules such as urea. However, because the technology to control the pore size of the membrane is limited, larger molecules (middle molecules) such as β -2 microglobulin are not removed from the patient's body as they are supposed to be with normal kidneys [2]. Typically, only 10~40% of the middle molecules are removed during a hemodialysis session. Consequently, these toxins reach abnormally high levels and damage the body over time. The toxin level can be up to fifty times higher in long term hemodialysis patients, and the toxin depositions are associated with various clinical manifestations and eventually constitute a major cause of morbidity in long term hemodialysis patients [3, 4].

1.2 Proposed Configuration

This work proposes a new dialyzer design that could increase the waste removal rate, including middle molecules, while reducing bioincompatibility. The new configuration is proposed based on currently used dialyzers. Instead of only blood flowing through the tubule, sheath fluid is added. A close-up view of each tubule of the proposed dialyzer is shown in Figure 1-2.

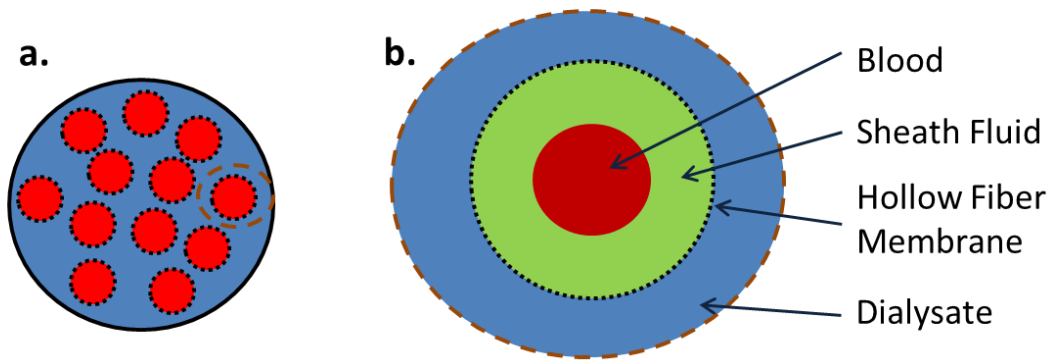


Figure 1-2. a. Cross-section of a typical dialyzer and b. close-up view of proposed configuration

The blood stream is surrounded by sheath fluid so that blood and membrane contact is completely avoided. Removing the direct contact between the blood and membrane and replacing the solid membrane with liquid can increase waste removal rate and reduce side effects [5]. The sheath fluid will be a plasma-like fluid so that the blood is not contaminated in case any mixing occurs. Waste diffusion happens simultaneously in two places, 1. from blood to sheath fluid and 2. from sheath fluid to dialysate. Middle molecules will easily diffuse into sheath fluid since no membrane is blocking the way. The proposed design can result in a system very similar to typical hemodialysis systems, but with improved waste filtration rate.

1.3 Research Questions and Hypothesis

The proposed dialyzer requires maintaining laminar flow of both blood and sheath fluid so that mixing does not occur inside each tubule. As blood flows through the dialyzer, blood cells and proteins, such as albumin, should be retained in the blood stream while providing enough time for waste molecules, such as urea and β -2 microglobulin, to diffuse into the sheath stream. In order to identify such feasible conditions, an understanding of cell migration behavior and waste diffusion should be developed by studying the effect of flow conditions and

dimensions in a micro-fluidic channel. Figure 1-3 shows the scope of two research questions answered in this research.

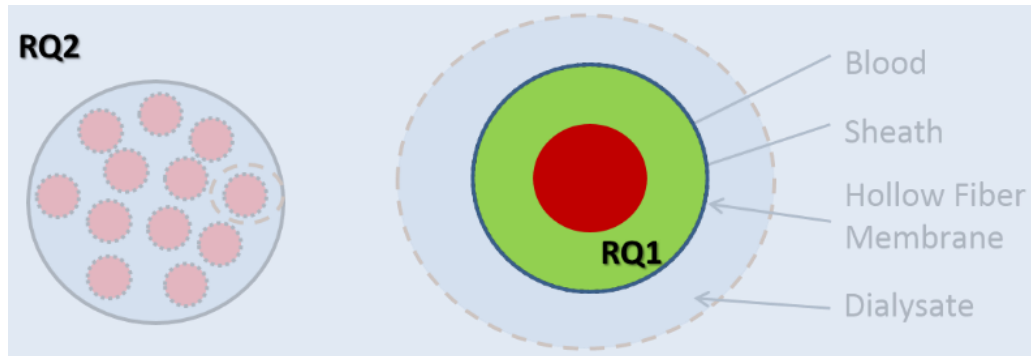


Figure 1-3. Scope of research questions

The first research question focused on understanding the cell migration behavior for a pressure driven laminar flow when blood flows in the center with sheath fluid in a circular channel. The cells cannot migrate across the membrane in the proposed filter design. Thus, the study of blood cell migration behavior is limited to the central region that involves only the blood and sheath stream. It is studied with Lattice Boltzmann and Spectrin Link (LB-SL) method based direct numerical simulations (DNS) of RBCs and platelets for accurate direct analysis of each different cell motion in the suspension. Research question 1 is as follows.

RQ 1. What are the conditions that retain blood cells in the blood stream when it flows with sheath fluid in a micro-fluidic channel?

Hypothesis 1: A meta-model that predicts migration of RBCs and platelets can be created by a parametric study with LB-SL method based direct numerical simulations. Then, the meta-model can be used to specify the conditions that will retain blood cells in the blood stream.

The second research question expanded the study region to the whole dialyzer, which includes membrane and dialysate as well. Molecular diffusion is studied with a Comsol tubule

model of fluid and molecule diffusion, but no blood cell suspensions. The two studies of blood cell migration behavior and molecule diffusion behavior are used together with a hemodialysis system model, which predicts the waste level change over time for a given dialyzer and patient information, to define the feasible design space. It provides improved waste removal rate while retaining blood cells in the central blood region with acceptable amount of dialysate and sheath fluid usage. Research question 2 is as follows.

RQ 2. What is the feasible design space of the proposed dialyzer with improved waste removal rate while retaining blood cells?

Hypothesis 2: The meta-model of blood cell migration behavior, a tubule model of molecule diffusion, and a hemodialysis system model can be used together to identify the feasible design space of the proposed dialyzer by studying the effect of design variables on the blood cell loss, molecule diffusion, dialyzer size, and the amount of sheath and dialysate usage.

Research question 1 is answered in Chapter 4, and research question 2 is answered in Chapter 5.

1.4 Summary

This thesis investigates a new dialyzer design based on a blood cell migration study and a molecule diffusion study in order to find a feasible design space that prevents blood cell loss and improves middle molecule filtration rate. Chapter 1 provided the motivation and the context of this work. Chapter 2 provides the background information based on literature review. Chapter 3 provides the explanation and validation of the DNS method, Lattice Boltzmann – Spectrin Link method, used for the study of blood cell migration in non-uniform

suspension flows in Chapter 4. Chapter 4 investigates the effect of channel dimensions and flow conditions on the blood cell extraction ratios (ER), the amount of cells lost into the sheath stream, and the conditions that will retain blood cells in the blood stream are identified. A meta-model of RBC ER is also created, and it can be applied for the manipulation of cells in a micro-fluidic channel. Chapter 5 identifies a feasible design space for the proposed dialyzer based on the Comsol tubule model and a hemodialysis system model. Chapter 6 concludes by providing an analysis of the provided work and suggestions for future work.

CHAPTER TWO

LITERATURE REVIEW

In this chapter, blood cell migration behaviors in suspension flows are reviewed in the context of general suspension flows. Existing micro-fluidic devices with non-uniform suspension flows that have similar configuration as the proposed dialyzer design are documented. Research directions are suggested based on the literature review.

2.1 Blood Composition and Relevant Dimensionless Parameters in Blood Flow

Blood is composed of blood cells and plasma. Plasma is a Newtonian fluid, but whole blood is a dense suspension of blood cells. Red blood cells (RBCs) constitute about 45% of whole blood by volume. They contain hemoglobin and distribute oxygen. They are deformable and have a biconcave disk shape with diameter of 6-8 μm . Platelets are responsible for blood clotting. They are rigid and disk shaped with diameter of 2-3 μm . One microliter of blood contains 0.2M-0.5M platelets [6] compared to 4.2M-6.1M RBCs. RBCs outnumber platelets and white blood cells by a factor of around 15 and 1000 [7]. Whole blood exhibits non-Newtonian behavior such as shear thinning, a decrease in the viscosity with increased shear rate. The complex behavior of whole blood has always been of interest for researchers.

The primary dimensionless parameter that is relevant to single-phase flow through a micro-fluidic channel is the Reynolds number. Inclusion of particles in the flow adds the particle Reynolds number, the volume fraction of particles, and Peclet number. If deformable particles, such as RBCs, are added, the capillary number is another important parameter to be considered. The dimensionless parameters relevant in blood flow are listed in Table 2-1.

Table 2-1. Relevant Dimensionless Parameters in Blood Flow

| | Symbol | Definition |
|---------------------------------|-----------------|-------------------------------|
| Reynolds Number | Re | $\frac{Du}{\nu}$ |
| Particle Reynolds Number | Re _p | $\frac{a^2\dot{\gamma}}{\nu}$ |
| Hematocrit | HCT | $\frac{NV_{RBC}}{V_{domain}}$ |
| Capillary Number | Ca | $\frac{a\dot{\gamma}\mu}{G}$ |

The Reynolds number is the ratio of inertial force and viscous force. D is the channel diameter or height, u is the average velocity in the channel, and ν is the kinematic viscosity of the suspending fluid, plasma. All of the simulations conducted in this research are well within the laminar flow region ($Re \ll 2100$) where the viscous force is dominant.

The RBC based particle Reynolds number, Re_p , is the ratio of the inertial to viscous forces on the local level of RBC. a is the RBC diameter, $\dot{\gamma}$ is the shear rate. $\dot{\gamma}$ is supposed to be the actual shear rate that a RBC is experiencing. However, in this research, the wall shear rate was used, unless noted otherwise, to specify the maximum possible Re_p . Most of simulations were run with Re_p values less than 0.4, but for some of simulations, it was as high as 0.7.

Hematocrit is the volume fraction of RBCs. It is defined as the number of RBCs, N , multiplied by the volume of a RBC, V_{RBC} , divided by the volume of the fluid domain, V_{domain} .

The Capillary number is the ratio of forces due to viscous fluid motion to the elasticity of the RBC membrane where G is the RBC membrane shear modulus. Most of simulations in this research were run with Ca values of less than 1.

The Peclet number is the transport rate ratio of advection to diffusion, and it is defined as $Pe = \frac{6\pi a^3 \dot{\gamma} \mu}{k_B T}$. k_B is Boltzmann's constant and T is temperature. It can be used for characterizing a suspension flow by emphasizing the effect of Brownian motion. The Peclet number of blood cell suspension in this work goes to infinite since Brownian motion of blood cell is negligible compared to the migration due to deformation, hydrodynamics, and particle-particle interaction. Thus, Peclet number is not included in the list of relevant dimensionless parameters in blood flow.

2.2 Uniform Suspension Flows

Deformability, shear rate, and particle density affect the equilibrium position of particles in suspension. In the dilute limit where particle interactions are negligible, for rigid spherical particles, no migration occurs at very low flow rates where no inertial force exists. As flow rate and hence shear rate increases and inertial effects are involved, the particle concentration at the center of the tube and close to the wall decreases, and maximum concentration occurs around 0.6 of radius from the tube's center. It is due to a well-known fluid separation effect that neutrally buoyant spherical particles equilibrate around 0.6R for dilute suspension in laminar pressure driven pipe flow, which is called the tubular pinch effect or the Segre Silberberg equilibrium position [8, 9]. It is due to the competition between the inertial lift forces that drive particles towards the wall and pressure forces that drive particles towards the center. Rigid platelets [10] and rigid RBC ghost cells [11] behave the same as rigid spheres. However, deformable RBCs tend to migrate to the center until a high shear rate (5000/s) is reached [12, 13]. Above the high shear rate, RBCs will also exhibit tubular pinch effect: the effect was shown at $Re_p=0.001$ and it vanished at $Re_p=5e-6$ [10]. The general trend of RBCs showing tubular pinch

effect on high shear rate or Re_p is agreed among different researchers. However, the equilibrium position and exact cut-off that the tubular pinch effect appears is a little controversial as another study showed RBCs showing the effect nearer to the center, not exactly 0.6 or tubule radius [11].

The trajectories of two isolated spheres that interact with each other are symmetric and reversible in creeping flow conditions, Stokes flow where inertial force is negligible [14]. However, interactions of more than three spheres [15] lead to asymmetry and irreversible displacement. Particle migration in a suspension across streamlines and against concentration gradients may be found even under Stokes flow when undergoing bounded shear flow. It is different from the tubular pinch effect that is due to inertial forces. The particle migrations are dominated by the flow, since Brownian diffusion can be neglected in such particle migration with high Peclet number, so it is called shear-induced migration and observed in many experimental studies [16, 17]. Several attempts have been made to explain the phenomenon of shear-induced particle migration behavior and related rheology of Stokes flow in suspension using constitutive models, which are presented in section 2.3.

The shear-induced migration that drives particles from the low to high shear region works against the wall-induced lift force that drives particles away from the wall in a pipe flow. The particle migration based on the balance of these driving forces lead particle concentration distribution to be non-uniform [18] and velocity profile to be blunt in comparison to the Hagen-Poiseuille parabolic velocity profile for Newtonian fluids [19]. Increasing volume fraction of particles increases the concentration of particles in the central region and more velocity blunting [20]. When two different types of particles flow as a dense suspension, the different effect of shear force and wall-lift force on particles and particle-particle interactions lead to the

segregation of the particles. Large particles will concentrate in the central region compared to small particles [21]. Whole blood is a dense suspension of large deformable RBCs and small rigid platelets. Initially uniformly distributed blood cells will show very different migration behavior as they flow through a channel or a pipe and create a non-uniform distribution. RBCs migrate to the center and platelets marginate to a cell-free-layer close to the wall. And the trend is stronger for increased shear rate [22]. RBC aggregation in tube flow also tends to create a more blunted velocity profile and leads to a greater axial migration, which results in a larger cell-free layer [23]. The platelet margination results in an order of magnitude higher platelet concentration near the wall. Due to the presence of RBCs in blood [24], the rate of platelet flux to the vessel walls is several orders of magnitude higher compared to the transport due to simple Brownian motion [25]. This higher transport rate of platelets due to RBCs is termed "enhanced diffusivity" [26, 27]. The platelet margination was explained by RBC-enhanced shear-enhanced diffusion [28]. A thorough review of dense suspension rheology can be found in the review of Stickel and Powell [29].

2.3 Constitutive Models of Particle Migration in a Sheared-Suspension

Leighton and Acrivos proposed a phenomenological model, diffusive flux model, that assumes that the particle migration is due to a gradient in the shear rate and the concentration [30]. Although it provides valid predictions of particle concentration profiles for homogeneous shear flow, it is not valid in general.

Nott and Brady proposed a suspension balance model (SBM) where macroscopic mass, momentum, and energy balances are constructed and solved simultaneously [31]. They proposed that the velocity orthogonal to the suspension velocity is driven by the divergence of

the hydrodynamic portion of particle phase stress $\langle \boldsymbol{\sigma} \rangle^p$, which is equated to the particle stress $\boldsymbol{\Sigma}^{(p)}$, which denotes the particle contribution to the suspension stress [32]. The hydrodynamic part of the particle stress is equated as stresslet, the symmetric part of the first moment of the fluid traction on the particle surface [32]. They also showed that the diffusive flux model can be recovered from the suspension balance model showing that the two models share the same physical origin.

Many researchers derived equations of motion for general two phase flows, and their results showed that there is no hydrodynamic contribution to the particle phase stress for the Stokesian suspensions. The effect of the fluid is only felt as an average hydrodynamic force on the particles which has traditionally assumed to be interphase drag. The discrepancy regarding hydrodynamic contribution to the particle phase stress was pointed out by Lhuillier [33], and he proposed an additional part, stress-induced migration. Nott et al. [34] reaffirmed the statement of Lhuillier and showed that although the form of the equations of the motion in the SBM is correct, the identification of the hydrodynamic part of the particle phase stress $n\langle \boldsymbol{\sigma}^h \rangle^p$ with that of particle stress $\boldsymbol{\Sigma}^{h(p)}$ is incorrect, and stresslet contributes only to the stresses of fluid phase and suspension, not particle phase. And they showed that the hydrodynamic force on the particle phase $n\langle \boldsymbol{f}^h \rangle^p$ should be the sum of the interphase drag $n\langle \boldsymbol{f}^h \rangle_{drag}$ and the divergence of the hydrodynamic part of the particle phase stress $n\langle \boldsymbol{\sigma}^h \rangle^p$. Particle migration is likely driven by the divergence of the stress $\langle \boldsymbol{\sigma}^h \rangle^p$. They also noted that their forms of $\langle \boldsymbol{f}^h \rangle_{drag}$ and $\langle \boldsymbol{\sigma}^h \rangle^p$ needs further verification either by analytical calculation or by Stokesian Dynamics simulation to make a definitive statement.

Many studies based on the original SBM that calculate particle phase stress using stresslet to simulate particle migration in a sheared suspension are incorrect due to the discrepancy explained. Although the simulation results closely match with experiments [20, 21, 35, 36], it is limited to rigid particles. Simulation studies using LBM that studied microstructure and rheology also used the original method that involves stresslet [37-39].

The divergence of the hydrodynamic portion of particle phase stress $\langle \boldsymbol{\sigma} \rangle^P$ is used to explain the shear-induced migration, and it does not take into account the stress-induced migration. Lhuillier [33] provided systematic descriptions of the nondrag part of the hydrodynamic force leading to shear-induced migration and a stress-induced force which involved Irving-Korkwood (IK) stress bound to the direct (non-hydrodynamic) interaction forces between the particles. The proposed phenomenological expressions require analytical calculation and numerical simulations for further verification. Nott et al. [34] also noted that particle migration could also be driven by the divergence of the particle phase contact stress, which is the same as IK stress. They also noted that the importance of particle-particle interaction on the particle migration increases with concentration.

As described, the description of the particle migration in Stokes suspension flow is still controversial concerning the forces acting on the particles, and further numerical simulation studies are required to complete the understanding of particle migration in Stokes suspensions.

2.4 Blood Cell Migration Behaviors in Non-Uniform Suspension Flows

Blood cell migration behavior in uniform suspension flow where only the blood flows through a pipe or channel are relatively well understood although some controversies exist on

the driving force of the particle migration. However, the blood cell migration in non-uniform suspensions that sheath fluid flows in direct-contact with the blood are rarely studied.

One of a very few studies considered non-uniform suspensions of RBCs [40]. Their experiments were conducted using dilute to semi-dilute (~30%) RBC suspensions in channels of $0.5 \times 0.05 \times 600$ mm or similar other dimensions. They showed that the spreading of a stream of blood cells in channel flow is characterized by a sub-diffusive behavior with exponent $1/3$. The subdiffusive behavior is expected to be generic to systems where advected particles undergo short-range pairwise hydrodynamic interactions or collisions.

Although there are few studies on the rheology of non-uniform suspension flows, there are a few micro-fluidic devices that utilize the non-uniform suspension flow configuration. Reviewing such application's experimental results can suggest what study range should be used for this research in order to find the conditions that will retain the blood cells in the blood stream in the proposed dialyzer design.

2.4.1 Blood Cleansing Device for Sepsis Treatment

Yung et al. developed an extracorporeal blood cleansing device that can selectively remove pathogens from contaminated blood using microbeads controlled with a magnetic field [41]. They used micro-fabricated PDMS layers to assemble a micro-fluidic device where blood and saline flow in parallel with direct contact. The flow channel dimensions were $0.5 \times 0.2 \times 20$ mm with the blood and sheath stream thickness of 0.1 mm each. They found that 50-60% of the blood would be lost in the outlet when the flow rate ratio of phosphate buffer saline (PBS) to the blood flow was 1. Replacing PBS with 6% Dextran solution to match the viscosity of the blood did little to reduce blood loss. The loss was significantly reduced to ~13% when the flow

ratio increased by 4-fold in order to hydrodynamically confine the blood stream. However, there is a concern for the increased saline flow, since it may exert a momentum transfer into the blood phase, which can potentially impede the motion of magnetic particles and reduce separation efficiency. Although the channel cross-section dimension may be larger than a typical dialyzer tubule, this study is a good example of utilizing saline for blood cleansing purposes. It suggests that there is huge blood cell loss for the large sheath stream thickness, and that the flow ratio is an important factor, while viscosity ratio is not for reducing blood loss in such flow conditions.

2.4.2 Hemodialysis Filtration System

Leonard et al. proposed a 2-stage serial filtration system that consists of a rectangular micro-fluidic channel and a dialyzer [42, 43] as shown in Figure 2-1.

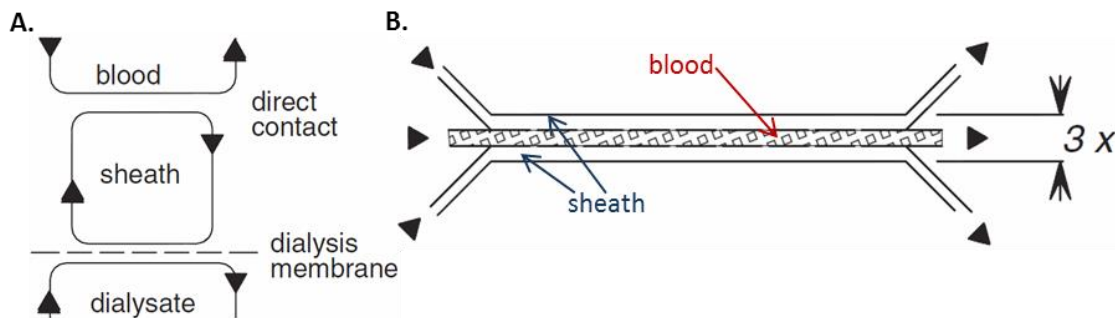


Figure 2-1.A. Overview of the system and B. flow configuration of the micro-fluidic channel for direct contact [42]

Figure 2-1.A shows the overview of the system, and Figure 2-1.B shows the cross-section view of the first stage micro-fluidic channel. In the micro-fluidic channel, the blood stream flows, in the center with 1/3 height of the channel, sandwiched between sheath fluids on both sides without membranes in between. Thus, the blood and sheath fluid flow in contact without mixing, and this eases mass transfer of waste molecules. The sheath is a plasma-like fluid so that the blood

is not contaminated in case any mixing occurs. Then, in the second stage in serial connection to the first stage micro-fluidic channel, the sheath fluid is filtered through a typical dialyzer, and the sheath fluid is reused until it is totally replaced by a new sheath fluid after several cycles. This system may increase waste removal rate compared to currently used dialyzers. The dimensions of the micro-fluidic channel are provided in Table 2-2 with the dimensions of currently used dialyzer membrane for reference.

Table 2-2. Dimensions of Leonard’s micro-fluidic channel and currently used dialyzer tubule

| | | |
|--------------------------|--------------------|----------------------|
| Leonard’s Channel | Length | 1.5~14.6 cm |
| | Height | 75~300 μm |
| | Depth | 1.25 cm |
| Dialyzer Tubule | Diameter | 200 μm |
| | Membrane thickness | 6~35 μm |
| | Pore diameter | 0~6 nm |

For such micro-fluidic channels, the most important requirement is preventing possible blood cell loss. Aucoin experimentally studied how RBCs would migrate away from the center using the same configuration [44]. The study showed the potential of the design for hemodialysis treatment, but the best conditions in thin, microfluidic flows were not well defined. In the specific operating ranges studied, they found that fluid mechanics alone were insufficient to completely prevent blood cell loss [45]. As a result, the use of nanopore filters that block the cells in the sheath flow from entering the second stage is suggested [42]. This is an important reason that their proposed configuration is serial, not parallel. The parallel configuration that is suggested with this research is possible when flow conditions that can prevent blood cell loss are identified.

Using the micro-fluidic channel, they also studied the effect of different flow conditions on the diffusion rate of solutes. It is known that the diffusivity enhances with increased shear rate and particle volume fraction. Although many studies were conducted in various experimental settings for different solutes and suspension particles [46-51], most authors report quantitatively different results. Leonard et al. studied how bovine serum albumin diffuses from the center to peripheral sheath fluid regions for varied shear rates and hematocrits using the configuration shown in Figure 2-1.B. [44]. Nanne et al. studied the effect of particle suspension on diffusivity of waste solutes using the same configuration. The results did not permit a clear determination of the physical cause of diffusion enhancement. However, results generally agree on the augmentation of diffusivity with increasing particle volume fraction and shear rate, and the diffusivity enhancement ratio of about 2.5 was found for bovine albumin in 40% hematocrit of bovine blood suspension flow for the interface shear rate of 100 /s [52].

2.4.3 Hydrodynamic Focusing

Hydrodynamic focusing is a method for handling a sample stream. A device includes an inlet for the sample stream and various numbers of inlets [53-58] for sheath fluids that surround the sample stream. The sample stream and sheath stream flow with direct contact in the micro-fluidic channel, and the sample stream can be controlled by varying flow geometry, dimension, flow rates, number of sheath fluid inlets, etc. Hydrodynamic focusing has a number of applications in microfluidics such as micromixers, microcytometers, and fluidic switches [53]. Although applications are generally for enhancing mixing in the viscosity-dominant laminar flow condition or making cells align without the separation of sample stream and sheath stream at the outlet, the fact that manipulation of sample stream is possible when two different fluids

flow with direct contact in a micro-fluidic channel shows the possibility of the proposed filter configuration.

2.5 Simulation Studies of Blood Flow

A simple 2-D simulation of red blood cells and a leukocyte successfully reproduced the increasingly blunted velocity profiles, increased leukocyte margination in a micro-vessel, and the existence of a cell free layer close to the wall [59]. Stokesian dynamics simulations successfully showed velocity blunting [31]. It is also used to study self-diffusion of particles [60] and rheology in dense suspensions [61]. Even with the limited number of particles studied, results qualitatively matched with experimental results. Recently, the Lattice Boltzmann Method (LBM) coupled with several particle models was successfully implemented to simulate vesicles (deformable capsules), RBCs, and platelets in a sheared flow in large scale 3-D simulations with physiological particle volume densities by Aidun et al. [37-39, 62]. Using the LBM, the dynamics, RBC migration and platelet margination [62] and microstructure and rheology [37-39] were studied with up to 1090 RBCs and 40 platelets. Normal stresses and particle phase stresses in suspensions were also calculated which are the key information needed to study rheology and understand why particle migration happens according to the suspension balance model. The LBM is used as a direct numerical simulation method in this thesis, and more details follow in Chapter 3.

2.6 Summary

The literature review revealed that there have been similar attempts to clean blood using direct-contact in micro-fluidic channels. There has been limited success yet due to the

problem of blood cell loss. Only a few researchers [40, 45, 52] studied particle migration of non-uniform suspensions in which blood cells populate only in the central region, as proposed in this study. In order to realize the proposed filter design, it is important to understand how blood cell migration happens and how blood cells can be retained in the blood stream when it flows with sheath stream. The literature review shows that previous study of the blood cell migration behavior in non-uniform suspension flow was conducted in a limited range of channel dimensions due to limits on the experimental settings. The direct numerical simulation study based on LBM that follows enables the study to address a wider range of channel sizes.

CHAPTER THREE

LATTICE BOLTZMANN AND SPECTRIN LINK METHOD AND VALIDATION

This chapter explains the direct numerical simulation (DNS) methodology based on the Lattice Boltzmann and Spectrin Link (LB-SL) method. The LBM is used for modeling plasma as a Newtonian fluid, and the Spectrin-Link (SL) method is used for modeling the RBC membrane. The parameter values for the new RBC properties with fewer nodes are presented and validated. The LB-SL method is also validated for the study of blood cell migration in non-uniform suspension flows. The computational performance of the code is also presented in this chapter.

3.1 Fluid Simulation Method - Lattice Boltzmann Method

The LBM is an Eulerian approach that recovers the solution of the incompressible Navier-Stokes equations via the Chapman-Enskog expansion. It is used for low Mach, low Reynolds number flows with inertia characteristic of blood flow [63]. With LBM, the fluid phase is modeled by solving simplified microscopic kinetic equations to update the distribution function in each simulation time step. The distribution function, which gives the probability of finding a fluid particle at position \mathbf{x} and time t , is updated based on the collision and streaming process of fluid particles moving in given discrete directions i . Figure 3-1 is an example three-dimensional fluid lattice structure where fluid particles move in 19 discrete directions along the horizontal, vertical, and diagonal links.

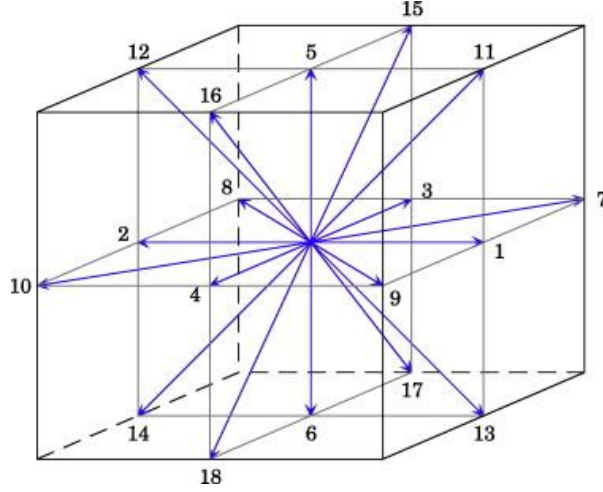


Figure 3-1. D3Q19 lattice

Updating the distribution function requires information concerning only the neighboring fluid node locations. Due to the simple and local nature of the calculation, LBM is widely used for fluid phase modeling that utilizes parallel computing. Aidun and Clausen reviewed recent developments of LBM, its applications in complex and multiphase flows, and its remarkable scalability for parallel processing [64]. This study utilized Aidun et al.'s LBM, which used the 3D lattice with 19 velocities (D3Q19), having the form

$$f_i(\mathbf{x} + \mathbf{e}_i, t + 1) - f_i(\mathbf{x}, t) = -\frac{1}{\tau} [f_i(\mathbf{x}, t) - f_i^{(0)}(\mathbf{x}, t)] \quad (3-1)$$

where f_i is a fluid particle distribution function, $f_i^{(0)}$ is an equilibrium distribution function, and τ is the relaxation time. The distribution function gives the probability of finding a particle at position \mathbf{x} and time t , moving in the discrete direction i . The equilibrium distribution function satisfying the Navier-Stokes equations is

$$f_i^{(0)}(\mathbf{x}, t) = w_i \rho \left[1 + \frac{1}{c_s^2} (\mathbf{e}_i \cdot \mathbf{u}) + \frac{1}{2c_s^4} (\mathbf{e}_i \cdot \mathbf{u})^2 - \frac{1}{2c_s^2} (\mathbf{u} \cdot \mathbf{u}) \right] \quad (3-2)$$

where w_i are appropriate lattice weights set by the geometry of the lattice, and isotropy given as

$$w_i = \begin{cases} 1/3 & i = 0, \\ 1/18 & i = 1 \dots 6, \\ 1/36 & i = 7 \dots 18. \end{cases} \quad (3-3)$$

The single relaxation time is used with a pseudo-sound-speed of $c_s = \sqrt{1/3}$ and a kinematic viscosity of $\nu = c_s^2 \rho (\tau - 0.5)$ [65].

Calculating the moments of the equilibrium distribution function provides the macroscopic fluid properties. The first moment is the local density, which is given in the following equation.

$$\rho(\mathbf{x}, t) = \sum_i f_i(\mathbf{x}, t) \quad (3-4)$$

The second moment is momentum, and the macroscopic velocity is given in the following equation.

$$\mathbf{u}_\alpha(\mathbf{x}, t) = \frac{1}{\rho(\mathbf{x}, t)} \sum_i f_i(\mathbf{x}, t) \mathbf{e}_{i\alpha} \quad (3-5)$$

α denotes a Cartesian direction.

The third moment is related to the pressure, as shown in the following equation.

$$c_s^2 \rho(\mathbf{x}, t) \delta_{\alpha\beta} + \rho(\mathbf{x}, t) \mathbf{u}_\alpha(\mathbf{x}, t) \mathbf{u}_\beta(\mathbf{x}, t) = \sum_i f_i(\mathbf{x}, t) \mathbf{e}_{i\alpha} \mathbf{e}_{i\beta} \quad (3-6)$$

In the LB formulation, the pressure is proportional to the density, as given in the following equation.

$$P_f = c_s^2 \rho(\mathbf{x}, t) = 1/3 \rho(\mathbf{x}, t) \quad (3-7)$$

3.2 Platelet Simulation Method

Platelets are modeled using a finite element model with triangular surface elements to model each platelet as a rigid ellipsoid. The position and angle of the platelet models suspending in the plasma are updated based on the forces generated from interaction with the plasma and RBCs. The calculation is based on a simple Newtonian dynamics solver in each simulation time step: 1. Using the forces on each surface element generated from the particle-particle interaction and fluid-solid coupling, the total applied force and torque applied on the entire particle are calculated. 2. The total force and torque are used to update the acceleration, velocity, and location of each triangular surface. More details of the method can be found in Reasor et al. [39] and MacMeccan et al. [66]. This study used exactly the same method as that presented in the literature, with the exception of a coarser platelet model, which is introduced in 3.9.2.

3.3 Red Blood Cell Simulation Method – Spectrin-Link Method

A RBC is modeled as a deformable membrane in order to capture the complex behavior whereby an RBC deforms into various shapes under different flow conditions. The spectrin-link (SL) method is used for RBC membrane modeling [39, 67, 68]. The RBC model consists of points $\{\mathbf{x}_n, n \in 1 \dots N_v\}$, which are the vertices of the RBC surface triangulation. It is similar to the spectrin links found on real RBCs. Figure 3-2 shows the discretization of LB fluid nodes and SL RBC vertices.

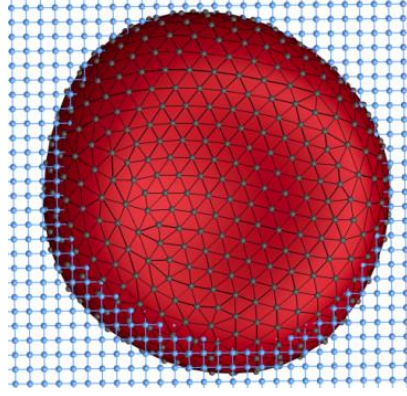


Figure 3-2. Discretization of fluid and solid phases [69]

The dynamics of each vertex are updated based on three forces, according to Newton's equations of motion via

$$\mathbf{v}_n = \frac{d\mathbf{x}_n}{dt}; \quad M \frac{d\mathbf{v}_n}{dt} = \mathbf{f}_n + \mathbf{f}_n^{\text{LB}} + \mathbf{f}_n^{\text{PP}} = \mathbf{f}_n^{\text{total}} \quad (3-8)$$

where M is the average amount of mass at each point, \mathbf{f}_n^{LB} is the force due to the fluid-solid coupling with the LB method, and \mathbf{f}_n^{PP} is the force due to particle interactions. \mathbf{f}_n is found by minimizing the Helmholtz free energy, $E\{\mathbf{x}_n\}$, of the RBC membrane as follows:

$$E\{\mathbf{x}_n\} = E_{\text{in-plane}} + E_{\text{bending}} + E_{\text{volume}} + E_{\text{area}}; \quad \mathbf{f}_n = -\frac{\partial E\{\mathbf{x}_n\}}{\partial \mathbf{x}_n} \quad (3-9)$$

The Helmholtz energy is calculated based on the temporal information and initial RBC mesh information, such as the vertex locations and angle between adjacent surfaces, RBC surface area and volume to match experimentally known RBC bending energy and in-plane energy while conserving the volume and surface area. More details follow in the next subsections.

3.3.1 Helmholtz Energy Calculation

The in-plane energy, $E_{\text{in-plane}}$, is related to shear properties, and is calculated as follows with contracting spring energy and expanding surface energy.

$$E_{\text{in-plane}} = \sum_{j \in 1 \dots N_s} U_s(l_j) + \sum_{k \in 1 \dots N_t} \frac{C_q}{A_k} \quad (3-10)$$

N_s is the number of links that connects two vertices as springs, N_t is the number of triangular surface elements, and A_k is area of the k th triangle. $U_s(l_j)$ is the spring energy where l_j is the length of the link j and $k_{\text{in-plane}}$ is the constant that is chosen to match the Capillary number.

$$U_s(l_j) = \frac{k_{\text{in-plane}} l_{\text{max}}}{4p} \frac{3x^2 - 2x^3}{1 - x} \quad (3-11)$$

l_{max} is the maximum spring extension, and p is the persistence length. $x = l/l_{\text{max}} \in (0,1)$ where l is the length of the spring. The spring energy that exerts purely attractive forces yields triangular area compression of each surface element. The second term of the in-plane energy produces triangular area expansion with the following equation.

$$C_q = \frac{\sqrt{3} A_0^{q+1} (4x_0^2 - 9x_0 + 6)}{4pql_{\text{max}}(1 - x_0)^2} \quad (3-12)$$

A_0 is $\sqrt{3} l_0^2/4$ where l_0 is the equilibrium link length, and $x_0 = l_0/l_{\text{max}} = 1/2.2$. Exponent q is set to 1 [67].

The bending energy takes into account the instantaneous angle between two adjacent triangles having the common edge j , as shown in the following equation.

$$E_{\text{bending}} = \sum_{j \in 1 \dots N_s} k_b [1 - \cos(\theta_j - \theta_0)] \quad (3-13)$$

k_b is the bending constant, θ_j and θ_0 are the instantaneous and spontaneous angles between two adjacent triangle elements sharing the edge j . The spontaneous angle θ_0 is set according to the total number of vertices N_v , as shown in the following equation [67].

$$\theta_0 = \cos^{-1} \left(\frac{\sqrt{3}(N_v - 2) - 5\pi}{\sqrt{3}(N_v - 2) - 3\pi} \right) \quad (3-14)$$

Volume energy takes into account the conservation of the volume of the RBC by comparing the instantaneous volume, V , to the desired volume, V_0 .

$$E_{\text{volume}} = \frac{k_v(V - V_0)^2}{2V_0} \quad (3-15)$$

k_v is the volume constant that is set to adjust the contribution of the volume energy compared to other energy values.

Area energy is similar to the volume energy calculation, but it considers the local energy conservation of each triangular element as well.

$$E_{\text{area}} = \frac{k_{aG}(A - A_0^G)^2}{2A_0^G} + \sum_{k \in 1 \dots N_t} \frac{k_{aL}(A_k - A_0^L)^2}{2A_0^L} \quad (3-16)$$

k_{aG} and k_{aL} are the global (total RBC) area and the local area constants, and A_0^G and A_0^L are the desired global area and local area. A is the instantaneous global area of the RBC, and A_k is the instantaneous area of the k -th triangular element.

3.3.2 Macroscopic Mechanical Properties Calculation

The behavior of the RBC membrane is calculated using the SL parameters and microscopic equations introduced in the previous section. The parameters also determine the macroscopic mechanical properties of RBC membrane, including shear modulus, Young's modulus, area compression modulus, and Poisson's ratio.

The shear modulus, G , of the RBC membrane is given as the following equation [39].

$$G = \frac{\sqrt{3}k_{in-plane}}{4pl_{max}x_0} \left(\frac{3}{4(1-x_0)^2} - 0.75 + 4x_0 + \frac{x_0}{2(1-x_0)^3} \right) \quad (3-17)$$

The elastic area compression modulus, K , is given as the following equation [67].

$$K = \frac{\sqrt{3}k_B T}{4pl_{max}(1-x_0)^2} \left[(q+0.5)(4x_0^2 - 9x_0 + 6) + \frac{1+2(1-x_0)^3}{1-x_0} \right] + k_{aG} + k_{aL} \quad (3-18)$$

Young's modulus, Y , is calculated using the membrane shear modulus and elastic area compression modulus as shown in the following equation.

$$Y = \frac{4KG}{K+G} \quad (3-19)$$

Poisson's ratio, ν , is given as the following equation.

$$\nu = \frac{K-G}{K+G} \quad (3-20)$$

In section 3.7, the mechanical properties of the RBC model calculated based on the presented equations are compared to experimentally measured property values in order to assure realistic RBC modeling.

3.3.3 Coarse Graining Method

A coarse graining method that allows the use of fewer vertices (~500) for a RBC model than are found on a real RBC (~30,000 vertices) has been developed by several researchers [67, 70]. The coarse graining method scales lengths based on the number of vertices in the fine model that is close to the real RBC and the number of vertices in the coarse model. The

superscript f denotes the fine model, and c denotes the coarse model in the following equations.

$$l_0^c = l_0^f \sqrt{\frac{N_v^f - 2}{N_v^c - 2}}, \quad l_{max}^c = l_{max}^f \sqrt{\frac{N_v^f - 2}{N_v^c - 2}} \quad (3-21)$$

The equilibrium length, l_0 , and the maximum spring extension length, l_{max} , are scaled using the number of vertices in the fine model N_v^f and in the coarse model N_v^c [67]. The persistence length, p , is scaled as the following equation.

$$p^c = p^f \frac{l_0^f}{l_0^c} = p^f \sqrt{\frac{N_v^c - 2}{N_v^f - 2}} \quad (3-22)$$

3.4 Fluid-Solid Coupling – Standard Bounce-back Method

The LBM based fluid model is coupled with particle models of blood cells using the standard bounce-back (SBB) boundary condition, which enforces the no-slip condition on surfaces by utilizing links to adjust the LB fluid particle distributions on link endpoints. The implementation of the SBB, the most common and simple of LB methods for no-slip conditions, is identical to that implemented by MacMeccan et al. [66].

The SBB method interpolates the force due to the bounce-back operation between the interior and exterior nodes onto the SL based RBC model. More details can be found in MacMeccan et al. [66] and Clausen et al. [71].

For a link in the i' direction, the particle distributions on link endpoints are adjusted as shown in the following equation.

$$f_i(\mathbf{x}, t + 1) = f_{i'}(\mathbf{x}, t^+) + 6\rho w_i \mathbf{u}_b \cdot \mathbf{e}_i \quad (3-23)$$

i' is the direction opposite of i , t^+ is the time after the collision but prior to the streaming process, and \mathbf{u}_b is the local solid velocity at the link intersection point, where the fluid links and RBC vertex links intersect.

i' is the direction normal and into the RBC membrane surface, and i is the direction normal to and out of the membrane surface. Momentum transfers of equal amount with opposite direction occur as shown in the following equation.

$$\mathbf{f}^b\left(\mathbf{x} + \frac{1}{2}\mathbf{e}_{i'}, t\right) = -2\mathbf{e}_i[f_{i'}(\mathbf{x}, t^+) + 3\rho w_i \mathbf{u}_b \cdot \mathbf{e}_i] \quad (3-24)$$

The force is linearly interpolated to the nearest vertices. The interior fluid nodes do not impact the dynamics of the rigid particles such as platelets. However, the SBB procedure occurs twice for each link between the internal and external LB fluid nodes, since SL based RBC models are filled with internal fluid.

As the fluid filled RBCs move through the LB fluid domain, the LB nodes are covered and uncovered by the domain inside the RBC membrane. In order to take into account the effects of the interior fluid viscosity for covering, the momentum of the particle is adjusted as shown in the following equation.

$$\mathbf{f}^c\left(\mathbf{x}, t + \frac{1}{2}\right) = \rho(\mathbf{x}, t)[\mathbf{u}(\mathbf{x}, t) - \mathbf{u}_b(\mathbf{x}, t)] \quad (3-25)$$

For the uncovering case, the sign of this force would change. For the SL based RBC, $\mathbf{f}^{LB} = \mathbf{f}^b + \mathbf{f}^c$.

3.5 Subgrid Modeling – Contact and Lubrication Model

When the gap between two solid surfaces, either from two particles or from a particle and a wall, becomes shorter than a lattice unit, the LB method fails to resolve the flow in the gap. In this case, subgrid modeling is required to capture the effects of contact forces. The contact and lubrication force model used in this work is similar to what is implemented and improved by Reasor et al. [39] and MacMeccan et al. [66] based on the original work of Ding and Aidun [72]. Details including the lubrication and contact force theories that are referenced can be found in the previous work.

A contact force that applies a short range exponential force prevents particles overlapping, as shown in the following equation.

$$d\tilde{\mathbf{f}}^{\text{contact}} = -\tilde{A}_c \exp\left(\frac{\tilde{g}_c - \tilde{g}}{\tilde{\sigma}_c}\right) \frac{\mathbf{e}_i}{\|\mathbf{e}_i\|} \text{ if } \tilde{g} \leq c_i \quad (3-26)$$

The variables normalized by the particle radius are denoted by a tilde. $\tilde{A}_c = 5$ is a contact force scaling constant, $\tilde{g}_c = 0.03$ is the specified cutoff gap, and \tilde{g} is the local gap distance. $\tilde{\sigma}_c = 0.005$ determines the range of contact force. The contact force is applied in the direction of the vector \mathbf{e}_i . c_i is the cutoff distance to apply the lubrication and contact force in the lattice direction.

The lubrication force is calculated as follows.

$$d\tilde{\mathbf{f}}^{\text{lub}} = \begin{cases} 0 & \text{if } c_i < \tilde{g} \\ -\frac{\bar{q}}{4\pi} \frac{\tilde{U}_{app}}{\tilde{\lambda}\tilde{g}^2} \mathbf{n}_{avg} & \text{if } \tilde{g}_c \leq \tilde{g} \leq c_i \\ -\frac{\bar{q}}{4\pi} \frac{\tilde{U}_{app}}{\tilde{\lambda}\tilde{g}_c^2} \mathbf{n}_{avg} & \text{if } \tilde{g} \leq \tilde{g}_c \end{cases} \quad (3-27)$$

$\bar{q} = 0.4$ is a fitting parameter that is determined experimentally [66]. \tilde{U}_{app} is the approach velocity of two surfaces, and λ is the curvature calculated based on the tangent vector of the surface and vectors connecting the surface element centroid to that of neighboring elements. The parameters presented employed the same values as were used in the previous work [39].

After both lubrication and contact forces are calculated following the above equations, force values that are exceptionally large and, therefore, not realistic were set to the maximum force value allowed in order to prevent stability problems from arising. The maximum force value was set to 1.0 in the previous work [39]. The sum of the final lubrication and contact forces is the particle-particle interaction force, \mathbf{f}^{PP} , that appears on the equation for the update of RBC model vertices.

3.6 Simulation Domain – Boundary Conditions

No-slip boundary conditions are used for the channel walls that are modeled as rigid. Periodic boundary conditions are used for the inlet and outlet so that the computational domain can be reduced, avoiding the use of an extremely long vessel and continuous seeding of blood cells at the inlet. A schematic of the simulation domain of rectangular and circular channels is shown in Figure 3-3.

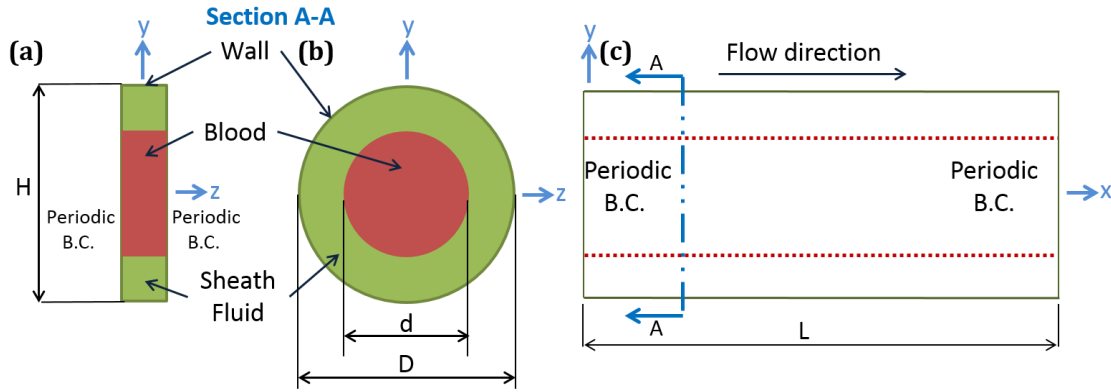


Figure 3-3. Schematic of simulation domain (a) cross-section of a rectangular channel (b) cross-section of a circular channel (c) front-view

Figure 3-3 (c) shows the front-view of the simulation domain in the flow direction. To study non-uniform suspension flow, the blood cells are initially populated in the center. The inlet and outlet are marked with periodic boundary conditions. Circular channel walls are treated with no-slip boundary conditions. The top and bottom walls of rectangular channels are also treated with no-slip boundary conditions. A cross-section view is shown in Figure 3-3 (a) and (b), which are views of the cut-section A-A in Figure 3-3 (c). For the rectangular channel, the z-direction (the vorticity direction) is also treated with periodic boundary conditions to reduce the computational domain. Thus, the rectangular channel case simulates an infinitely wide microfluidic channel with no side wall effect on the vorticity direction (z-direction). Because the blood cell movement in that direction is not of interest, the minimum length that will allow 2~3 RBCs is used (2.7 RBC diameter). The flow direction domain length, L , is set to $40 \mu\text{m}$, and the validity of this length value is studied in the following validation section.

3.7 RBC Model Creation

SL based RBC modeling has been studied by several researchers [39, 73-81], and different strategies for the initial triangulation of biconcave RBCs are introduced. One strategy

is to take the average geometry of healthy RBCs and mesh the membrane accordingly, and another strategy is to start from a meshed sphere and deflate it to the average RBC volume while minimizing the Helmholtz free energy to find the equilibrium shape. Another strategy is to start from the average shape of RBCs, and go through the energy relaxation process while allowing the vertex movements. Depending on the strategy and parameter values of the Helmholtz energy calculation used to find the initial RBC mesh, the shapes of the RBCs can vary. Although the bending energy, κ_b , is reported as $2.2 \pm 0.3E - 19$ J [82], which corresponds to a $k_{\text{bending}} = 200k_B T$ where k_B is Boltzmann's constant and T is temperature, different researchers have found values of k_{bending} from $200k_B T$ to $4000k_B T$ that yield the stable biconcave RBC shape. In the study of Aidun et al., because LBM is independent of temperature, $k_{\text{in-plane}}$ is set to $k_B T$ and chosen to match the capillary number, which is the most important non-dimensional number for studying blood rheology. The capillary number represents the ratio of forces due to viscous fluid motion to the elasticity of the RBC membrane. Other parameters are chosen arbitrarily, such that $E_{\text{volume}} > E_{\text{area}} > E_{\text{in-plane}} > E_{\text{bending}}$, similar to Dupin et al. [80], while area and volume are conserved and stable RBC shape is close to the real biconcave RBC shape.

In this study, coarser models of RBCs are created in order to reduce the computational cost for simulating dense suspensions. The new models have 492 nodes, compared to the previously used RBC model [39], which had 613 nodes. Also, the coarse graining method of the RBC model was updated from the version of Pivikin [78] to Fedosov [75], as was explained in section 3.3. The first RBC model was created with the fluid LB resolution of 3 lattice units per 1 micron ($3\text{lu}/\mu\text{m}$), and the second model was updated to the coarser fluid resolution of $2.5\text{lu}/\mu\text{m}$. RBC properties were also updated to yield behaviors that are closer to the experimental

results reported in the literature. Validation results that compare the RBC model to the experimental results are presented in the next section.

The RBCs are created by deflating a sphere to the target volume and size while minimizing the Helmholtz free energy. During the deflation process, the desired volume, $V_{\text{desired}}(t)$, was changed in each time step, as shown in the following equation.

$$V_{\text{desired}}(t) = V(0) + \frac{t}{t_{\text{defl}}} [V_{\text{target}} - V(0)] \quad (3-28)$$

$V_{\text{desired}}(t)$ is used as V_0 for the volume energy calculation. The initial volume, $V(0)$, is the volume of the sphere, and t_{defl} is the duration that the deflation occurs, which was 20,000 simulation time steps in this study. After the deflation time step of 20,000, the energy minimization process continued with $V_{\text{desired}}(t) = V_{\text{target}}$ until the equilibrium was reached. The shape change of the RBC model during the deflation process is shown in Figure 3-4.

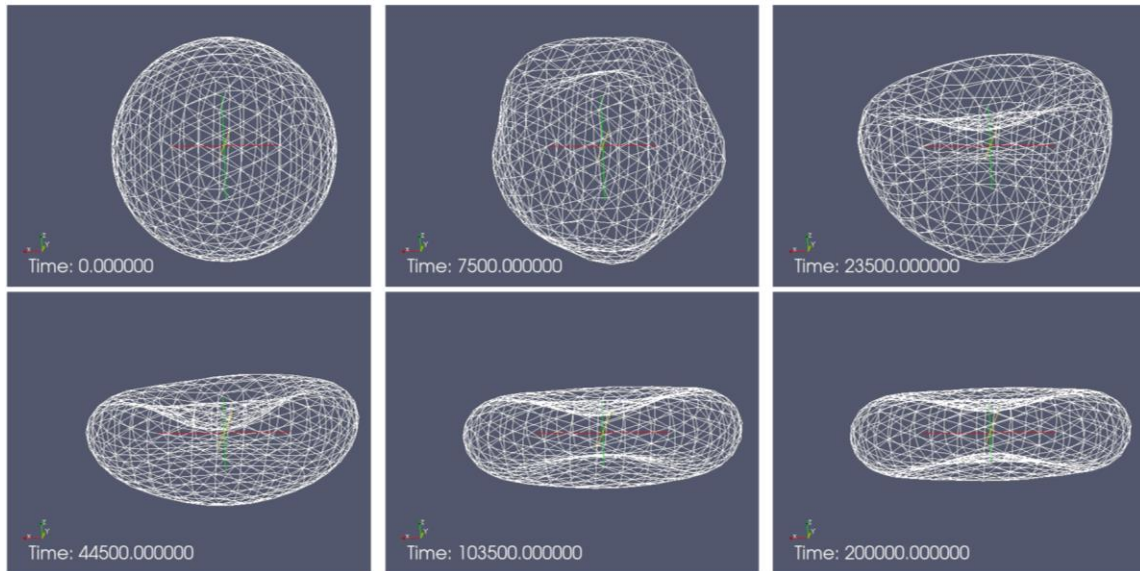


Figure 3-4. The shape change of RBC model during the deflation process

The equilibrium RBC shapes are compared to the analytically known RBC shape as shown in Figure 3-5.

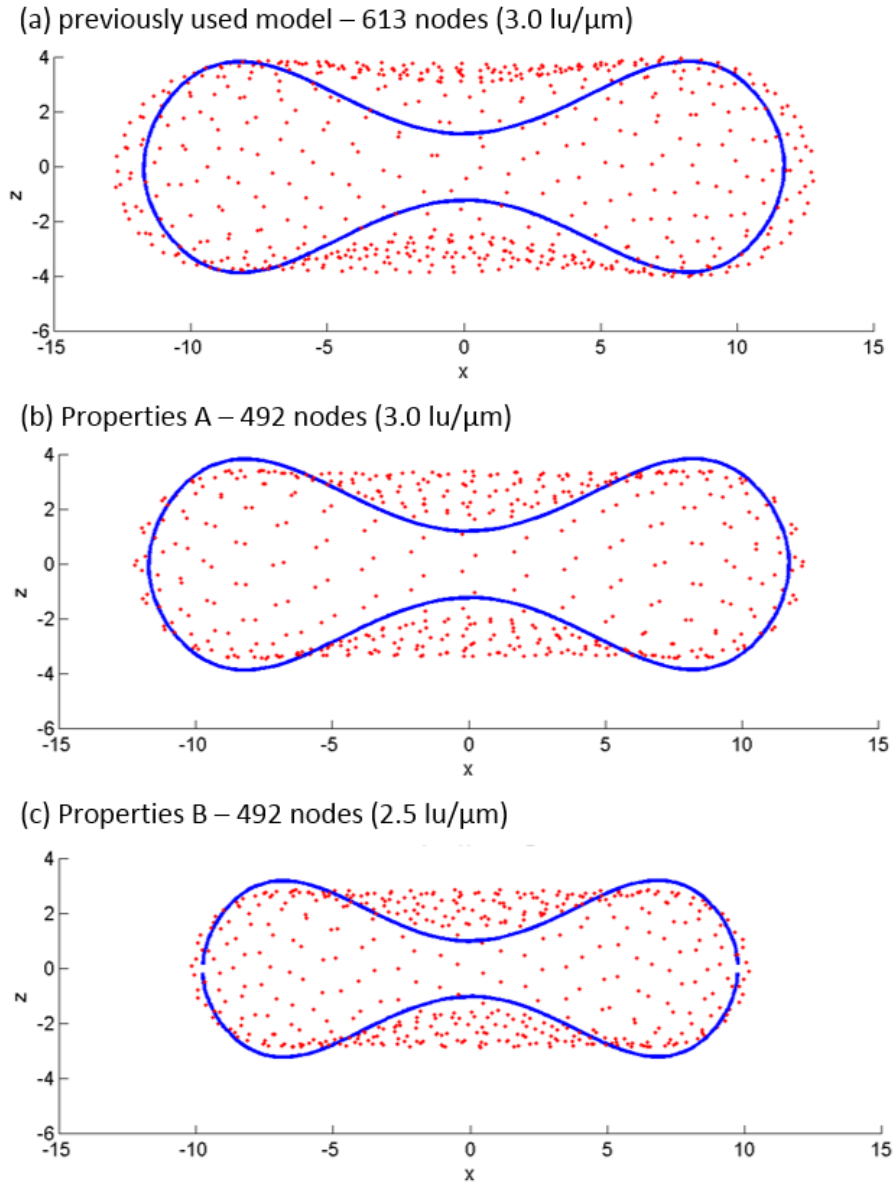


Figure 3-5. Side view of RBC models (red) in comparison to analytical RBC shape (blue)

Neither the number of nodes on the RBC nor the fluid resolution greatly affect the RBC behavior as long as the minimum resolution is provided. However, parameter values change RBC properties and do affect the behavior of RBCs as shown in Figure 3-5. The new RBC models with

updated parameters are closer to the analytical RBC shape, especially in the central concave region. The axis in the figure is in the lattice unit, so RBC B with lower resolution is smaller than the other two RBCs.

The change of the Helmholtz energy, volume, and area during the RBC creation process with parameters B and 2.5 μm resolution is plotted in Figure 3-6.

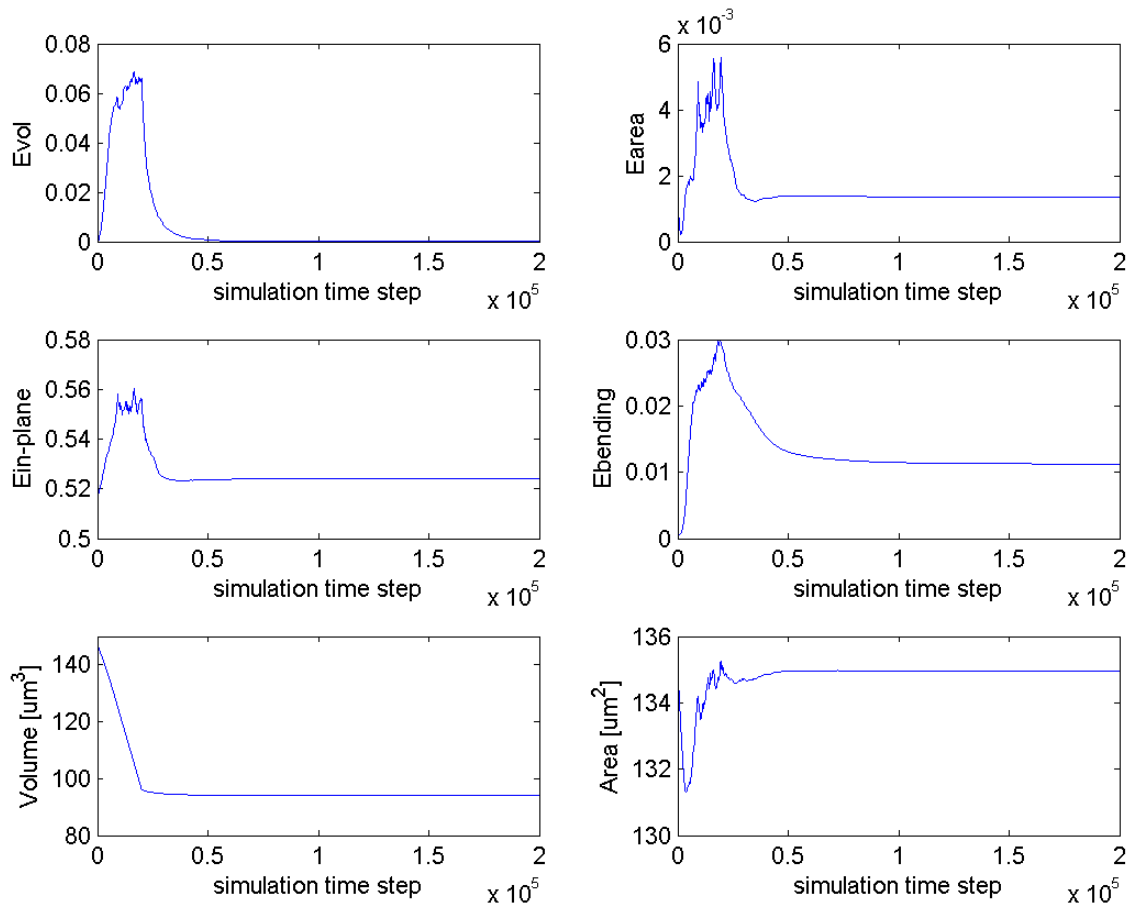


Figure 3-6. Helmholtz energy, volume, and area change during RBC creation process

The values of Helmholtz energy in Figure 3-6 are plotted without units, as was calculated in the simulation, and only the change in relative magnitude needs to be noted. The plot shows that the equilibrium shape is reached at time step of 200,000. Similar results were obtained for the

RBC creation with properties B and 3 lu/ μm resolution; the equilibrium volumes and areas of the two RBC models are shown in Table 3-1.

Table 3-1. Equilibrium volume and area of the two RBCs

| | $V_{eq} [\mu\text{m}^3]$ | $A_{eq} [\mu\text{m}^2]$ |
|---------------------|--------------------------|--------------------------|
| Parameters A | 94.037 | 134.88 |
| Parameters B | 93.996 | 134.97 |

The surface area and volume of a real RBC are assumed to be $135 \mu\text{m}^2$ and $94 \mu\text{m}^3$ with $7.80 \mu\text{m}$ diameter, based on the experimental study that measured the shape of a healthy RBC [83]; the size of the sphere is matched to have the same surface area as a real RBC. The parameter values used for the creation of RBC models are $k_{aL} = 100k_{in-plane}$, $k_v = 120000k_{in-plane}$, $N_v^f = 27344$, and $p^f = 18.7\text{nm}$. The parameter values, which are different for the two RBC models, are listed in Table 3-2.

Table 3-2. Parameter values of the two RBCs

| | $\frac{k_{bending}}{k_{in-plane}}$ | $\frac{k_{aG}}{k_{in-plane}}$ | $l_0^f [\text{nm}]$ | $V_{target} [\mu\text{m}^3]$ | $A_{target} [\mu\text{m}^2]$ |
|---------------------|------------------------------------|-------------------------------|---------------------|------------------------------|------------------------------|
| Parameters A | 1140 | 7400 | 75.5 | 94.00 | 135.78 |
| Parameters B | 800 | 9900 | 90.6 | 93.952 | 132.88 |

A_{target} is used as A_0^G during the deflation process for the area energy calculation. The target volume and area value used in the deflation process are not the same as those of a real RBC, because equilibrium is reached where the sum of the four energy terms is minimized, including the bending energy and in-plane energy, and final equilibrium area and volume are not exactly the same as the target values. Thus, the target values were set with some offset based on experience to equilibrate with desired area and volume close to the real RBC area and volume.

LBM is independent of temperature, and $T = 300\text{K}$ is assumed for the RBC property calculation. The corresponding mechanical properties of RBC models are listed in Table 3-3.

Table 3-3. Mechanical properties of the two RBCs

| | G [$\mu\text{N/m}$] | K [$\mu\text{N/m}$] | Y [$\mu\text{N/m}$] | ν |
|---------------------|-------------------------|-------------------------|-------------------------|-------|
| Parameters A | 6.34 | 292.26 | 24.81 | 0.958 |
| Parameters B | 5.28 | 269.44 | 20.72 | 0.962 |

Shear modulus, G , is the most important property for characterizing RBC deformation, and it affects the rheology. The shear modulus of the modeled RBCs is close to the experimentally measured shear modulus of RBC, which is in the range of $4\sim 12\mu\text{N/m}$ [84, 85]. Validation results of these new RBC parameters are presented in section 3.9.

3.8 Initial Seeding of Blood Cells in Dense Suspension Flow

The initial positions of blood cells were generated using a method similar to that used in previous studies [39, 66, 86]. This method generates random locations and orientations of particles in the domain at specified distances away from one another. Then, the particles are grown from much smaller size to about 105% of the particle sizes while allowing for strong particle-particle forces. During the growth, all of the particles are treated as rigid particles.

During the initial random location generation, only one type of particle can be used. Two different approaches can be taken to specify which particles are RBCs and which are platelets. One method is to seed the total number of particles in the whole domain as RBCs, and then change some of the particle information to platelet information. In this case, platelets and RBCs should be carefully chosen in order to have a good distribution over a cross-section for

both types and to avoid the situation where all the platelets are located in the bottom half or top half. Another method is to generate seeding separately in smaller domains. For example, for the case in which 100 RBCs and 10 platelets are flowing in a 100 lattice unit length channel, 100 RBCs' locations are generated in a separate 84 lu channel, and 10 platelet locations are generated in a separate 4 lu channel. Then, the two separately generated sets of particle information can be merged with the platelet locations translated over a distance of about 90 lus in the flow direction. Screenshots of the initial seeding of RBCs and platelets before growth are shown in Figure 3-7.

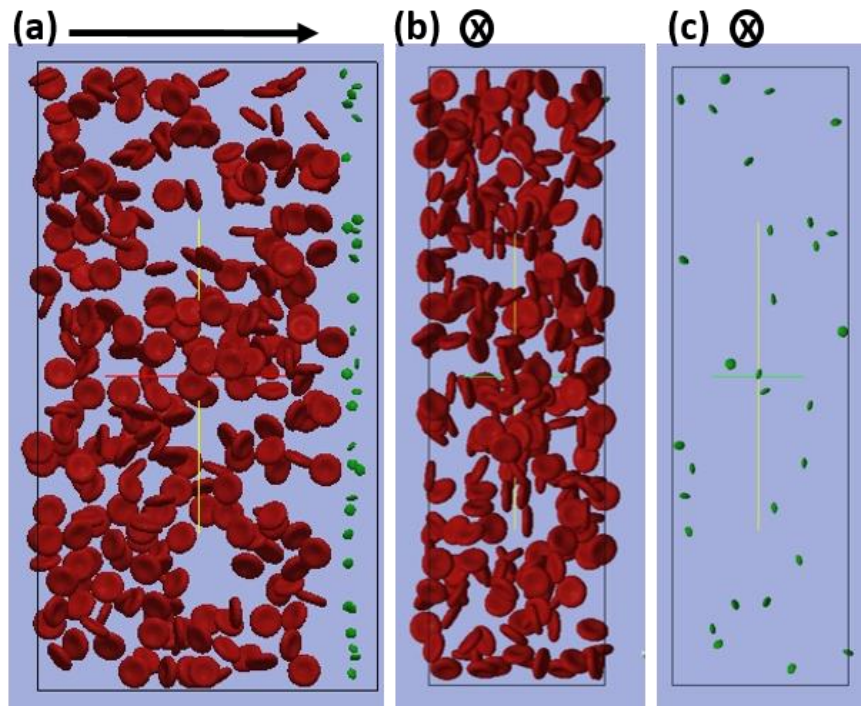


Figure 3-7. Initial random location generation: (a) flow direction view of the whole channel (b) cross-section view of RBCs (c) cross-section view of platelets

In Figure 3-7 (a), the flow direction is from left to the right. Because this random location is generated for a very dense suspension case (40% HCT), about 20% sized particles are used. Figure 3-7 (b) and (c) show that both RBCs and platelets are well distributed in the cross section.

To grow particles to full size from the initially generated locations as shown in Figure 3-7, two different approaches can be taken. One is to grow the particles over a long period of time (about 20,000 simulation timesteps) with the hope of successfully growing the particle to the full 105% size in one trial, since such slow growth will avoid particle overlapping. Should particles overlap and the simulation crash, the growing should be redone until it is successful. Another strategy is to plan several short cases with different growth rates based on the initial size of the particle for each case. An example of such a strategy is shown in Table 3-4.

Table 3-4. Example growth plan for 2078 RBCs and 138 platelets with 40% HCT

| | Growth 1 | Growth 2 | Growth 3 |
|------------------------------|-----------------|-----------------|-----------------|
| Restart File Timestep | - | 1600 | 800 |
| Initial Size | 0.15 | 0.8 | 0.92 |
| Growth Time | 2000 | 1500 | 1500 |
| Crash Timestep | 1708 | 961 | Success! |
| Size @ Crash | 0.8691 | 0.936 | - |

Initially, 15% sized particles are were used to grow to 105% size in 2000 timesteps. Because such a fast growth rate was used, the simulation crashed at timestep 1708 when the particles reached 86.91% size. Then, at the timestep 1600, the particle locations were taken as the initial positions of particles for the second growth with the initial size of 80%. In this case, only 25% more growth was required during 1500 timesteps, so the growth rate was much slower than the first case. This case required a total of 3 growth phases with a total of 5000 time steps until the particles successfully grew to the full 105% size. Because the particle overlapping usually occurs when the particles have grown above 80%, using fast growth rate initially, and then reducing the growth rate for the following growth trials can reduce the total simulation cost for seeding. In this study, the second approach was mostly used except for a few initial cases.

3.9 Validation

3.9.1 Isolated RBC

The new RBC models were validated by comparing simulation results to two common isolated RBC experiments used to validate a RBC model [39, 67, 76, 87]. The first of these is the parachuting experiment, whose result measure the RBC's axial length and diameter during flow through a $9.3\ \mu\text{m}$ pipe [88]. When a RBC with diameter of $8.185\ \mu\text{m}$ flows through such a small pipe, it deforms to a parachuting shape as shown in Figure 3-8.

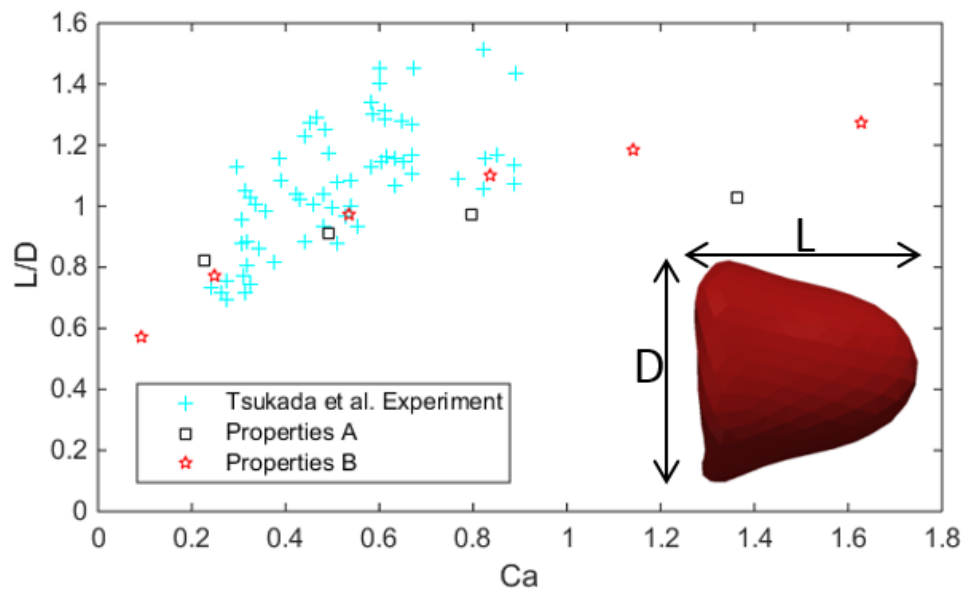


Figure 3-8. Deformation index vs. Capillary number for a RBC flowing through a $9.3\ \mu\text{m}$ pipe

It shows the deformation index that measures the ratio of length and diameter plotted against capillary number. The experimental results were available with flow velocity only, so this was converted to capillary number with an assumed RBC shear modulus of $5.28\ \mu\text{N/m}$. The simulation results with the two new RBC properties are in the lower end of the experimental results, and the results with properties B match the experimental results better.

The second validation simulations compare simulation results to optical tweezer experiments that stretch a RBC with different forces and measure the axial and transverse length [89]. Figure 3-9 shows a stretched RBC and the simulation results in comparison to the experimental results.

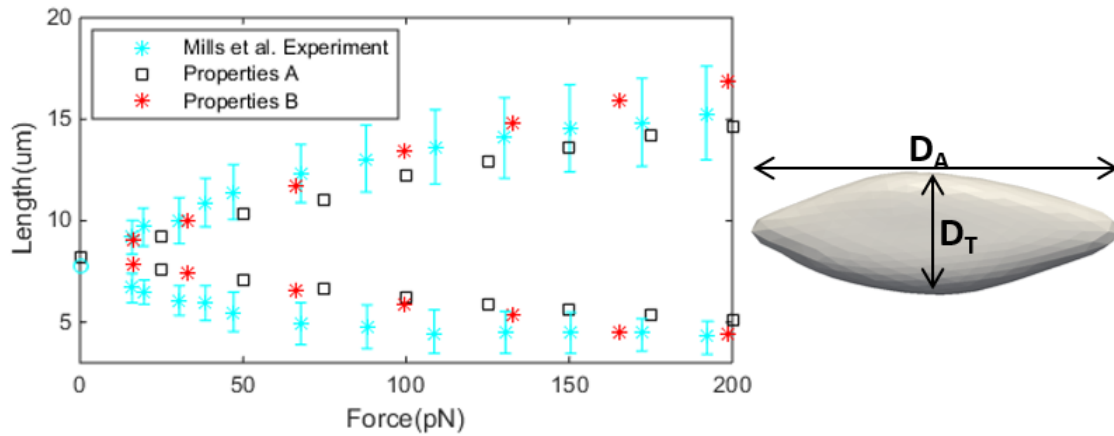


Figure 3-9. Tweezer simulation results and a stretched RBC

It shows that the simulation results generally match well with experiment results.

Based on the two validation results, the RBC model with properties B is used for further simulations.

3.9.2 Isolated Platelet

Platelets are modeled as rigid ellipsoids with major axis diameters of $2.8\mu\text{m}$ and a minor axis diameter of $1.3\mu\text{m}$. 90 nodes are used, in contrast to previously used 142 nodes [86, 90, 91], in order to reduce the computational cost. Figure 3-10 shows the new platelet model with the new RBC model.

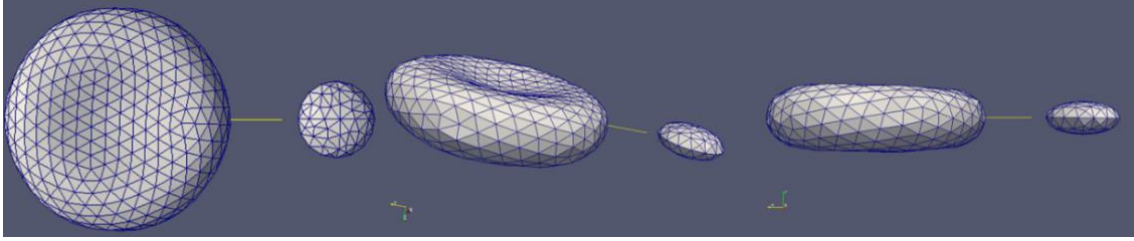


Figure 3-10. New platelet model with the new RBC B in 2.5 μm resolution

The new platelet model was validated by comparing the simulation results of the platelet in a simple shear to the Jeffery's analytical solution of a solid ellipsoid in a simple shear [92]. The boundary of the ellipsoid is given by the following equation.

$$\frac{x^2}{a^2} + \frac{y^2}{a^2} + \frac{z^2}{b^2} = 1 \quad (3-29)$$

When one of the principal axes is aligned with the vorticity direction as shown in Figure 3-11,

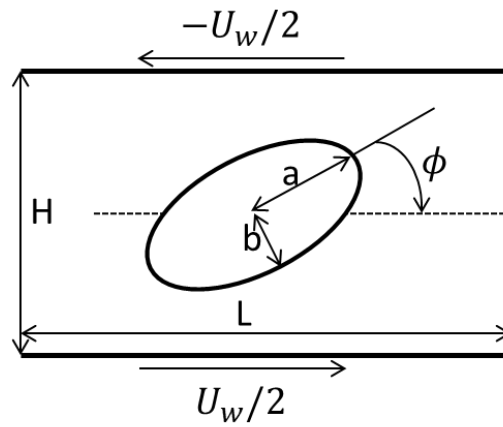


Figure 3-11. A ellipsoid aligned with the vorticity direction and immersed in simple shear flow
the rotation angle, ϕ , and the angular rate of rotation, $\frac{\partial\phi}{\partial t}$, of the ellipsoid in the simple shear flow with the shear rate, $\dot{\gamma}$, can be analytically solved as shown in the following equation.

$$\phi = \tan^{-1} \left(\frac{b}{a} \tan \frac{ab\dot{\gamma}t}{a^2 + b^2} \right) \quad (3-30)$$

$$\frac{\partial \phi}{\partial t} = \frac{\dot{\gamma}}{a^2 + b^2} (b^2 \cos^2 \phi + a^2 \sin^2 \phi) \quad (3-31)$$

In the validation simulation, the computational domain was $36 \times 36 \times 18$ lattice nodes, and the particle Reynolds number, $Re_p = \dot{\gamma}(2a)^2/\nu$, was 0.064. The angle and the angular velocity over time are plotted in Figure 3-12.

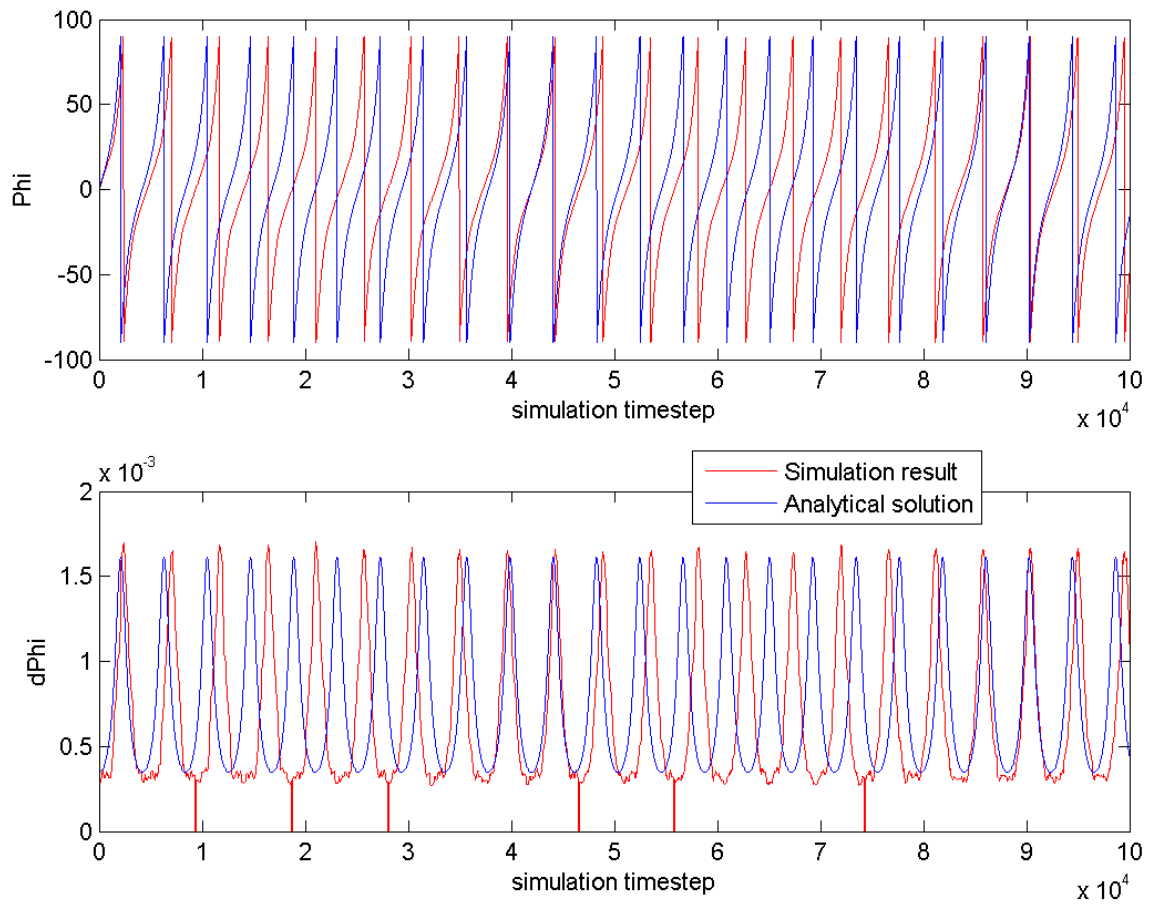


Figure 3-12. Angle and angular velocity of the platelet over time in comparison to Jeffery's solution

A close-up view of the plot is shown in Figure 3-13.

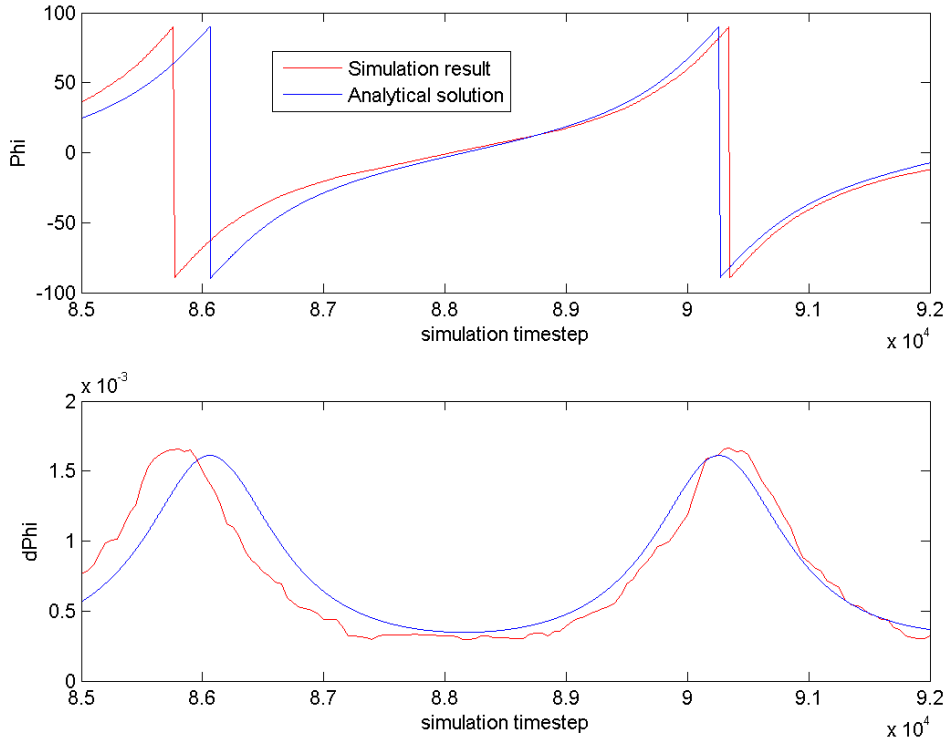


Figure 3-13. Angle and angular velocity of the platelet over time in comparison to Jeffery’s solution (close-up view)

The plot shows that the simulation result and Jeffery’s analytical solution generally match, although there is some offset. This is due to the coarse meshing of the platelet model. A perfect ellipsoid with the same dimension as the platelet model ($2.8 \times 2.8 \times 1.3 \mu\text{m}$) would have $5.3 \mu\text{m}^3$ volume, but the coarse meshed platelet model volume is $4.9 \mu\text{m}^3$. Considering the difference between the model and a perfect ellipsoid, the results show that the no-slip boundary condition and the dynamics of the platelet model are satisfied.

3.9.3 Domain Size

As was mentioned in section 3.6, periodic boundary conditions are used in the flow direction in order to reduce the computational cost. With the periodic boundary condition applied at the inlet and outlet, the blood cells that pass through the outlet will appear in the inlet and continue the simulation. If the domain length in the flow direction is too short, the

simulation result may not reflect reality. Thus, the simulation domain should be longer than the diameter of several particles, although a minimum length is preferred to reduce the simulation cost. The domain length of 40 μm has been commonly used in previous studies, with the LB fluid resolution of 3.0 $\text{lu}/\mu\text{m}$. The logic behind the choice of the channel length is that with the domain of 120 lu and particle velocity slower than 0.05 $\text{lu}/\text{timestep}$, the channel length is long enough to diminish the effect of periodicity. The same 40 μm and 80 μm lengths have been studied and compared with the new 2.5 $\text{lu}/\mu\text{m}$ resolution in order to confirm the validity of the channel length. Screenshots of the simulation domains of the two cases are shown in Figure 3-3.

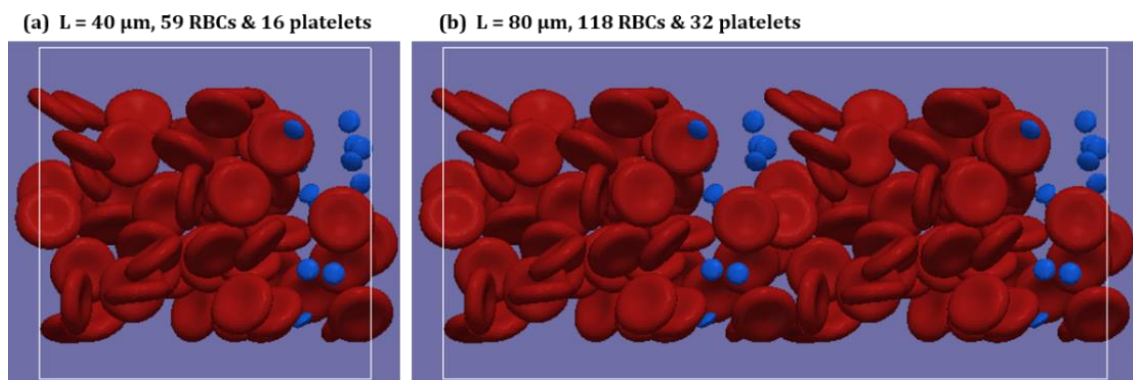


Figure 3-14. Simulation domains with two different domain lengths in the flow direction

The white box is the simulation domain, and the flow is from left to right. The channel has no-slip boundary conditions on the top and bottom walls. In the vorticity direction, the domain size is set to 21.6 μm , which is the same as 2.62 RBC diameters. RBCs and platelets are colored in red and blue, respectively. The blood cells are flowing in a rectangular channel of 40 μm height, with 32 μm initial blood stream height in the center, with 20% hematocrit. Figure 3-3 (b) has the double channel length, and RBCs and platelets in 40 μm length were copied twice in the 80 μm length case in order to start the simulations with exactly the same distribution of the cells.

Thus, the number of cells was also doubled. The results of the two cases were plotted as shown in Figure 3-15.

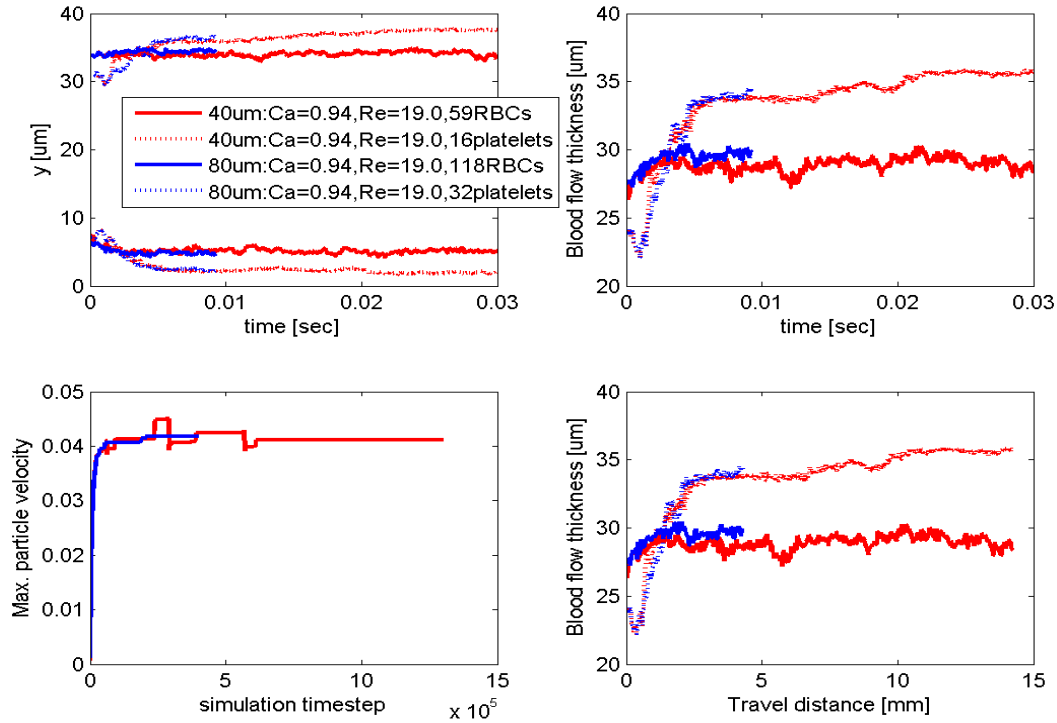


Figure 3-15. Blood cell migration behavior results with two different domain lengths

RBC results are plotted in solid line, and platelet results are plotted in dotted lines. Red is used for the 40 μm length case (a), and blue is used for the 80 μm length case (b). The top left plot shows the height of maximum and minimum blood cells over time. It visualizes how the blood stream thickness varies over time. The top right plot shows the evolution of the blood stream thickness, which is the difference between maximum and minimum heights shown in the top left plot. The bottom left plot shows the maximum particle velocity for each simulation time step. The travel distance was calculated by integrating the average particle velocity over time. The blood flow thickness change over travel distance is plotted in the bottom right. The results are almost identical for the two cases for both RBCs and platelets, proving that 40 μm is long enough. Thus, further studies used the 40 μm flow direction channel length.

3.9.4 Subgrid Modeling – Effect of Contact and Lubrication Parameters

As was mentioned in section 3.5, subgrid modeling is used when the gap between two solid surfaces becomes shorter than a lattice unit. Because of the frequent use of subgrid modeling and crashes in the simulation for dense suspension cases, special attention was given to study the effect of the subgrid modeling parameters on the blood cell migration behavior.

The contact and lubrication model ensures that the particles do not overlap and that they flow as closely to real flow as possible based on contact and lubrication force theories. However, stability issues were noted from earlier studies, especially in dense suspensions [69, 93], and these include severe cases that cause simulations to crash. Many different strategies were used in order to mitigate the issue, such as changing the contact force for a while, and results showed that the flow behavior was not affected because the parameter change was local. For 20% hematocrit cases, manually changing some of the parameters can sufficiently handle the stability issue. However, for 40% cases, this becomes very demanding due to the increased instability caused by the densely packed particles. Hence, the means for addressing such instability is critical.

In this study, when stability issues arose during the simulation, the system automatically changed the maximum value of allowable lubrication and contact force that still avoids application of exceptionally large forces. In previous studies, the maximum value was set to 1.0 in the simulation. In this study, the maximum value varied between 0.1 and 1.0, and mostly, values between 0.3 and 0.7 were used. Occasionally, the fitting parameter, $\bar{q} = 0.4$, was changed to $\bar{q} = 0.3$. This strategy allowed the simulation to run without excessive crashing. However, it is important to determine whether or not this approach had a significant effect on

the results. The effect of the parameter adjustment was studied by comparing the following three different cases:

- start with the maximum value (lubForceMax) of 0.6, then change to 0.3 at simulation time step of 5000. $\bar{q} = 0.4$
- start with the maximum value (lubForceMax)=0.6, and $\bar{q} = 0.4$
- start with the maximum value (lubForceMax)=0.6, and $\bar{q} = 0.3$.

The results of the three different cases when 958 RBCs and 64 platelets flow in 120 μm diameter channel with the initial blood stream diameter of 84.7 μm are shown in Figure 3-16.

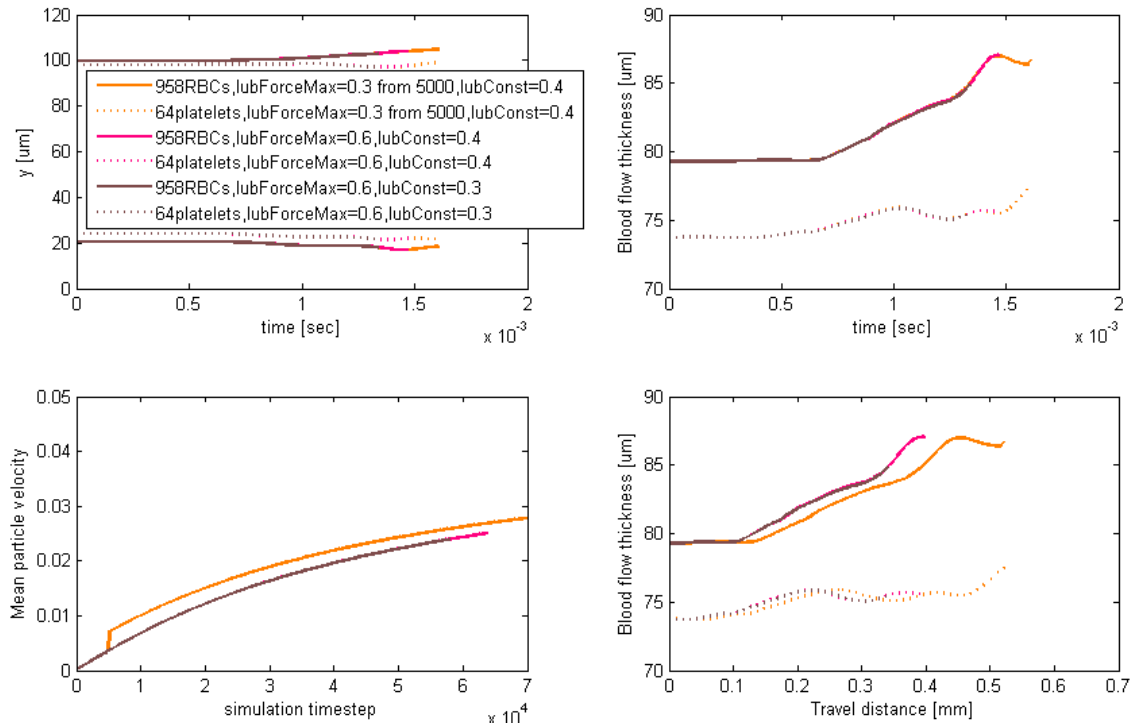


Figure 3-16. Blood cell migration behavior flowing in 120 μm diameter channel with the initial blood stream diameter of 84.7 μm for three different contact and lubrication parameter values

RBC flow results are plotted in solid lines, and platelet flow results are plotted in dotted lines.

The top left plot shows the height of maximum and minimum blood cells over time. It visualizes how the blood stream thickness varies over time. The top right plot shows the evolution of the

blood stream thickness, which is the difference between maximum and minimum heights shown in the top left plot. The bottom left plot shows the average particle velocity for each simulation time step. By integrating the average particle velocity over time, the travel distance is calculated. The blood flow thickness change over travel distance is plotted in the bottom right. The results show that there is little difference between the three different cases except for the small increase in the particle velocity when the parameter value is changed at timestep of 5000. The average trajectory of the particles is plotted over the travel distance as shown in Figure 3-17.

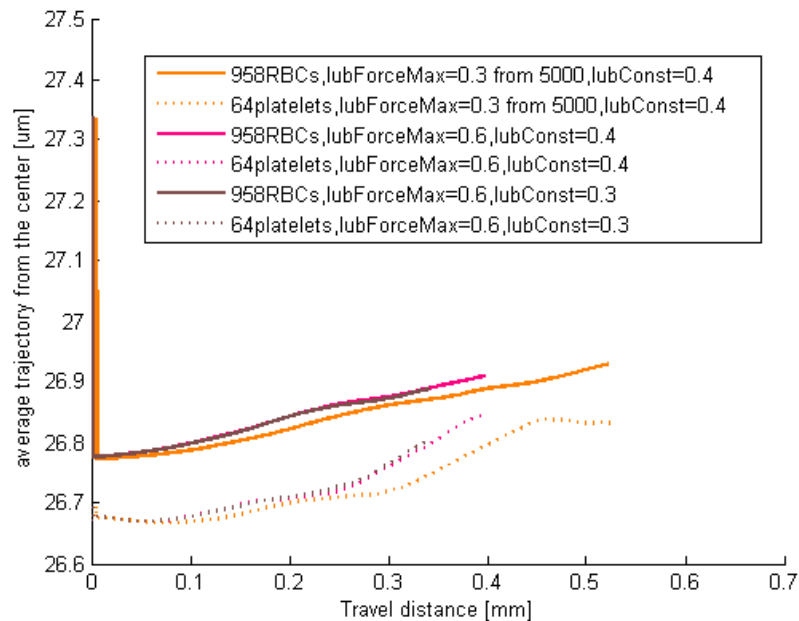


Figure 3-17. Average trajectory of blood cells flowing in 120 μm diameter channel with the initial blood stream diameter of 84.7 μm for three different contact and lubrication parameter values

The average distance from the center is the average of all the blood cells at the timestep. It shows that when the parameter changed, the RBCs were suddenly moved in the radial direction towards the wall. However, this is a local effect, and the plot shows that the cells would go back to the original location, and continue the normal trend. Because the contact and lubrication model is used only when particles are closer than one lattice unit, and many different

combinations lead to the same flow behavior as shown; such parameter adjustment is acceptable and necessary for dense suspension studies. When the parameters are adjusted, careful analysis is required to exclude the peak values that result from the parameter change, which mitigates the stability issues while not affecting the flow behavior.

3.9.5 Cell Migration in Non-uniform Suspension Flows

The use of the finalized RBC models coupled with LBM for the study of non-uniform suspension flow was validated by comparing the simulation results to the published experimental results on RBC diffusivity in non-uniform suspension flows.

One of a very few studies considered down-gradient diffusion in non-uniform suspensions of RBCs [40]. They studied the spreading of a stream of blood cells in channel flow, as shown in Figure 3-18, using dilute to semi-dilute (~30%) RBC suspensions in channels of $0.491 \times 0.053 \times 600\text{mm}$ or similar other dimensions.

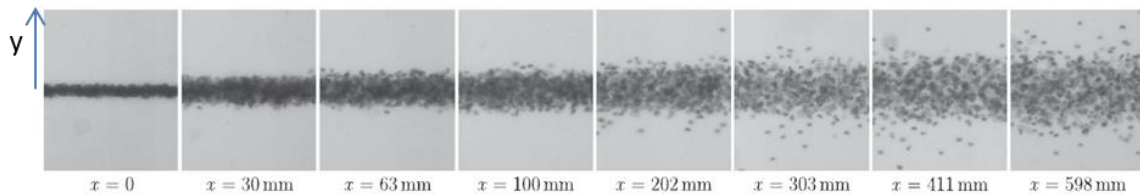


Figure 3-18. RBC diffusion in a flat channel with 15% hematocrit blood stream and PBS solution [40]

The flow is in the x-direction, and RBC spreading is shown in the y-direction (width) in Figure 3-18. This spreading of a stream of blood cells in channel flow is characterized by the subdiffusive behavior with exponent $1/3$. This phenomenon is expected to be generic to systems in which shear-advected particles undergo short-range pairwise hydrodynamic

interactions or collisions. The concentration profile in four sections of the channel is shown in Figure 3-19 (a).

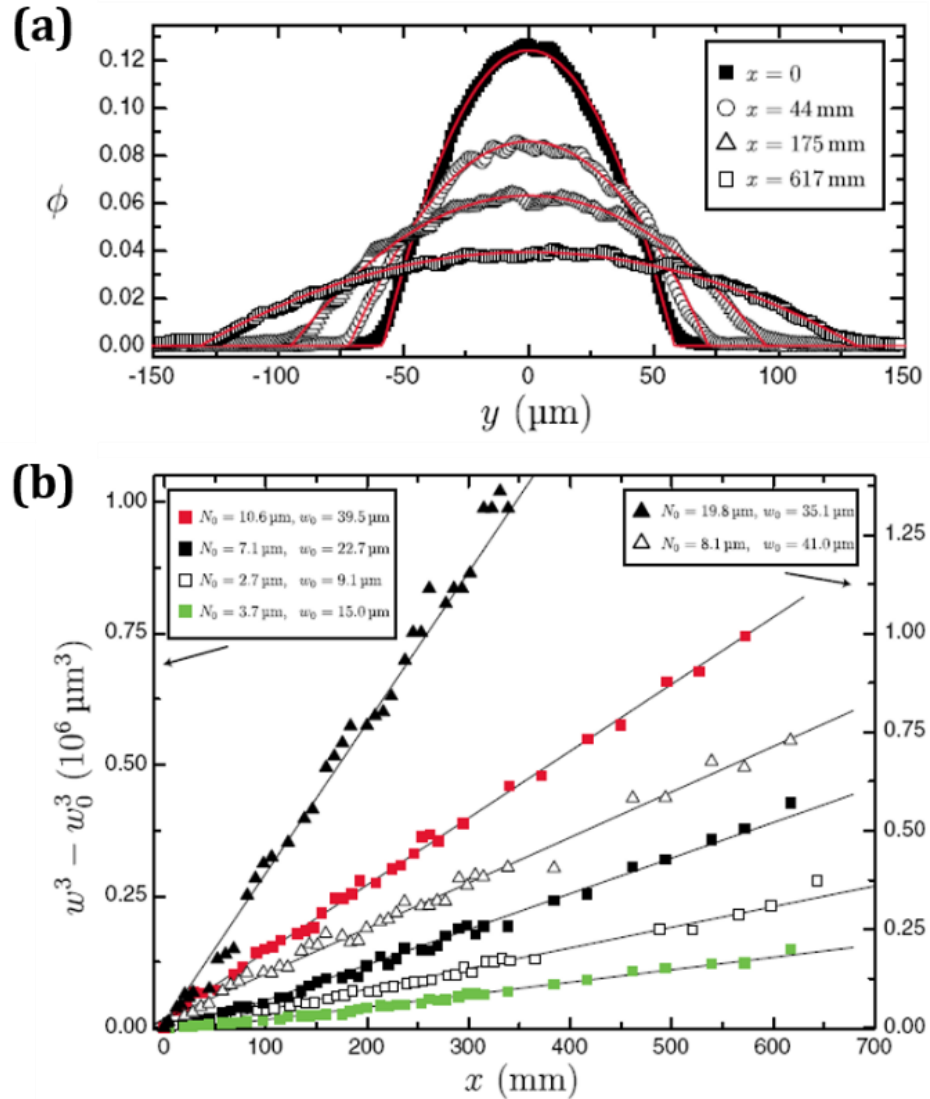


Figure 3-19. (a) Concentration profile in four sections of a flat channel, (b) Clouds half-width w along the channel for several different conditions and for two different thicknesses (empty symbols: $2h=53\mu\text{m}$, full symbols: $2h=101\mu\text{m}$) [40]

Based on the subdiffusive behavior with exponent 1/3, the blood stream half-width, w , at half-height of the RBC cloud is expected to increase according to the following equation with the initial half-width, w_0 .

$$w(x)^3 - w_0^3 = Ax = \frac{27f_3R^2N_0}{8\sqrt{2}h}x \quad (3-32)$$

f_3 is the dimensionless diffusivity in the width direction (y-direction), R is the particle characteristic size, $N_0 = \int \phi(x, y)dy$ is the conserved number of particles (with the unit of length) where ϕ is hematocrit, and h is the channel depth (z-direction). Figure 3-19. (b) plots $w(x)^3 - w_0^3$ over flow distance, x , for several different experimental conditions with different initial blood stream conditions (hematocrit and blood stream thickness) and channel dimensions. This display shows the linear relationship (as expected from the above equation), and based on the slope, A , the dimensionless diffusivity of RBCs is calculated. With $2R = 7.2\mu\text{m}$, $\phi = 0.16$, and effective hematocrit $\phi_{eff} = \frac{\phi V_e}{V}$ based on the assumption that effective occupied volume of RBC, $V_e = 4\pi R^3/3$, is much larger than the actual RBC volume, V , due to the tumbling, $f_3 = 0.05$ is found for RBCs. In order to compare this simulation to the experimental results, two cases were studied with channel depth of $2h = 53\mu\text{m}$ and width of $491\mu\text{m}$ with the simulation conditions as listed in Table 3-5.

Table 3-5. Initial seeding conditions of simulations

| | Initial seeding width | Initial seeding HCT, ϕ | N_0 | No. RBC |
|--------------------|-----------------------|-----------------------------|--------------------|---------|
| Case A - Δ | 82 μm | 0.099 | 8.11 μm | 183 |
| Case B - \square | 18.2 μm | 0.148 | 2.69 μm | 91 |

The two cases are comparable to the empty triangle and rectangle cases in Figure 3-19 (b). Simulation conditions were set to be as close to the experimental study as possible by matching N_0 and using the same initial seeding width as $2w_0$ of the experiments. The initial seeding width is the channel width used to seed and grow RBC particles for generating initial RBC locations. Then, the RBC locations are translated in the y-direction to position them in the

middle of the large $491\mu\text{m}$ channel width. Initial concentration profiles of the two simulation cases are shown in Figure 3-20.

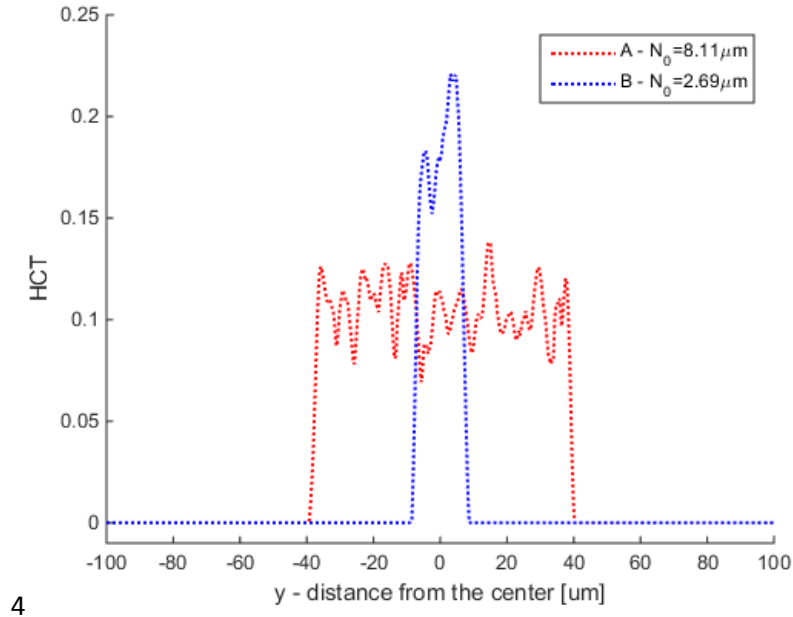


Figure 3-20. Initial concentration profile of the two simulation cases

Because the initial positions are randomly generated in the small channel, with the initial seeding width and the initial seeding hematocrit, ϕ , the initial concentration profile is closer to a step function than to the parabolic curves shown in Figure 3-19 (a). Figure 3-21 shows fitted parabolic curves with the initial concentration profiles.

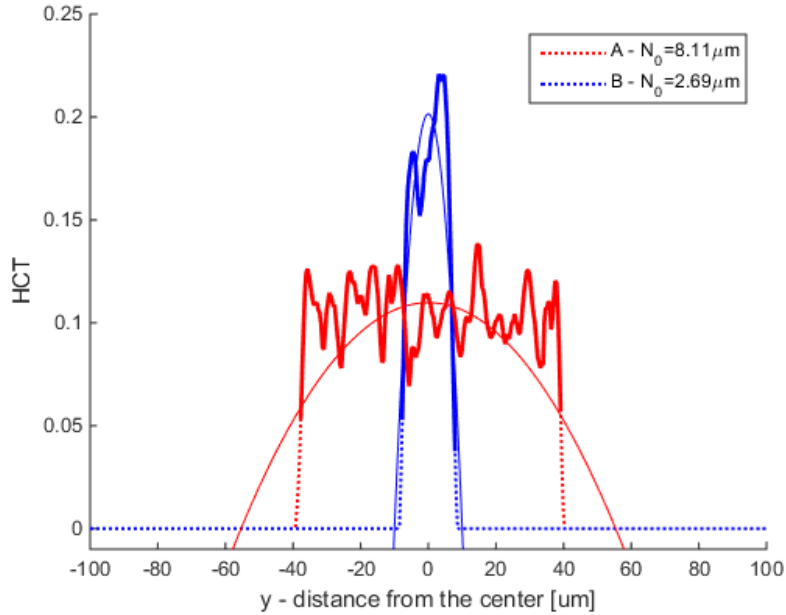


Figure 3-21. Fitted parabolic curves (thin solid lines) of the initial concentration profile (dotted line) with concentration data used for the fitting shown in thick solid line

For the curve fitting, extremely low concentration data (less than 5% for case A, and 3.1% for case B) are excluded. Because the study range is relatively dilute and a limited number of RBCs is used for the simulation, inclusion of the low concentration data can result in poor fitting. Thus, the data shown with thick solid lines is used to fit the parabolic curve shown in the thin solid line. The area between the horizontal axis and the fitted curves was set to match N_0 of each case. Figure 3-21 shows that the concentration profile of case A is not very close to parabolic shape because of the lower HCT and wider initial width. It was found that the concentration profile of case A grows closer to a parabolic shape from 28mm of flow distance (simulation time step $2e6+1$). Thus, case A was analyzed by setting the 28mm data as the initial condition (0 mm). The adjusted condition of the simulations (maximum values) is listed in Table 3-6 with additional information for further analysis.

Table 3-6. Adjusted initial conditions of simulations for analysis

| | w_0 | N_0 | Ca | Re | Re_p | Shear Rate [1/s] |
|--------------------|---------------------|--------------------|-------|-------|--------|------------------|
| Case A - Δ | 40.75 μm | 8.11 μm | 0.403 | 176.5 | 0.68 | 539.2 |
| Case B - \square | 7.08 μm | 2.69 μm | 0.407 | 178.4 | 0.69 | 545.1 |

Figure 3-22 shows the evolution of concentration profiles along the channel for case A and B.

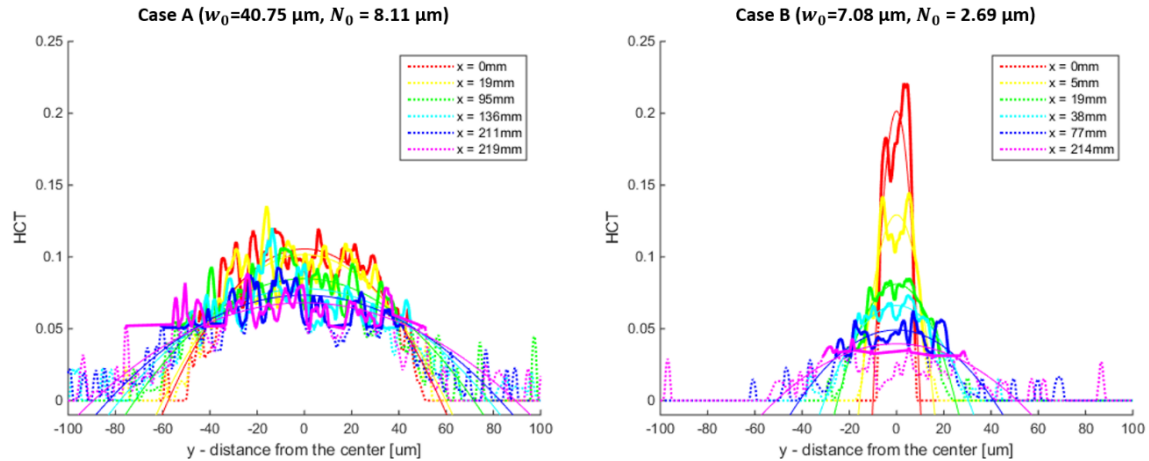


Figure 3-22. Concentration profile in several sections along the channel (dotted line: data, thin solid line: fitted parabolic curve, thick solid line: data used for fitting)

The data shown with thick solid lines are used to fit the parabolic curve shown in the thin solid line. Parabolic curves fit close to data, and it shows the spreading of RBC clouds along the channel similar to Figure 3-19 (a). The flow distance along the channel is calculated by integrating the average flow velocity over time. Based on the fitted parabolic curves, the blood stream half-width, w , at half-height of the RBC cloud is calculated for each case, as listed in Table 3-7 and Table 3-8.

Table 3-7. Half-width along the channel for Case A ($w_0 = 40.75 \mu\text{m}$, $N_0 = 8.11 \mu\text{m}$)

| | | | | | | | | |
|-------------------------------------|--------|--------|----------|---------|----------|---------|---------|---------|
| Simulation time step | 2e6+1 | 3e6+1 | 4e6+1 | 4.8e6+1 | 6e6+1 | 7.2e6+1 | 8e6+1 | 9e6+1 |
| Distance [mm] | 0 | 10 | 19 | 27 | 38 | 50 | 57 | 66 |
| w [μm] | 40.75 | 41.07 | 42.34 | 44.46 | 44.92 | 45.78 | 47.28 | 47.87 |
| Simulation time step | 10e6+1 | 11e6+1 | 12e6+1 | 13e6+1 | 14.1e6 | 15.1e6 | 16.2e6 | 17.1e6 |
| Distance [mm] | 76 | 86 | 95 | 105 | 116 | 125 | 136 | 144 |
| w [μm] | 48.94 | 50.03 | 50.70 | 51.57 | 53.55 | 54.33 | 55.21 | 56.02 |
| Simulation time step | 18.1e6 | 19.1e6 | 19.995e6 | 21.1e6 | 21.995e6 | 23.1e6 | 24.05e6 | 24.95e6 |
| Distance [mm] | 154 | 163 | 172 | 183 | 191 | 202 | 211 | 219 |
| w [μm] | 58.70 | 59.35 | 59.72 | 60.99 | 59.79 | 60.74 | 58.60 | 63.18 |

Table 3-8. Half-width along the channel for Case B ($w_0 = 7.08 \mu\text{m}$, $N_0 = 2.69 \mu\text{m}$)

| | | | | | | | | |
|-------------------------------------|-------|---------|--------|----------|----------|----------|-------|-------|
| Simulation time step | 1 | .5e6+1 | 1e6+1 | 2e6+1 | 3.95e6+1 | 5.35e6+1 | 6e6+1 | 7e6+1 |
| Distance [mm] | 0 | 5 | 10 | 19 | 38 | 51 | 57 | 67 |
| w [μm] | 7.08 | 11.03 | 13.45 | 17.62 | 21.56 | 24.54 | 26.23 | 30.97 |
| Simulation time step | 8e6+1 | 8.8e6+1 | 10e6+1 | 10.8e6+1 | 12e6 | 13e6 | 14e6 | 15e6 |
| Distance [mm] | 77 | 85 | 96 | 104 | 116 | 126 | 136 | 145 |
| w [μm] | 29.05 | 28.64 | 30.80 | 28.86 | 33.05 | 34.88 | 36.13 | 35.96 |
| Simulation time step | 16e6 | 17e6 | 18e6 | 20e6 | 21e6 | 22e6 | | |
| Distance [mm] | 155 | 165 | 175 | 194 | 204 | 214 | | |
| w [μm] | 38.26 | 34.13 | 37.90 | 36.72 | 35.24 | 36.12 | | |

In order to confirm the subdiffusive behavior with exponent 1/3, as was suggested from the literature [40], log-log plot of half-width, w , and flow distance, x , is plotted for both cases as shown in Figure 3-23.

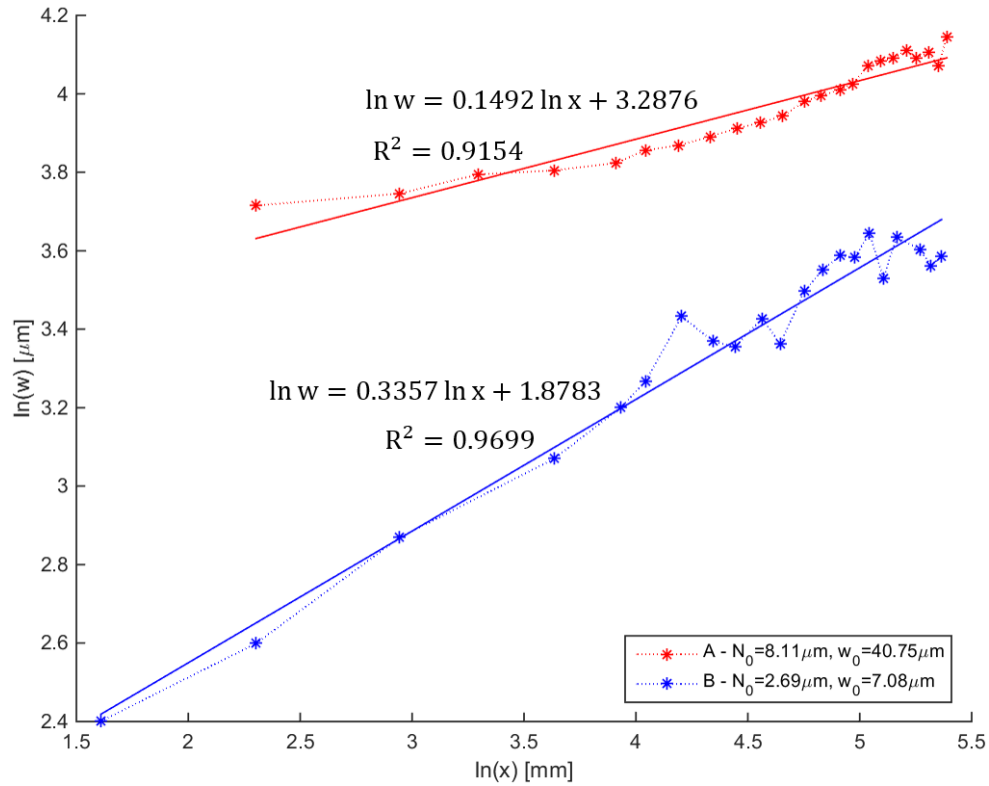


Figure 3-23. Log-log plot of w vs. flow distance x (stars: data, solid line: fitted linear line)

The straight solid line is the fitted line used to calculate the slope, exponent. It shows that the exponent of case A and B are $1/6.7$ and $1/2.97$, respectively. The result of case B is very similar to what was expected from the literature, but case A is not. Considering that the exponent value is supposed to reduce with increasing hematocrit due to increasing particle interactions, the result of case A is counter-intuitive. Case A result also shows lower R^2 suggesting that the quality of the data is not good. It is because of the rough fit that was made for the calculation of half width from the concentration profile as shown in Figure 3-22. Because of the huge simulation cost involving the large channel size, the minimum channel length was used for the simulation domain in the flow direction. Initial blood stream hematocrit of case A was about 10%, and that of case B was about 15%. Because of the low hematocrit, as the half-width increases, there were more locations where there is no blood cell at all in the middle of the

blood stream leading to a poor parabolic curve fit of concentration profile. Longer simulation domain would have allowed having more blood cells in the simulation so that more smooth concentration profile fitting can be achieved, but it was not affordable. Because case A had lower hematocrit, the fit was rougher for case A. However, the result of case B matches the experimental result very closely. In order to compare the dimensionless diffusivity values of RBCs to the experiment, $w(x)^3 - w_0^3$ over the flow distance, x , is plotted as shown in Figure 3-24.

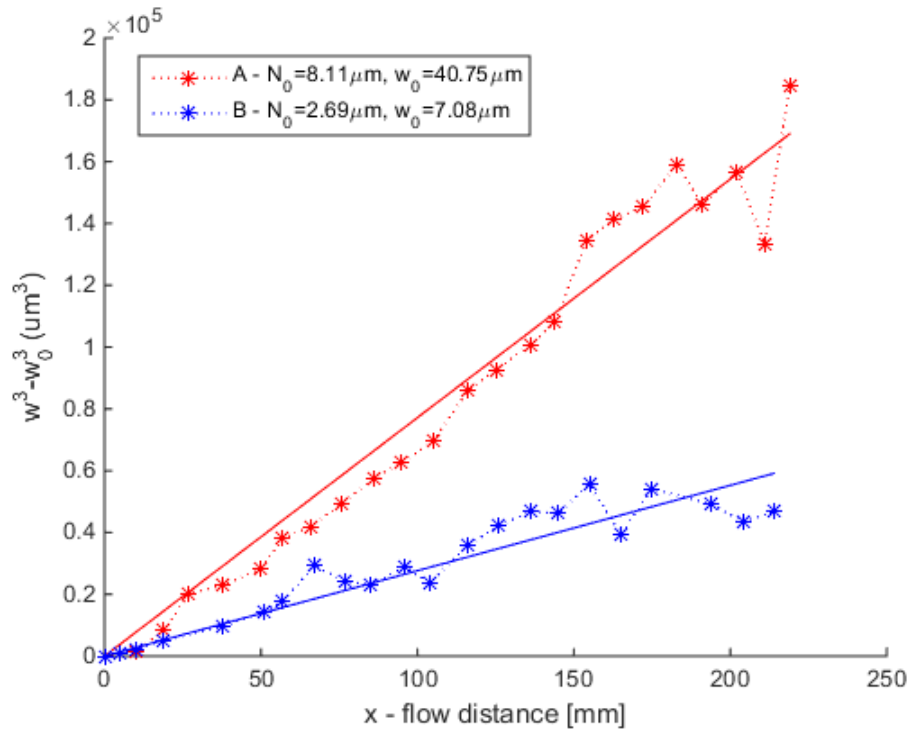


Figure 3-24. $w(x)^3 - w_0^3$ along the channel for several different conditions with simulations (stars: data, solid line: fitted linear line)

The straight solid line is the fitted line used to calculate the slope and the dimensionless diffusivity, $f_3 = 0.0413$ for case A and $f_3 = 0.0446$ for case B, based on RBC effective volume with diameter of $2R = 8.185\mu\text{m}$. It is very close to the experimental result of $f_3 = 0.05$.

A cross-sectional view of the channel was not available from the experimental study [40], but this simulation study provided the data as shown in Figure 3-25 and Figure 3-26.

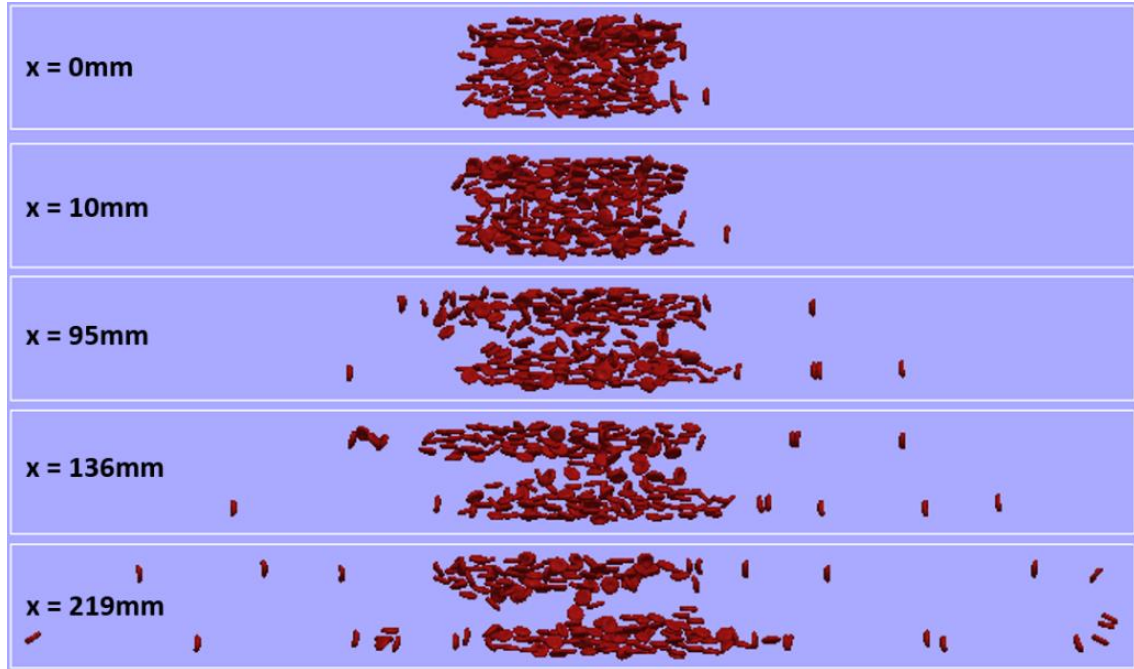


Figure 3-25. Cross-section view of the channel for case A ($w_0=40.75\ \mu\text{m}$, $N_0 = 8.11\ \mu\text{m}$)

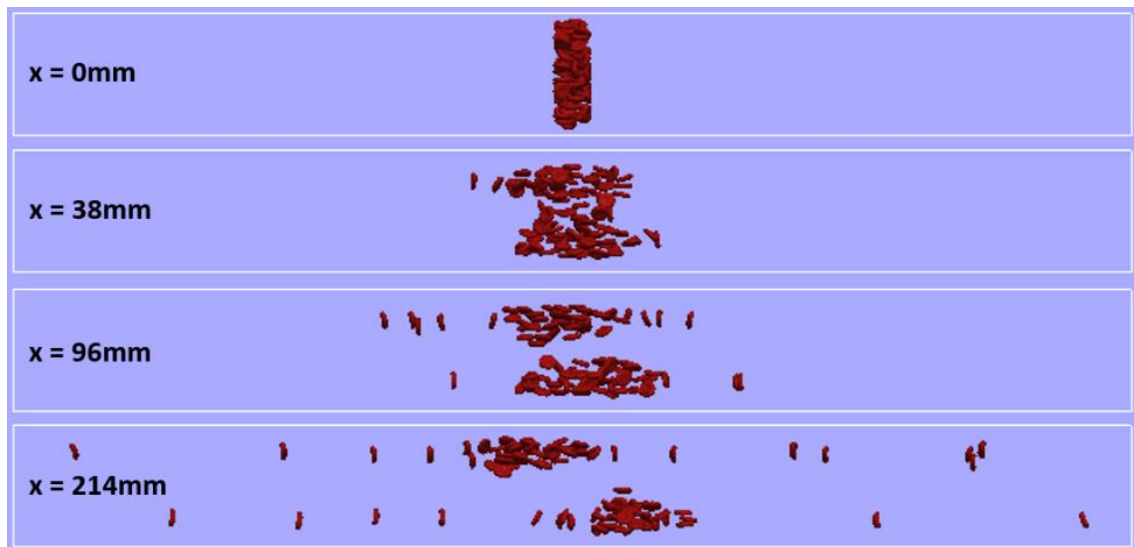


Figure 3-26. Cross-section view of the channel for case B ($w_0=7.08\ \mu\text{m}$, $N_0 = 2.69\ \mu\text{m}$)

The flow is into-the-page direction (x), channel width is in the horizontal direction (y), and channel depth is in the vertical direction (z). The figures show RBC spreading in the y-direction (width) along the channel as was described with concentration profiles in Figure 3-22. In addition, the Segre Silberberg effect is found in that the RBCs concentration decreases in the center and close to wall area in the depth (z) direction. For the further analysis, concentration profiles in the depth direction are plotted in Figure 3-27.

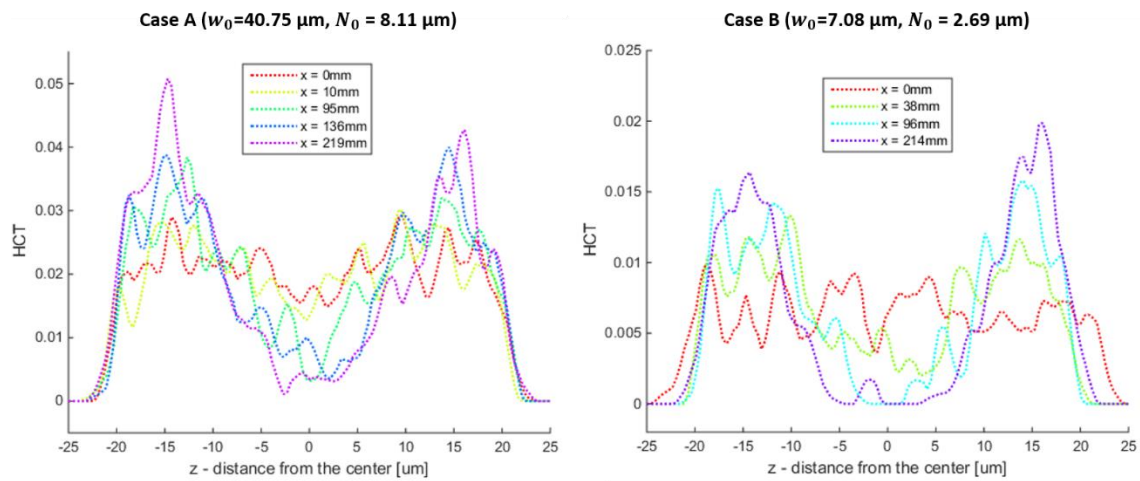


Figure 3-27. Concentration profile (depth direction) in several sections along the channel

The simulation results show that the maximum concentration of RBCs is around $0.6 d$, where d is the half of channel depth. The experimental study was conducted with $Re_p = 0.001$, and this simulation study was conducted with $Re_p = 0.07 \sim 0.7$ depending on the length that is considered, the depth or the width. Due to limitations on the computational resources available, Re_p was set to be much higher than was used in the experimental condition. However, considering that the Segre Silberberg effect is expected to be found when $Re_p > 0.001$ [10], these simulation results reasonably represent the experimental condition. This suggests that the Segre Silberberg effect might have been present in the experiment, although

the data is not available and the analysis of the experiment was conducted with the assumption that the concentration profile was homogeneous in the depth direction (z).

This simulation study showed that the blood cell migration behavior found using the LB-SL method based simulation is comparable to what is found in experiments and revealed additional information on the depth-direction concentration profile.

3.10 Computational Performance

The hybrid LB-SL code is written entirely in the C programming language. For the huge simulation that is required for this research, the high performance computing system called Stampede at Texas Advanced Computing Center (TACC) was utilized to run the simulation with multiple cores. The performance of the code on the system was measured with *speedup* and *efficiency* of scaling results. The term *speedup* is defined as the following equation.

$$\text{Speedup} = \frac{\text{Time to Solution for } N_{\min} \text{ cores}}{\text{Time to Solution for } N \text{ cores}} \quad (3-33)$$

N_{\min} is the minimum number of cores required to run the simulation. And *efficiency* is defined as the following equation.

$$\text{Efficiency} = \frac{N_{\min}}{N} \times \text{Speedup} \times 100\% \quad (3-34)$$

Simulations were performed for a case of pressure driven flow with a domain size $160\mu\text{m} \times 160\mu\text{m} \times 160\mu\text{m}$ with 8715 RBCs (20% volume fraction) as shown in Figure 3-28.

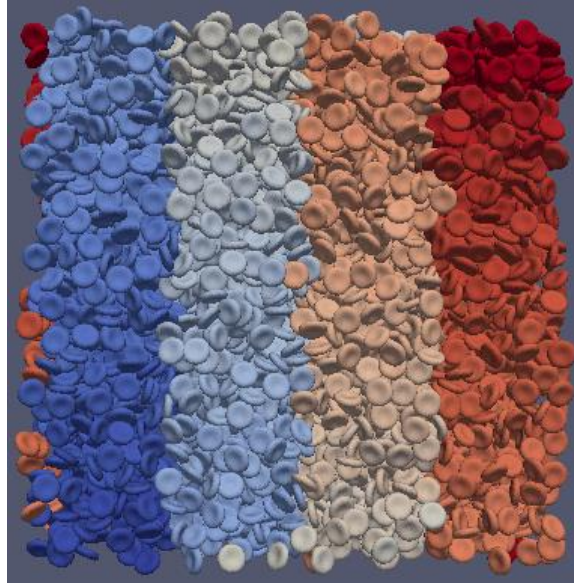


Figure 3-28. Screenshot of 8715 RBCs in $(160\mu\text{m})^3$ domain

Different colors in the figure are meant to aid visualization. Both $2.5 \text{ lu}/\mu\text{m}$ (low-resolution) and $3.0 \text{ lu}/\mu\text{m}$ (high-resolution) resolution cases are studied, and $400 \times 400 \times 400$ and $480 \times 480 \times 480$ lattice unit domains are used, respectively. Subdomain size of the scaling simulations are listed in Table 3-9.

Table 3-9. Subdomain size of scaling simulations with 8715 RBCs in $(160\mu\text{m})^3$ domain

| No. of cores | Subdomain size | Subdomain size for $2.5 \text{ lu}/\mu\text{m}$ | Subdomain size for $3.0 \text{ lu}/\mu\text{m}$ |
|---------------------|---|---|---|
| 128 | $20\mu\text{m} \times 40\mu\text{m} \times 40\mu\text{m}$ | $50 \times 100 \times 100$ | $60 \times 120 \times 120$ |
| 256 | $20\mu\text{m} \times 20\mu\text{m} \times 40\mu\text{m}$ | $50 \times 50 \times 100$ | $60 \times 60 \times 120$ |
| 512 | $20\mu\text{m} \times 20\mu\text{m} \times 20\mu\text{m}$ | $50 \times 50 \times 50$ | $60 \times 60 \times 60$ |
| 1024 | $10\mu\text{m} \times 20\mu\text{m} \times 20\mu\text{m}$ | $25 \times 50 \times 50$ | $30 \times 60 \times 60$ |
| 2048 | $10\mu\text{m} \times 10\mu\text{m} \times 20\mu\text{m}$ | $25 \times 25 \times 50$ | $30 \times 30 \times 60$ |
| 4096 | $10\mu\text{m} \times 10\mu\text{m} \times 10\mu\text{m}$ | $25 \times 25 \times 25$ | $30 \times 30 \times 30$ |

128 cores were selected as the base calculation for the speedup and efficiency calculation, since this is the minimum number of cores with access to enough memory to simulate the domain size. The results are shown in Table 3-10.

Table 3-10. Scaling simulation results for 100 LB time steps with 8715 RBCs in $(160\mu\text{m})^3$ domain

| No. of cores | Time - 2.5 lu/ μm [sec] | Time - 3.0 lu/ μm [sec] |
|--------------|------------------------------------|------------------------------------|
| 128 | 90.28 | 116.71 |
| 256 | 54.51 | 68.74 |
| 512 | 36.19 | 41.20 |
| 1024 | 24.54 | 31.16 |
| 2048 | 22.54 | 22.78 |
| 4096 | 23.85 | 13.40 |

The speedup and number of LB time steps that are calculated per second for different numbers of cores are plotted in Figure 3-29.

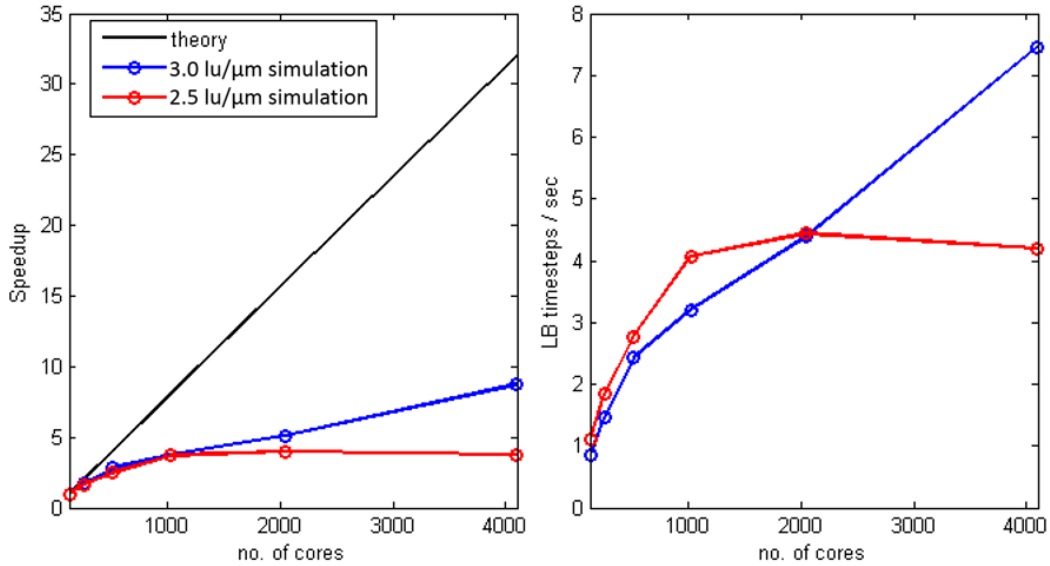


Figure 3-29. Scaling simulation results for 100 LB time steps with 8715 RBCs in $160\mu\text{m}^3$ domain

In theory, the speedup should increase linearly with increasing numbers of cores used. For a single-phase flow with only fluid, the speedup was shown to increase close to the theory [94].

However, because of the Message Passing Interface (MPI) communication overhead that accompanies information communication between cores, the speedup does not increase linearly, and the efficiency drops as the number of cores increases. It was noted that when more than 2048 cores were used for the lower resolution case ($2.5 \text{ lu}/\mu\text{m}$), the performance was worse than using 1024 cores because too much MPI communication overhead occurred. This study also shows that with the lower resolution, the simulation will run much faster and the cost would be cheaper up to 2048 cores. Further increasing the number of cores leads to the lower resolution case to be calculated slower than the higher resolution case due to the increasing ratio of the computation time consumed for particle-particle interactions. Because particle-particle interactions are calculated for the cases that two surfaces are closer than 1 lattice unit, and the length of 1 lattice unit is longer for the lower resolution ($0.4 \mu\text{m}/\text{lu}$) than the higher resolution ($0.33 \mu\text{m}/\text{lu}$), lower resolution case always requires more particle-particle interaction force calculation. Once the subdomain size reduces enough for the communication overhead due to the particle-particle interaction force calculation to occur too much, using lower resolution does not lead to the computational cost saving. Since the simulations are run with much less than 1000 cores for each case in this research, it is reasonable to use the lower resolution case, as that provides results comparable to the experimental results shown in previous chapters while saving the simulation cost.

3.11 Summary

In this chapter, the direct numerical simulation based on Lattice Boltzmann and Spectrin Link method is presented. The Spectrin Link method used for RBC modeling, subgrid modeling used for particle-particle interactions, restart function of the code, and initial seeding strategy of

RBC suspensions are refined for RBC suspension modeling with realistic dense hematocrits. The updated properties of RBC with less number of nodes were validated for both isolated RBCs in equilibrium stage and non-uniform suspension of RBCs in transient phase. The computational performance of lower fluid resolution was evaluated to reduce computational cost. The validated LB-SL method with lower resolution is used in Chapter 4 for the direct numerical simulation study of blood cell migrations in non-uniform suspension flows.

CHAPTER FOUR

MIGRATION OF CELLS IN NON-UNIFORM SUSPENSION FLOW

This chapter is devoted to creating the meta-model of blood cell migration behavior. This is done with a parametric study using LB-SL method based DNS. The goal of this study is to address the first research question: What are the conditions that retain blood cells in the blood stream when it flows with sheath fluid in a micro-fluidic channel? The meta-model can be used to predict blood cell migrations in non-uniform suspension flows for different flow conditions and channel geometry. The extraction ratio (the ratio of cells lost into the sheath stream) over the flow distance is measured to create the meta-model, which is used to identify the feasible conditions that will retain blood cells in the blood stream.

4.1 Relevant Variables and Parameters

Design variables investigated in this chapter for the meta-model creation of extraction ratio includes the channel dimensions, flow conditions, hematocrit, and geometry. Hematocrit is not a variable for the hemodialysis treatment since whole blood will flow through a dialyzer without dilution process. However, it was included as a variable to study the possibility of reducing computational cost by using lower hematocrit cases for prediction of higher hematocrit cases. Geometry was also added to reduce the computational cost by using rectangular channel results to predict circular channel results. Although circular channels are the main interest for the proposed dialyzer design, rectangular channel cases are computationally much cheaper especially for large channels. The independent variables relevant to the study of blood cell migration behavior in non-uniform suspension flow are listed in Table 4-1.

Table 4-1. Independent variables and parameters for the study of blood cell migration behavior

| | Symbol | Dimension |
|----------------------------|----------------|-------------------------------------|
| Channel Diameter (Height) | D (H) | [L] |
| Sheath Stream Thickness | δ | [L] |
| Flow Distance | L | [L] |
| Particle Radius | a | [L] |
| Wall Shear Rate | $\dot{\gamma}$ | [T ⁻¹] |
| Average Flow Velocity | u | [LT ⁻¹] |
| Plasma Dynamic Viscosity | μ | [ML ⁻¹ T ⁻¹] |
| Plasma Kinetic Viscosity | ν | [L ² T ⁻¹] |
| RBC Membrane Shear Modulus | G | [MT ⁻²] |
| Hematocrit | HCT | [-] |
| Extraction Ratio | ER | [-] |

This study considered both circular channels and rectangular channels; D and H, respectively, are used for the dimensions of these channels. Sheath stream thickness, δ , is defined as $(D - d)/2$ where d is the blood inlet channel diameter as shown in Figure 4-1 (c).

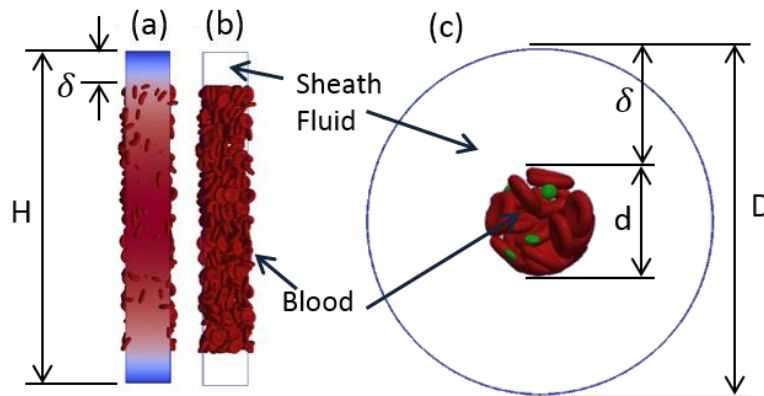


Figure 4-1. Cross-section of rectangular channels (a, b) and circular channel (c) with blood and sheath stream. (a. with fluid velocity field): flow direction is into the page

As was explain in section 3.6, rectangular channel cases simulate an infinitely wide micro-fluidic channel by having only the top and the bottom walls and applying periodic boundary conditions on the side; Figure 4-1 (a) shows the high flow velocity in the center with no side wall effects.

Because the minimum length, 2.7 RBC diameter, was used in the width direction with the

periodic boundary conditions, the simulation cost was much cheaper than circular channel cases for larger channel sizes. Flow distance, L , is calculated by integrating the average flow velocity over time, and it can be considered as the channel length of a dialyzer tubule. This study is limited to the case where the sheath stream viscosities are the same as the plasma viscosity, so the plasma viscosities, μ and ν , are the only relevant variables.

The relevant variables and parameters are non-dimensionalized based on dimensional analysis methods; this reduces the number of variables to study. Except for hematocrit and extraction ratio, which are already dimensionless, there are 9 variables to consider with 3 dimensions, length L , time T , and mass M . According to the Buckingham PI theorem, $9 - 3 = 6$ dimensionless parameters were constructed. The six dimensionless parameters are listed in Table 4-2.

Table 4-2. Dimensionless parameters

| | | | | | |
|--------------------|---------------|---------------|-----------------------|--------------------------------------|-----------------------------------|
| $\frac{\delta}{a}$ | $\frac{L}{D}$ | $\frac{D}{a}$ | $\frac{Du}{\nu} = Re$ | $\frac{a^2\dot{\gamma}}{\nu} = Re_p$ | $\frac{a\dot{\gamma}\mu}{G} = Ca$ |
|--------------------|---------------|---------------|-----------------------|--------------------------------------|-----------------------------------|

Thus, the relationship to study reduces as shown in the following equation.

$$ER = f\left(\text{HCT}, \frac{\delta}{a}, \frac{L}{D}, \frac{D}{a}, Re, Re_p, Ca\right) \quad (4-1)$$

Particle diameter, a , is included to compare the results of RBC migration behavior to that of platelets. Thus, δ and D are the design variables to explore, and the results can be analyzed by normalizing with particle diameters. The effects of Re , Re_p , and Ca are the same because the fluid property and RBC membrane shear modulus are set to realistic values so that Re , Re_p , and Ca linearly change with the flow velocity for the given channel dimension. In addition, the

effect of channel geometry (circular vs. rectangular) is also of interest. Thus, the final relationship to study further reduces as follows.

$$(ER, w) = f(HCT, Re, geometry, \delta, D, L) \quad (4-2)$$

In the following sections, the extraction ratios are analyzed for each of the simulation cases. In section 4.2, the effects of HCT and Re are presented. The effects of channel geometry and channel dimensions are presented in 4.3.

4.2 Effect of Hematocrit and Re

Hematocrit (HCT), the volume fraction of RBCs, is one of the important parameters that affect blood cell migration behavior. Although the realistic hematocrit level is about 40%, such a dense suspension flow study is very expensive, because the simulation cost largely depends on the number of blood cells and the size of the simulation domain. Thus, if low hematocrit case results can predict the behavior of blood cells in realistic hematocrit levels (~40%), the simulation cost can be saved. Three different hematocrit levels (20, 30, 40%) were tested in order to evaluate the possibility of using lower hematocrit cases, and screenshots of the simulations are shown in Figure 4-2.

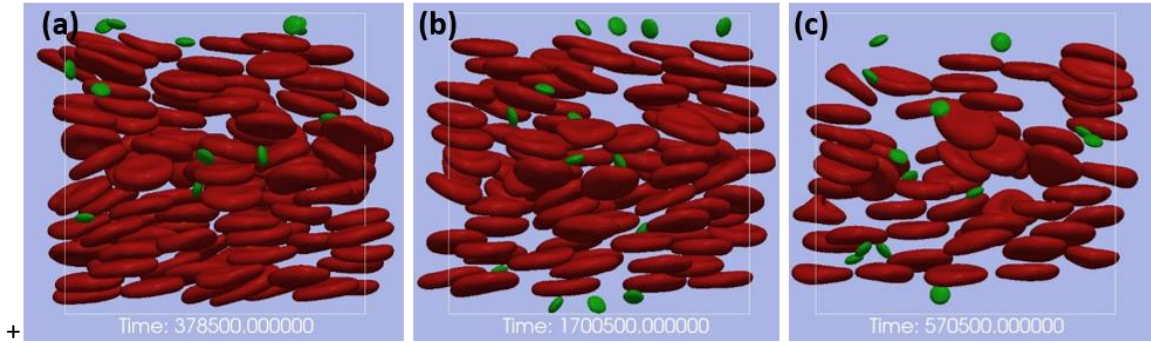


Figure 4-2. Screenshots of (a) 40%, (b) 30%, and (c) 20% hematocrit cases in 40 μm height channel with 32 μm initial blood stream height

Figure 4-2 shows a screenshot of RBCs and platelets flowing in a 40 μm height rectangular channel with 32 μm initial blood stream height in the center. It shows many more blood cells densely packed in the 40% case than other cases. For each of these cases, the number of cells lost into the sheath stream area in the top and the bottom 4 μm area was counted to calculate the extraction ratio, which is defined as the number of cells lost into the sheath stream region divided by the total number of the cells. The extraction ratios, ER, are plotted over the flow distance, L , and a dimensionless scale, L/H , is also shown on the top in Figure 4-3.

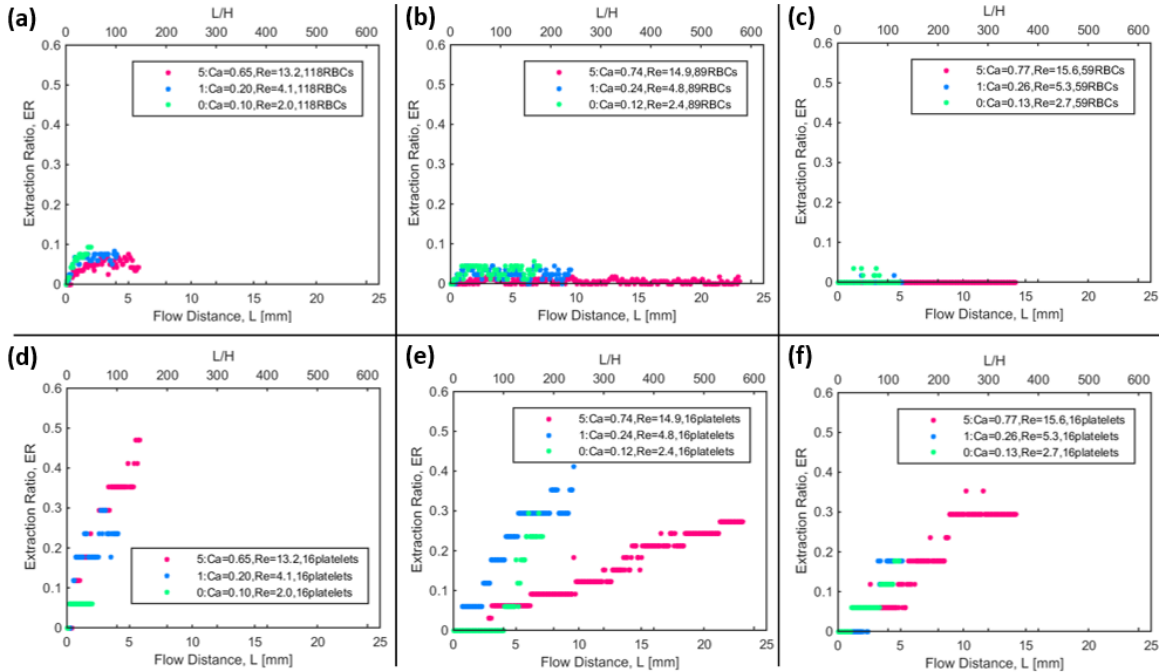


Figure 4-3. Extraction ratios of RBCs (a, b, c) and platelets (d, e, f) with 40% (a,d), 30% (b, e), and 20% (c, f)

The figure shows RBC results on the top row and platelet results on the bottom row; columns are arranged to display 40%, 30%, and 20% HCT cases from left to right. RBC results on the top are shown in a rescaled axis in Figure 4-4.

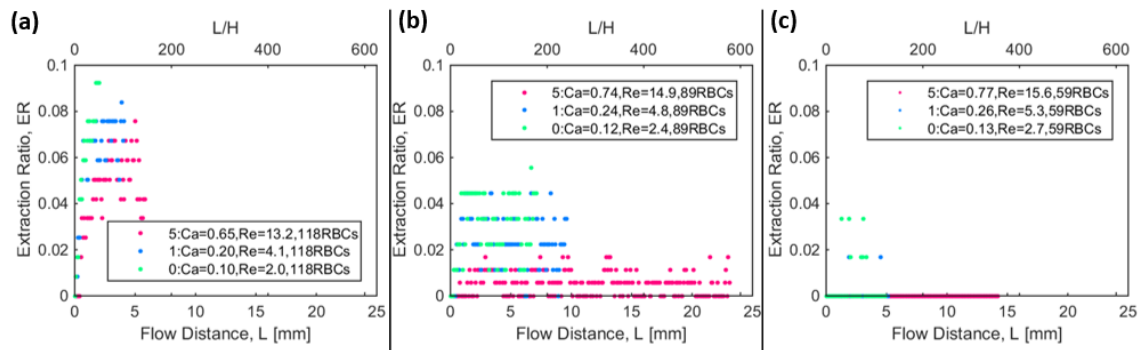


Figure 4-4. Extraction ratios of RBCs with 40% (a), 30% (b), and 20% (c)

Different colors represent different Re cases with 5 in the legend being the highest case; this figure shows that Re does not greatly affect the result. It shows that with 20% HCT, RBCs are

not lost into the sheath stream at all, but up to 10% are lost for 30 and 40% cases. For platelets, because of the platelet margination, platelet ER increases towards 100% loss, and the rate of ER is fastest for the 40% case. The platelet extraction ratio is much higher than that of RBCs, due to the platelet margination behavior. The sheath stream is only 4 μm high on the top and the bottom of the channel, which makes it hard for the 8 μm diameter RBCs to stay in the small region, compared to the 2.8 μm diameter platelets. Comparing the three different hematocrit cases, the extraction ratio increased with increasing hematocrit level. However, it is hard to define the exact relationship of the 20% or 30% cases to the 40% case. Thus, 40% hematocrit cases are selected for further study.

The blood cell migration behaviors of the 40% cases were analyzed further as shown in Figure 4-5.

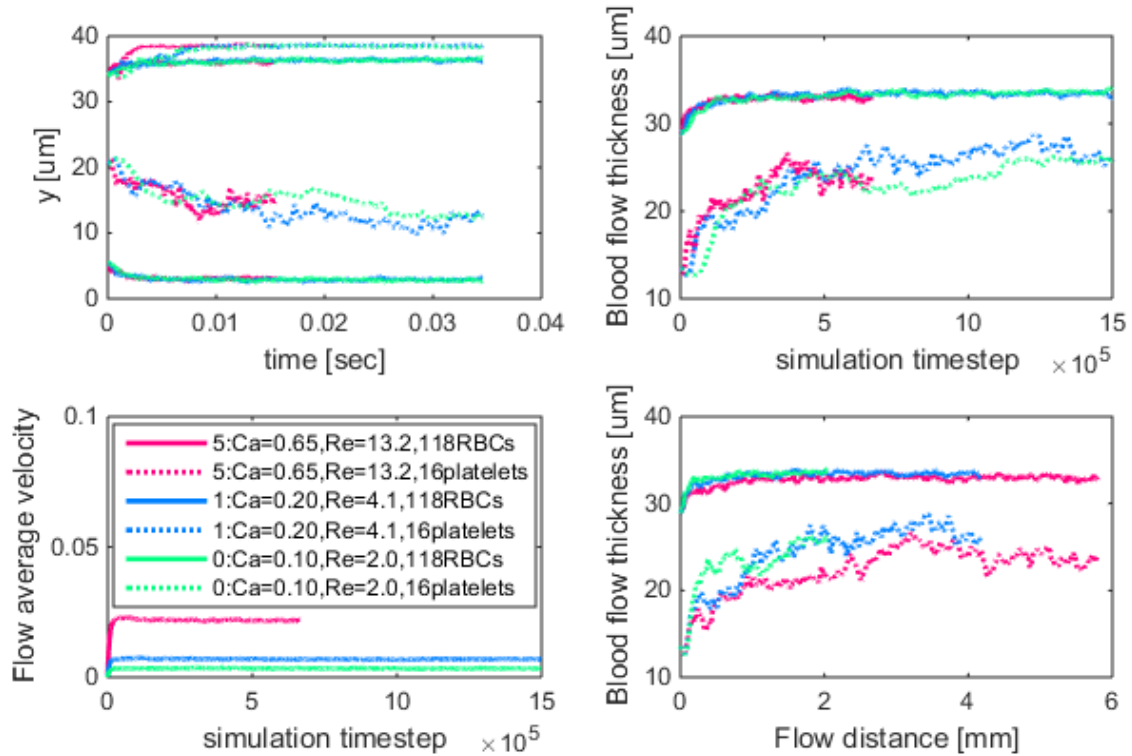


Figure 4-5. Blood cell migration behavior flowing in 40 μm diameter channel with the initial blood stream diameter of 32 μm for three different flow velocities with 40% HCT

RBC flow results are plotted in solid lines, and platelet flow results are plotted in dotted lines. Different colors represent different Re cases, with 5 in the legend being the highest case. The top left plot shows the height of maximum and minimum blood cells over time. It visualizes how the blood stream spreads over time. The top right plot shows the evolution of the blood stream thickness, which is the difference between the maximum and the minimum heights shown in the top left plot. The bottom left plot shows the flow average velocity for each simulation time step. By integrating the flow average velocity over time, the flow distance is calculated. The blood flow thickness change over flow distance is plotted in the bottom right. The results show that the results are almost identical when plotted over the flow distance. Confirmation that the particle migration depends on flow distance, is found in literature [40, 95], and the simulation

results agree with this. Based on this result, later studies investigated the particle margination behavior over flow distance, not Re , Re_{RBC} , or Ca .

4.3 Effect of Channel Dimensions and Geometry

Section 4.2 showed that the flow distance is the only important parameter. Thus, the effect of channel dimensions and geometries on the evolution of blood cell extraction ratios over flow distance is studied for realistic 40% HCT cases. Realistic numbers of platelets were used which are $\frac{1}{15}$ of the number of RBCs. However, for cases in which the realistic number of platelets was too few, 30 platelets were used for a reliable statistical analysis. All simulations started with uniformly suspended platelets and RBCs in the blood stream region.

4.3.1 Design of Experiments – Latin Hyper-Cube Method

Channels with the size of $40\mu m < D (H) < 200\mu m$ and sheath stream thickness of $3\mu m < \delta < 19\mu m$ were studied. In order to efficiently utilize limited computational resources, a Latin Hyper-Cube design of experiment method was used, as it evenly distributes the variables for the limited number of experiments possible. The simulation study space is shown in Figure 4-6 with dimensionless scales, D/a and δ/a , based on RBC radius of $a = 4.0925\mu m$.

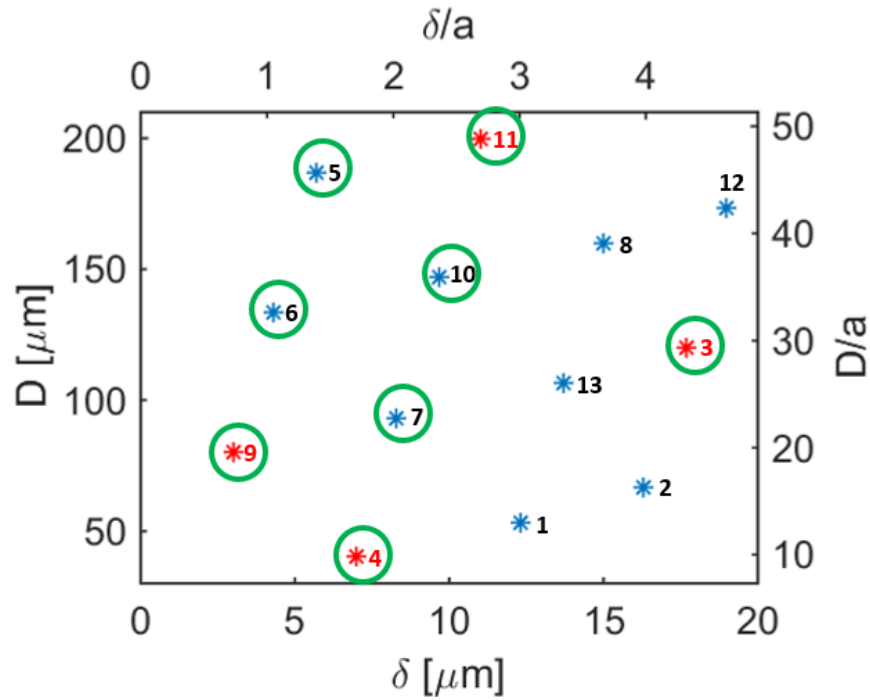


Figure 4-6. Simulation Study Space

Figure 4-6 shows cases 3, 4, 9, and 11 in red, as these cases were studied initially with circular channels. Based on the results of these four cases, it was found that the blood cell extraction ratio would decrease when the sheath stream thickness, δ , is small. Because circular channel cases are much more computationally expensive than rectangular channels, especially for large channels, the 8 cases that are circled in green were studied with circular channels. Then, all 13 cases were studied with rectangular channels. As was mentioned in section 3.6, for rectangular channels, periodic boundary conditions are used in both the flow direction and the vorticity direction, and the channel represents an infinitely wide channel that is not affected by side walls. Detailed information regarding the channel dimensions and the number of blood cells used is presented in Table 4-3 for circular channels and Table 4-4 for rectangular channels. In addition, the resulting flow characteristics, Re , Re_{RBC} , and Ca , are also presented based on RBC characteristic diameter of $a = 2.82\mu m$.

Table 4-3. Details of each cases studied with circular channels

| Case No. | δ [μm] | D [μm] | d [μm] | D [lu] | d [lu] | No RBC | No Plt | Ca | Re | Re_p | Shear Rate [1/s] |
|----------|----------------------------|---------------------|---------------------|--------|--------|--------|--------|------|------|--------|------------------|
| 3 | 17.7 | 120.0 | 84.7 | 300.0 | 211.7 | 958 | 64 | 0.57 | 46.4 | 0.15 | 893 |
| 4 | 7.0 | 40.0 | 26.0 | 100.0 | 65.0 | 134 | 30 | 0.60 | 13.0 | 0.39 | 937 |
| 5 | 5.7 | 186.7 | 175.3 | 466.7 | 438.3 | 4110 | 272 | 0.31 | 53.0 | 0.07 | 480 |
| 6 | 4.3 | 133.3 | 124.7 | 333.3 | 311.7 | 2078 | 138 | 0.39 | 38.5 | 0.10 | 601 |
| 7 | 8.3 | 93.3 | 76.7 | 233.3 | 191.7 | 786 | 52 | 0.40 | 23.6 | 0.13 | 628 |
| 9 | 3.0 | 80.0 | 74.0 | 200.0 | 185.0 | 732 | 49 | 0.46 | 26.7 | 0.20 | 724 |
| 10 | 9.7 | 146.7 | 127.3 | 366.7 | 318.3 | 2168 | 145 | 0.43 | 46.1 | 0.10 | 676 |
| 11 | 11.0 | 200.0 | 178.0 | 500.0 | 445.0 | 4236 | 281 | 0.38 | 51.2 | 0.06 | 592 |

Table 4-4. Details of each cases studied with rectangular channels

| Case No. | δ [μm] | H [μm] | h [μm] | H [lu] | h [lu] | No RBC | No Plt | Ca | Re | Re_p | Shear Rate [1/s] |
|----------|----------------------------|---------------------|---------------------|--------|--------|--------|--------|------|------|--------|------------------|
| 1 | 12.3 | 53.3 | 28.7 | 133.3 | 71.7 | 176 | 30 | 0.90 | 40.0 | 0.68 | 1404 |
| 2 | 16.3 | 66.7 | 34.0 | 166.7 | 85.0 | 185 | 30 | 1.05 | 52.6 | 0.56 | 1642 |
| 3 | 17.7 | 120.0 | 84.7 | 300.0 | 211.7 | 311 | 30 | 0.71 | 57.9 | 0.19 | 1115 |
| 4 | 7.0 | 40.0 | 26.0 | 100.0 | 65.0 | 153 | 30 | 0.85 | 18.4 | 0.55 | 1329 |
| 5 | 5.7 | 186.7 | 175.3 | 466.7 | 438.3 | 645 | 43 | 0.54 | 93.3 | 0.13 | 845 |
| 6 | 4.3 | 133.3 | 124.7 | 333.3 | 311.7 | 458 | 31 | 0.65 | 64.5 | 0.17 | 1007 |
| 7 | 8.3 | 93.3 | 76.7 | 233.3 | 191.7 | 282 | 30 | 0.64 | 37.6 | 0.21 | 997 |
| 8 | 15.0 | 160.0 | 130.0 | 400.0 | 325.0 | 478 | 32 | 0.53 | 75.8 | 0.14 | 821 |
| 9 | 3.0 | 80.0 | 74.0 | 200.0 | 185.0 | 272 | 30 | 0.74 | 42.6 | 0.32 | 1154 |
| 10 | 9.7 | 146.7 | 127.3 | 366.7 | 318.3 | 468 | 31 | 0.68 | 72.8 | 0.16 | 1068 |
| 11 | 11.0 | 200.0 | 178.0 | 500.0 | 445.0 | 654 | 44 | 0.54 | 72.6 | 0.09 | 838 |
| 12 | 19.0 | 173.3 | 135.3 | 433.3 | 338.3 | 498 | 33 | 0.93 | 126 | 0.20 | 1451 |
| 13 | 13.7 | 106.7 | 79.3 | 266.7 | 198.3 | 292 | 30 | 0.70 | 53.8 | 0.23 | 1093 |

4.3.2 Results

The evolution of blood cell extraction ratio over flow distance was found to follow an exponential curve as shown in the following equation.

$$ER = ER_{eq}(1 - e^{-L/L_\tau}) \quad (4-3)$$

This was shown in an experimental study as well [45]. One case is shown in Figure 4-7 with the fitted curve.

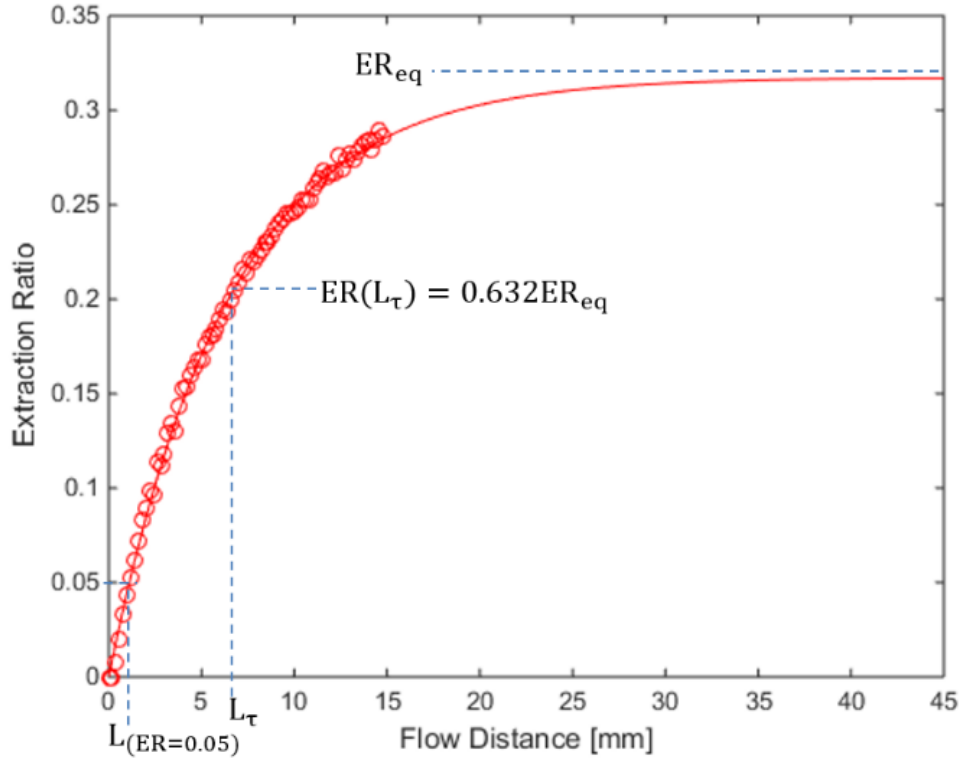


Figure 4-7. RBC extraction ratio vs. flow distance fitted to an exponential curve

ER_{eq} is the equilibrium extraction ratio, L is the flow distance, and L_τ is the length constant, which is the flow distance when the extraction ratio reaches 63.2% of ER_{eq} . Because of platelet margination behavior, platelets are expected to equilibrate close to the wall eventually, as was shown in section 4.2. Thus, ER_{eq} was set to 1 for platelets. $L_{(ER=0.05)}$ is the length when the extraction ratio reaches 5%. It is used for further analysis and meta-model creation in section 4.4.

4.3.2.1 Circular Channel Results

Extraction ratios for RBCs and for platelets through circular channels are plotted over flow distance for the 8 cases with fitted exponential curve, and the L/D scale is also shown on the top of each plot in Figure 4-8.

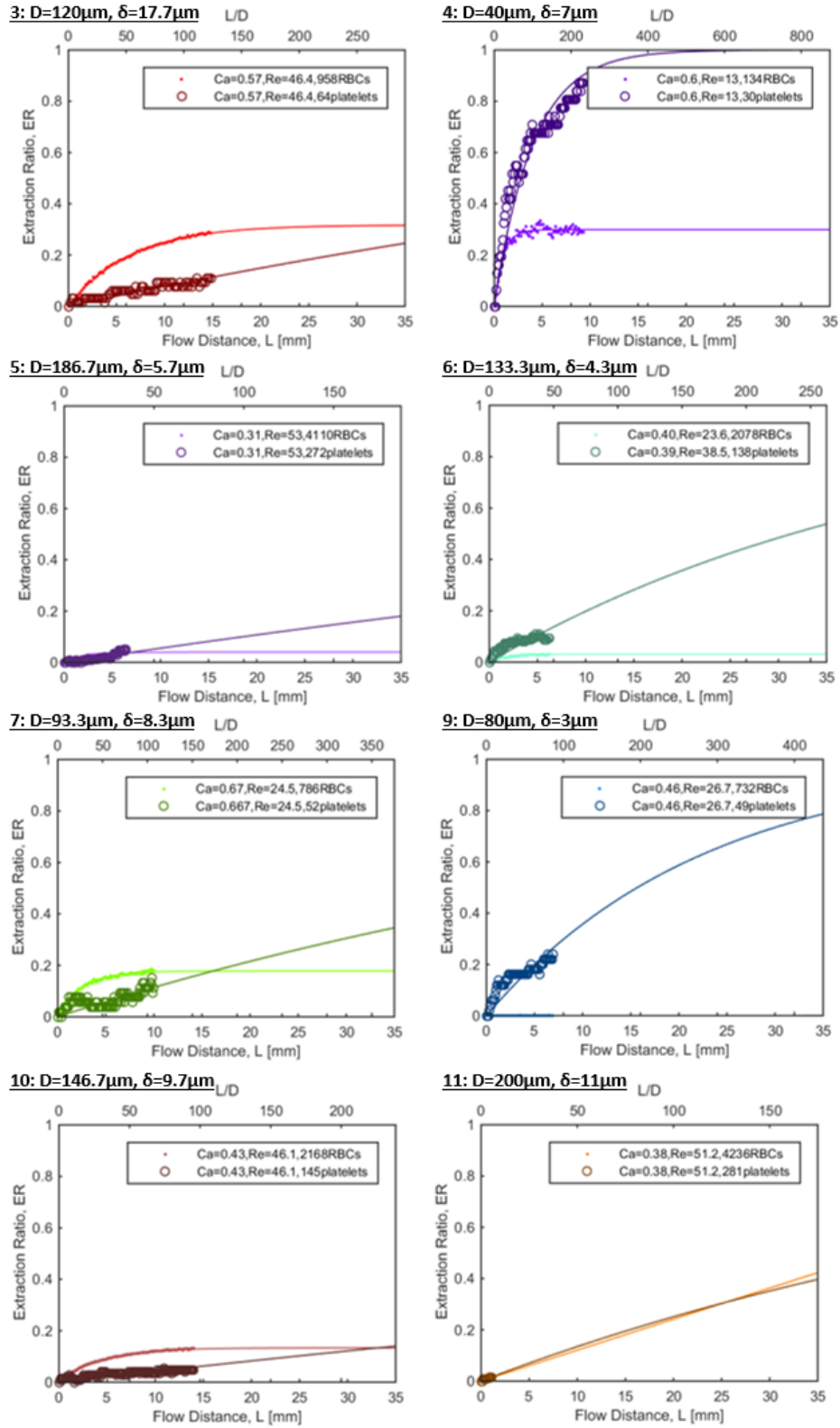


Figure 4-8. Extraction ratio of blood cells over flow distance for the 8 circular channel cases

In the figure, lighter colored small circular dots are for RBCs and darker colored stars are for platelets. Three cases are shown in Figure 4-9 with close-up view.

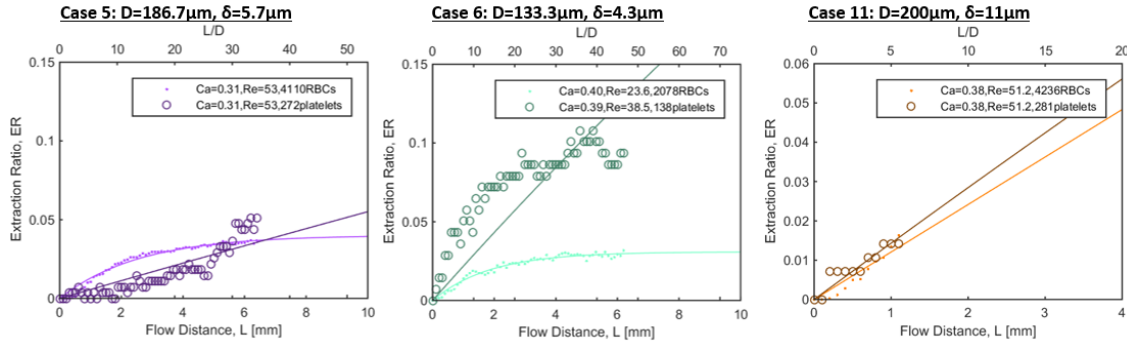


Figure 4-9. Close-up view of extraction ratio of blood cells over flow distance for 3 circular channel cases

The resulting ER curve parameters, ER_{eq} and L_{τ} , of each circular channel case are listed in Table 4-5.

Table 4-5. Resulting ER curve parameters of each cases studied with circular channels

| Case No. | δ [μm] | D [μm] | d [μm] | No RBC | No Plt | ER_{eq} RBC | L_{τ} RBC [mm] | L_{τ} Plt [mm] | $L_{(ER=0.05)}$ RBC [mm] | $L_{(ER=0.05)}$ Plt [mm] |
|----------|----------------------------|-----------------------|-----------------------|--------|--------|---------------|---------------------|---------------------|--------------------------|--------------------------|
| 3 | 17.7 | 120.0 | 84.7 | 958 | 64 | 0.3173 | 6.4806 | 123.93 | 1.1113 | 6.3568 |
| 4 | 7.0 | 40.0 | 26.0 | 134 | 30 | 0.2988 | 0.8783 | 4.00 | 0.1608 | 0.2052 |
| 5 | 5.7 | 186.7 | 175.3 | 4110 | 272 | 0.0402 | 2.5848 | 176.53 | ∞ | 9.0548 |
| 6 | 4.3 | 133.3 | 124.7 | 2078 | 138 | 0.0308 | 1.8606 | 45.33 | ∞ | 2.3251 |
| 7 | 8.3 | 93.3 | 76.7 | 786 | 52 | 0.1780 | 2.5712 | 82.44 | 0.8479 | 4.2286 |
| 9 | 3.0 | 80.0 | 74.0 | 732 | 49 | 0 | - | 22.64 | ∞ | 1.1613 |
| 10 | 9.7 | 146.7 | 127.3 | 2168 | 145 | 0.1336 | 4.3104 | 231.31 | 2.0207 | 11.8647 |
| 11 | 11.0 | 200.0 | 178.0 | 4236 | 281 | 7.8e+5 | 6.5e+7 | 69.26 | 8.5588 | 3.5526 |

For most of the cases, the flow distances were not long enough to analyze the platelet extraction ratio, due to the relatively long L_{τ} compared to that of RBC. For case 9, which is the smallest sheath stream thickness case, no RBCs were lost into the sheath stream. Because RBC

diameter is 8.185 μm , it would be very hard for a RBC to stay in the 3 μm sheath stream area.

Case 11, which is the largest channel case, was run too briefly to analyze anything. The simulation of this case was very hard to continue due to instability issues. Thus, case 11 was excluded for further analysis, which is presented in 4.4 for meta-model creation.

4.3.2.2 Rectangular Channel Results

The results of the 13 rectangular channel cases are shown in Figure 4-10 and Figure 4-11.

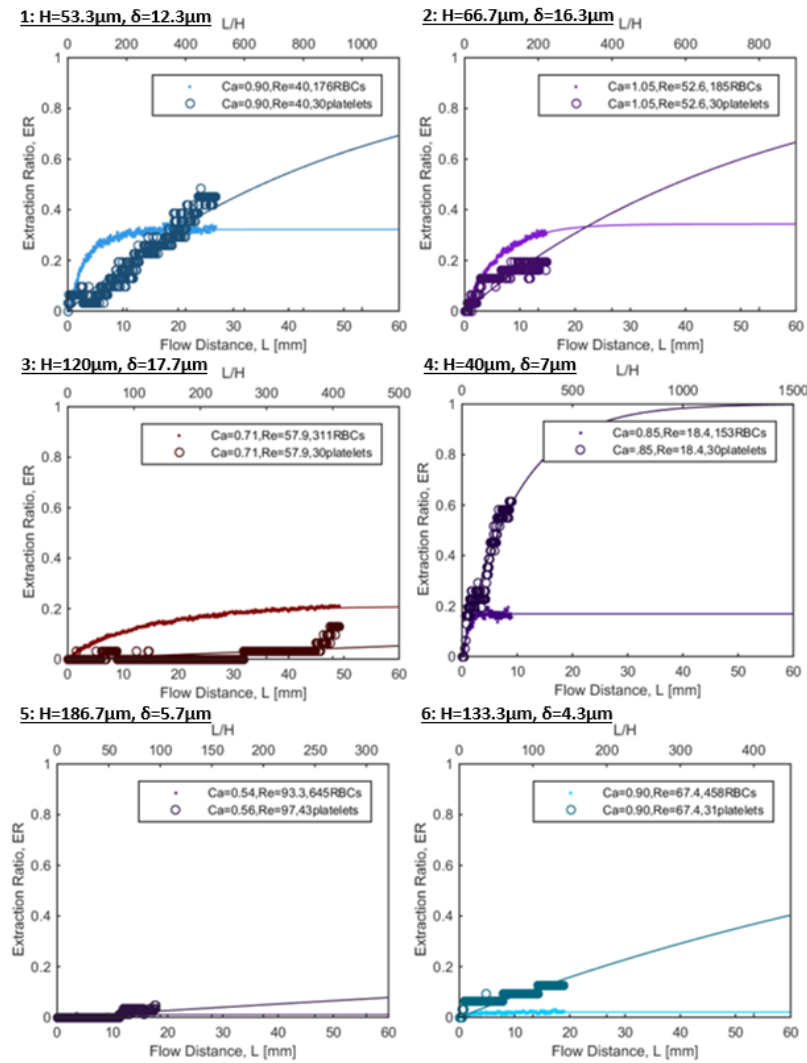


Figure 4-10. Extraction ratio of blood cells over flow distance for rectangular channel cases 1-6

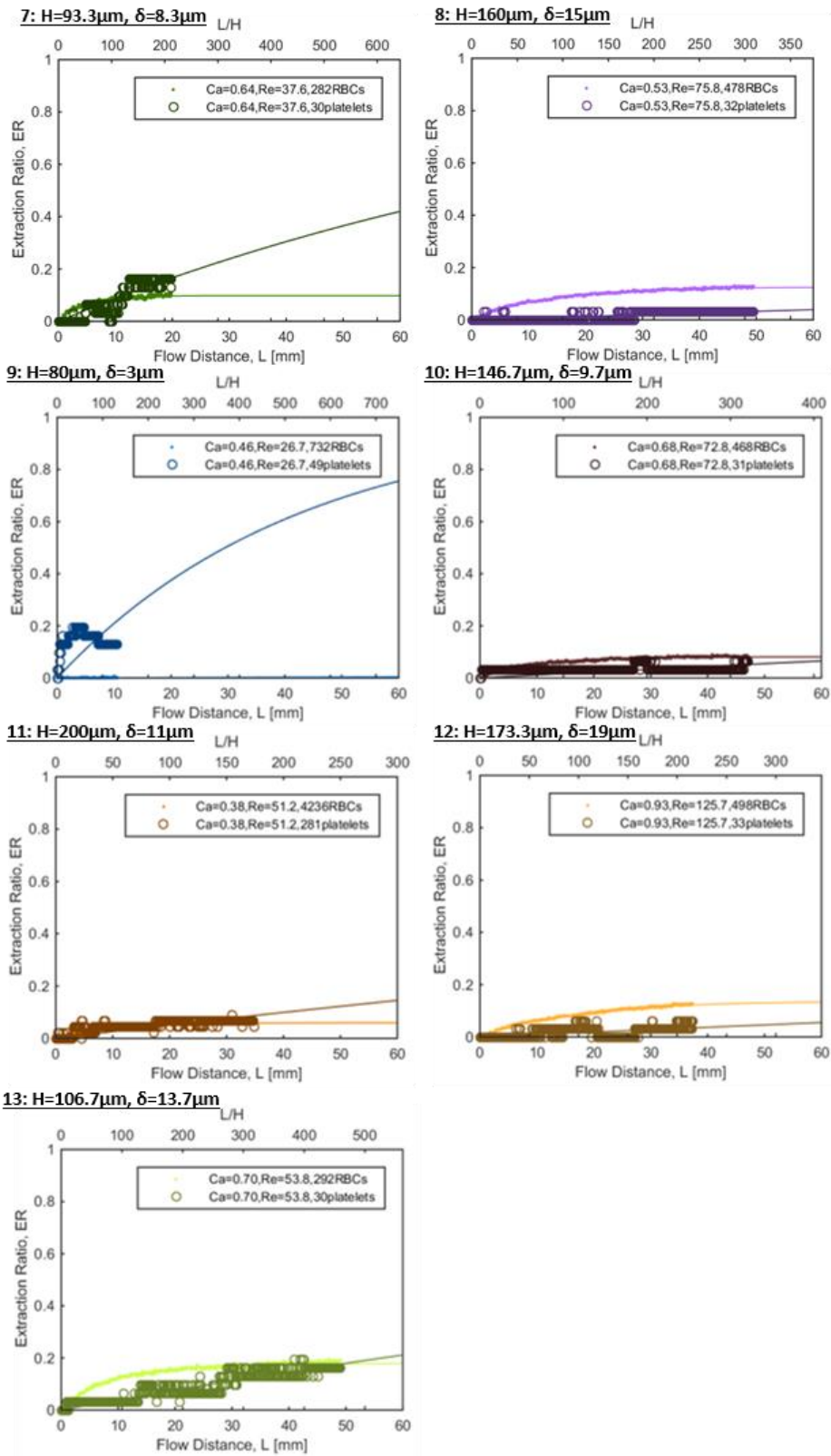


Figure 4-11. Extraction ratio of blood cells over flow distance for rectangular channel cases 7-13

In the figures, lighter colored small circular dots are for RBCs and darker colored stars are for platelets. Three cases are shown in Figure 4-12 with close-up view.

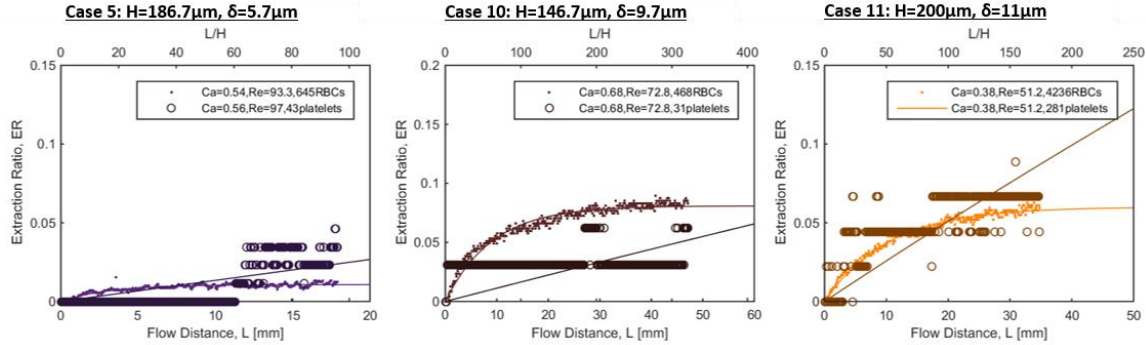


Figure 4-12. Close-up view of extraction ratio of blood cells over flow distance for 3 rectangular channel cases

The resulting ER curve parameters, ER_{eq} and L_{τ} , of each rectangular channel cases are listed in Table 4-6.

Table 4-6. Resulting ER curve parameters of each cases studied with rectangular channels

| Case No. | δ [μm] | D [μm] | d [μm] | No RBC | No Plt | ER_{eq} RBC | L_{τ} RBC [mm] | L_{τ} Plt [mm] | $L_{(ER=0.05)}$ RBC [mm] | $L_{(ER=0.05)}$ Plt [mm] |
|----------|----------------------------|---------------------|---------------------|--------|--------|---------------|---------------------|---------------------|--------------------------|--------------------------|
| 1 | 12.3 | 53.3 | 28.7 | 176 | 30 | 0.3217 | 3.5058 | 50.76 | 0.5922 | 2.6036 |
| 2 | 16.3 | 66.7 | 34.0 | 185 | 30 | 0.3433 | 6.3360 | 54.63 | 0.9973 | 2.8022 |
| 3 | 17.7 | 120.0 | 84.7 | 311 | 30 | 0.2098 | 14.3187 | 1112.7 | 3.8980 | 57.074 |
| 4 | 7.0 | 40.0 | 26.0 | 153 | 30 | 0.1688 | 1.1525 | 9.70 | 0.4048 | 0.4975 |
| 5 | 5.7 | 186.7 | 175.3 | 645 | 43 | 0.0107 | 3.0812 | 740.16 | ∞ | 37.965 |
| 6 | 4.3 | 133.3 | 124.7 | 458 | 31 | 0.0205 | 3.1551 | 116.24 | ∞ | 5.9623 |
| 7 | 8.3 | 93.3 | 76.7 | 282 | 30 | 0.0977 | 4.4751 | 110.21 | 3.2085 | 5.6530 |
| 8 | 15.0 | 160.0 | 130.0 | 478 | 32 | 0.1255 | 13.2715 | 1497.6 | 6.7442 | 76.817 |
| 9 | 3.0 | 80.0 | 74.0 | 272 | 30 | 0 | - | 42.57 | ∞ | 2.1836 |
| 10 | 9.7 | 146.7 | 127.3 | 468 | 31 | 0.0810 | 9.1322 | 882.88 | 8.771 | 45.286 |
| 11 | 11.0 | 200.0 | 178.0 | 654 | 44 | 0.0599 | 10.3973 | 382.74 | 18.717 | 19.632 |
| 12 | 19.0 | 173.3 | 135.3 | 498 | 33 | 0.1376 | 16.8866 | 1055.5 | 6.2708 | 54.140 |
| 13 | 13.7 | 106.7 | 79.3 | 292 | 30 | 0.1785 | 8.9568 | 252.80 | 2.9437 | 12.967 |

In all these results, the RBC extraction ratios closely match the fitted exponential line, but the match for platelets is rough due to its long L_τ . However, it was clear that the evolution of platelet extraction ratio is much slower than that of RBC extraction ratio for cases 3, 5, 8, 10, 11, and 12, which are the top right cases in Figure 4-6 with large channel diameters and sheath stream thicknesses. This result shows that platelet margination would be very slow when RBCs are spreading out a lot, due to the large sheath stream area. For case 9, which is the smallest sheath stream thickness case, no RBCs were lost into the sheath stream, as was the case for circular channels. Further analysis follows in the next section.

4.3.2.3 RBC Extraction Ratios

ER_{eq} of RBC of circular channels and rectangular channels are plotted over sheath to channel area ratio as shown in Figure 4-13; the area ratio is defined as $\frac{2\delta}{H}$ for rectangular channels, and $\frac{D^2 - (D - 2\delta)^2}{D^2}$ for circular channels.

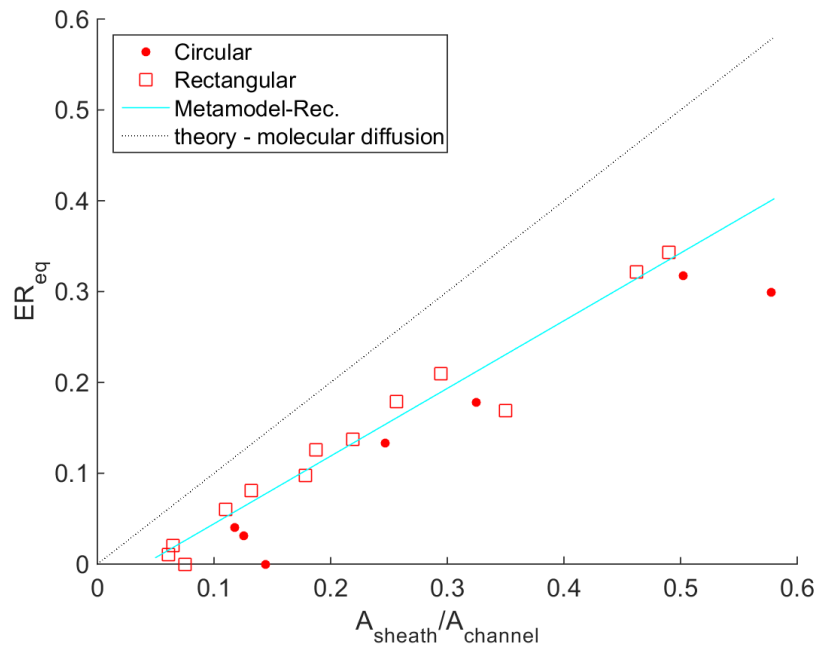


Figure 4-13. RBC ER_{eq} vs. area ratio of sheath to channel

This figure shows that ER_{eq} of RBC strongly depend on sheath to channel area ratio, and the trend is very similar for rectangular cases and circular cases. The linear fitted line of rectangular channel results, which is eventually used as the meta-model of RBC ER_{eq} , is also plotted together to compare the trend to the theoretical line of molecule diffusion.

For the molecule diffusion that purely relies on concentration gradient for diffusion, the ER_{eq} would be a linear function of the area ratio with slope of 1, and it would pass through the origin point. For the case of RBCs, the slope was less than 1, which is a preferable trend for the design space exploration of the proposed dialyzer with limited loss of blood cells into the sheath stream. The lower slope is because of the shear-driven migration behavior of deformable RBCs that tries to migrate towards the central area when it flows as a dense suspension. Thus, the equilibrium position of RBCs was determined as a balance of the tendency of RBCs to be away from the wall and the tendency to diffuse into the lower concentration region close to the wall.

The deviation of ER_{eq} from the fitted line is due to the finite particle size of RBCs. RBC diameter is $8.185 \mu\text{m}$, and the smallest sheath stream thickness studied was $3 \mu\text{m}$. Considering that the center point of RBCs was used to determine whether the RBC is in the sheath region or not, it is very hard for a RBC to stay in such a small thickness region no matter what the area ratio of sheath to channel is because of the wall-induced lift force.

The fitted line of RBC ER_{eq} does not pass through the origin point as is the case for molecular diffusion. For the dimensions that were studied in this research, the RBC sizes are comparable to the channel dimensions. Thus, for the cases that the area ratio is very small, the sheath stream thickness is also very small that RBCs cannot stay in the sheath region. However, if the

study space expands to much larger channel dimensions, the fitted line is expected to pass closer to the origin point.

The length constant, L_τ , of RBC was found to be related to the channel size and the area ratio of sheath to channel in a scaled form, $L_\tau \frac{a^2}{D^3}$. The scaling can be derived from the diffusion equation when the blood cell migration is mainly driven by shear-induced diffusivity [96]. The relations are shown in Figure 4-14.

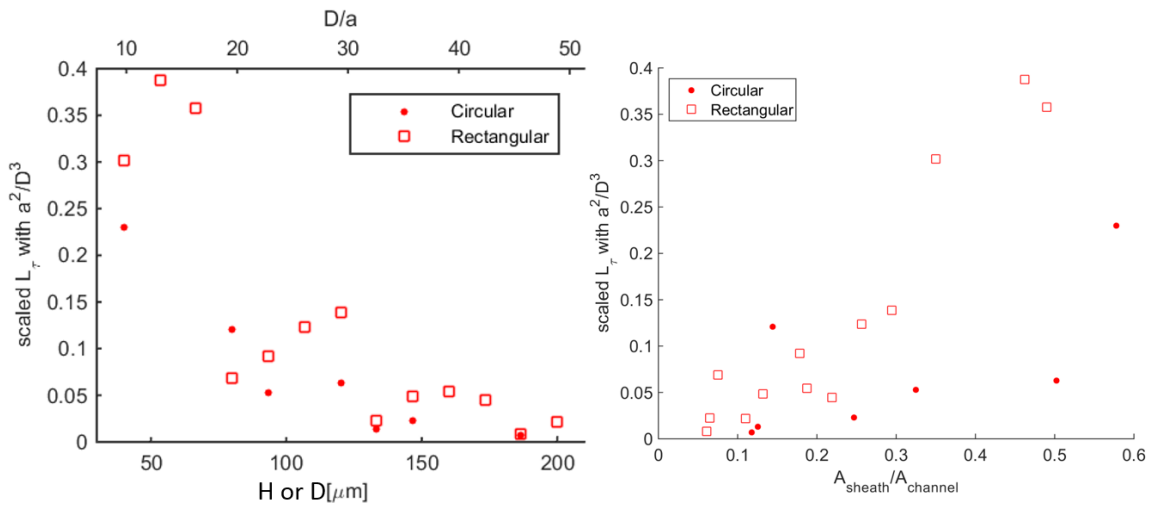


Figure 4-14. RBC scaled length constant $L_\tau \frac{a^2}{D^3}$ vs. channel size and area ratio of sheath to channel

This figure shows that scaled length constant, $L_\tau \frac{a^2}{D^3}$, has quadratic relations with channel size and the area ratio of sheath to channel. The trend is similar for both rectangular cases and circular cases. However, there are some deviations especially for the relation to the area ratio of sheath to channel. More data from various channel dimensions will help identify a clearer trend of the length constant. Slightly different trend of the circular cases and rectangular cases may be adjusted by adding a fitting constant that can be applied to match the rectangular channel results to the circular channel results more closely once more data is available.

Length constants of RBCs are plotted against channel size as shown in Figure 4-15 for more intuitive understanding.

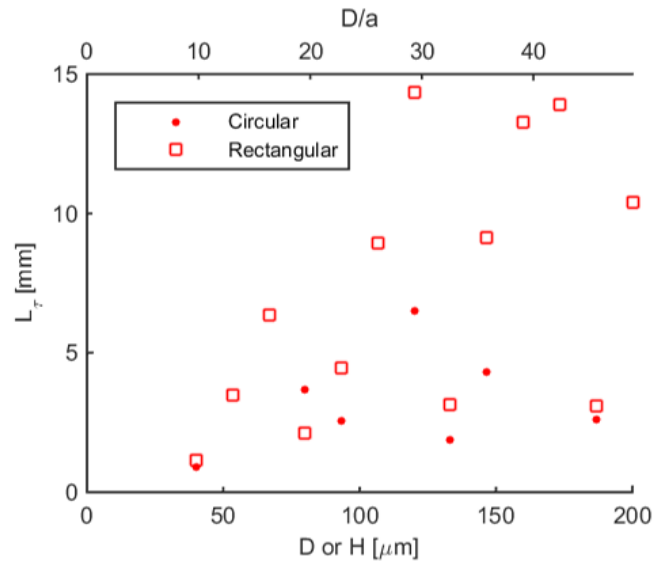


Figure 4-15. RBC length constant L_τ vs. channel size

This figure shows the general trend of increasing length constant with increasing channel size. Larger channel size increases the radial distance to travel to reach the sheath area for RBCs to migrate; thus, length constant, which is a measure of how long it takes to reach equilibrium, increases.

4.3.2.4 Platelet Extraction Ratios

Platelets are expected to equilibrate close to the wall because of the platelet margination behavior. Thus, ER_{eq} was set to 1 for platelets, and only L_τ is analyzed. Figure 4-16 shows the plots of scaled L_τ vs. the area ratio of sheath to channel and L_τ vs. channel size.

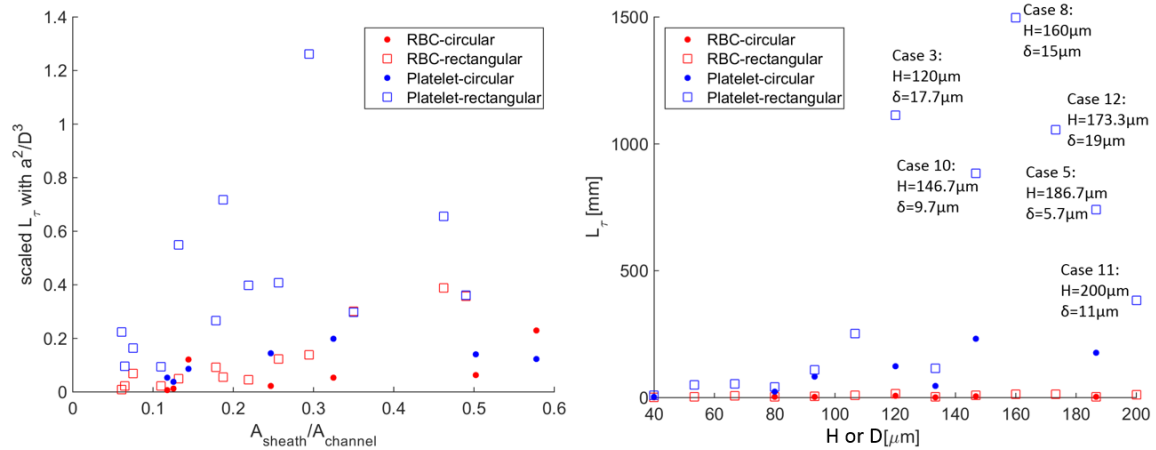


Figure 4-16. The relations of length constant L_τ vs. channel size and the area ratio of sheath to channel

For comparison, RBC results are plotted together; RBCs are in red markers and platelets are in blue markers. Circular dots represent circular channel case results, and empty rectangles represent rectangular channel case results. This figure shows that the length constants of platelet extraction ratios are much longer than those of RBCs. It was expected from the scaling, which is derived from the diffusion equation when the blood cell migration is mainly driven by shear-induced diffusivity [96], because the margination length is inversely related to the square of particle size, and platelets are much smaller than RBCs. Thus, many simulation results were long enough to show the clear trend of RBC extraction ratios, but not platelet extraction ratios. Platelet L_τ values may not be highly accurate, but the values were analyzed as-is. No clear trend was found for the platelet length constant, so the general trend was analyzed.

The right plot of Figure 4-16 is marked with the six cases with exceptionally high values of L_τ which were cases 3, 5, 8, 10, 11, and 12. These are the cases located on the upper and right corner of the simulation study space, as shown in Figure 4-6, with large channel size and large sheath stream thickness. Larger channel size and larger sheath stream thickness increase the flow distance to reach sheath region; thus, length constant increases. This trend is also in

agreement with the margination length scale that was found to be in a linear relation with the cubic of channel size.

4.4 Meta-Model Creation

In this section, meta-models of RBC and platelet extraction ratio curves are created based on the simulation results. The outline of the first research question is shown in Figure 4-17 in order to describe where this section fits in the big picture.

RQ1: Migration of cells in non-uniform suspension flow

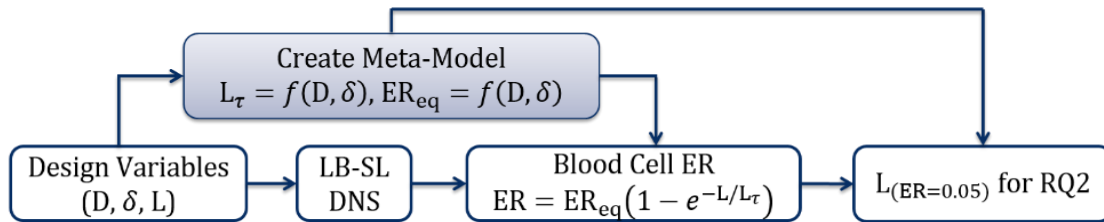


Figure 4-17. Outline of research question 1

The previous section used the LB-SL method to study rectangular channel cases having 13 different dimensions and circular channel cases having 8 different dimensions. Blood cell extraction ratio evolutions over flow distance were fitted to exponential curves, and L_τ and ER_{eq} were found for each case. $L_{(ER=0.05)}$, the length over which the extraction ratio would be 5%, was also found. For actual applications, including dialyzer design, this is the parameter that a designer would be most interested in. (5% was chosen arbitrarily to demonstrate the use of meta-models.) $L_{(ER=0.05)}$ is utilized in Chapter 5 to explore the design space of the proposed dialyzer, which will lose less than 5% of blood cells while filtering out middle sized waste molecules. In this section, the RBC meta-models of L_τ and ER_{eq} are created as functions of channel size and sheath stream thickness so that it can be calculated without the expensive LB-

SL based direct numerical simulation. Meta-model of platelet was not created since no clear trend was found from the simulation results. Since results of circular channels and rectangular channels were similar based on the area ratio and more results are available for rectangular channels, the rectangular channel results are used for the meta-model creation. $L_{(ER=0.05)}$ is also calculated for the whole parametric study region of $40\mu m < D (H) < 200\mu m$ and $3\mu m < \delta < 19\mu m$ for RBCs and compared to platelet's $L_{(ER=0.05)}$.

4.4.1.1 Meta-Model of RBC Extraction Ratio

ER_{eq} was found to strongly depend on sheath to channel area ratio as was shown Figure 4-13. A linear fitted meta-model is created for rectangular cases with $R^2 = 0.959$ as shown in the following equation.

$$ER_{eq} = c_1 + c_2 \frac{A_{sheath}}{A_{channel}} \quad (4-4)$$

The constants of the meta-model are listed in Table 4-7.

Table 4-7. Constants of the meta-model of ER_{eq}

| | |
|-------|--------------------|
| c_1 | -0.030058805096939 |
| c_2 | 0.744869626007254 |

The scaled length constant, $L_\tau \frac{a^2}{D^3}$, was found to be in a quadratic relation with the channel size and the area ratio of sheath to channel. Since case 9 did not lose any RBC into the sheath stream, $ER_{eq} = 0$, and L_τ can be any value. Thus, $L_\tau = 2.1\text{mm}$ is arbitrarily chosen to generate a good fit ($R^2 = 0.9968$) with the meta-model in a quadratic function of both channel height, H , and area ratio $\frac{A_{sheath}}{A_{channel}}$ as shown in Figure 4-18.

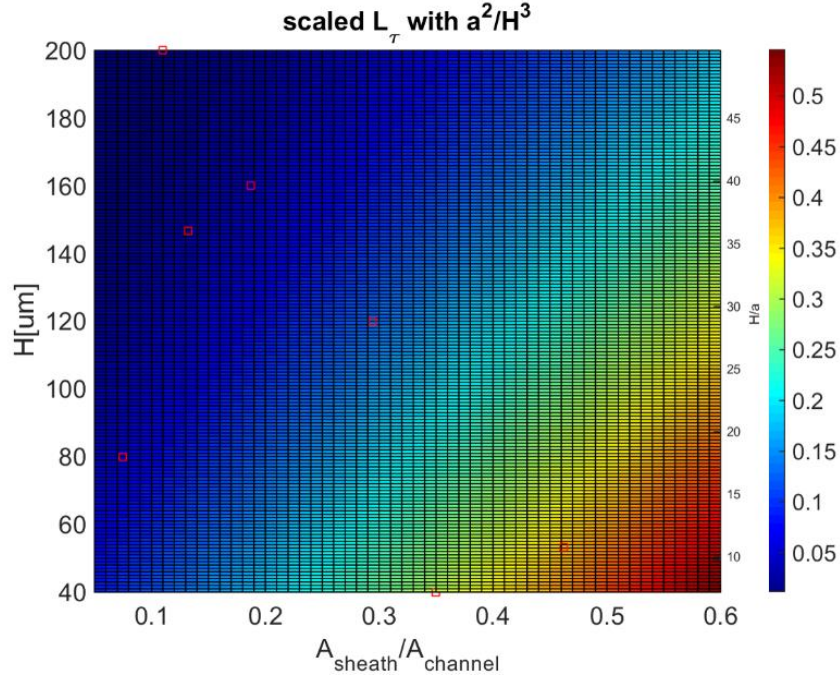


Figure 4-18. Meta-model of RBC $L_\tau \frac{a^2}{H^3}$ as a function of channel height and area ratio of sheath to channel

The meta-model equation of L_τ is shown below.

$$L_\tau \frac{a^2}{H^3} = c_1 + c_2 H + c_3 \frac{A_{\text{sheath}}}{A_{\text{channel}}} + c_4 H \frac{A_{\text{sheath}}}{A_{\text{channel}}} + c_5 H^2 + c_6 \left(\frac{A_{\text{sheath}}}{A_{\text{channel}}} \right)^2 \quad (4-5)$$

The constants of the meta-model are listed in Table 4-8.

Table 4-8. Constants of the meta-model of L_τ

| | |
|-------------------------|----------------------|
| a | 4.0925 μm |
| c_1 | 0.106336564709579 |
| c_2 | -0.001264030993316 |
| c_3 | 0.665558658171565 |
| c_4 | -0.003227034490143 |
| c_5 | 0.000003946954797 |
| c_6 | 0.448982443972123 |

For easier interpretation, the scaled L_τ plot shown in Figure 4-18 is converted to the plot of L_τ as shown in Figure 4-19.

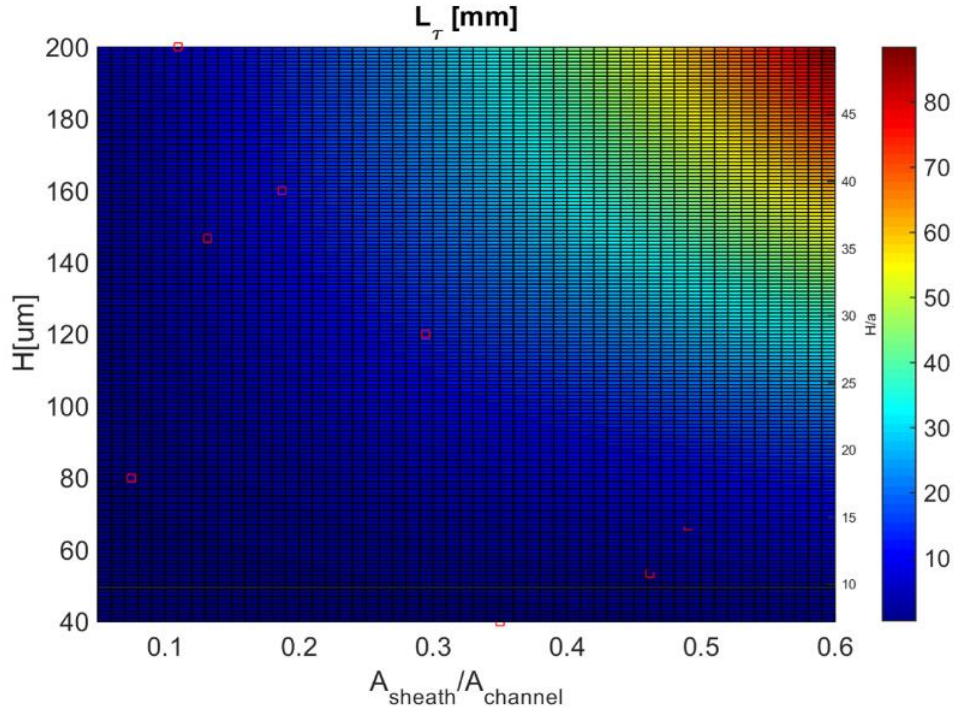


Figure 4-19. Meta-model of RBC L_τ in function of channel height and area ratio of sheath to channel for rectangular channels

As was shown in the results section, Figure 4-19 shows that larger channel size and larger sheath stream area increase L_τ , meaning that it will increase the flow distance to reach equilibrium.

These meta-models were created based on the results of rectangular channel and can be applied for circular channels as well with the area ratio chosen accordingly.

4.4.1.2 $L_{(ER=0.05)}$ of RBCs and Platelets

With the meta-models of L_τ and ER_{eq} , the extraction ratio of RBCs can be calculated for any given channel dimensions based on equation (4-3): $ER = ER_{eq}(1 - e^{-L/L_\tau})$. By setting

ER = 0.05 for the given channel size and sheath stream thickness, $L_{(ER=0.05)}$ can be calculated for rectangular and circular channels as shown in Figure 4-20.

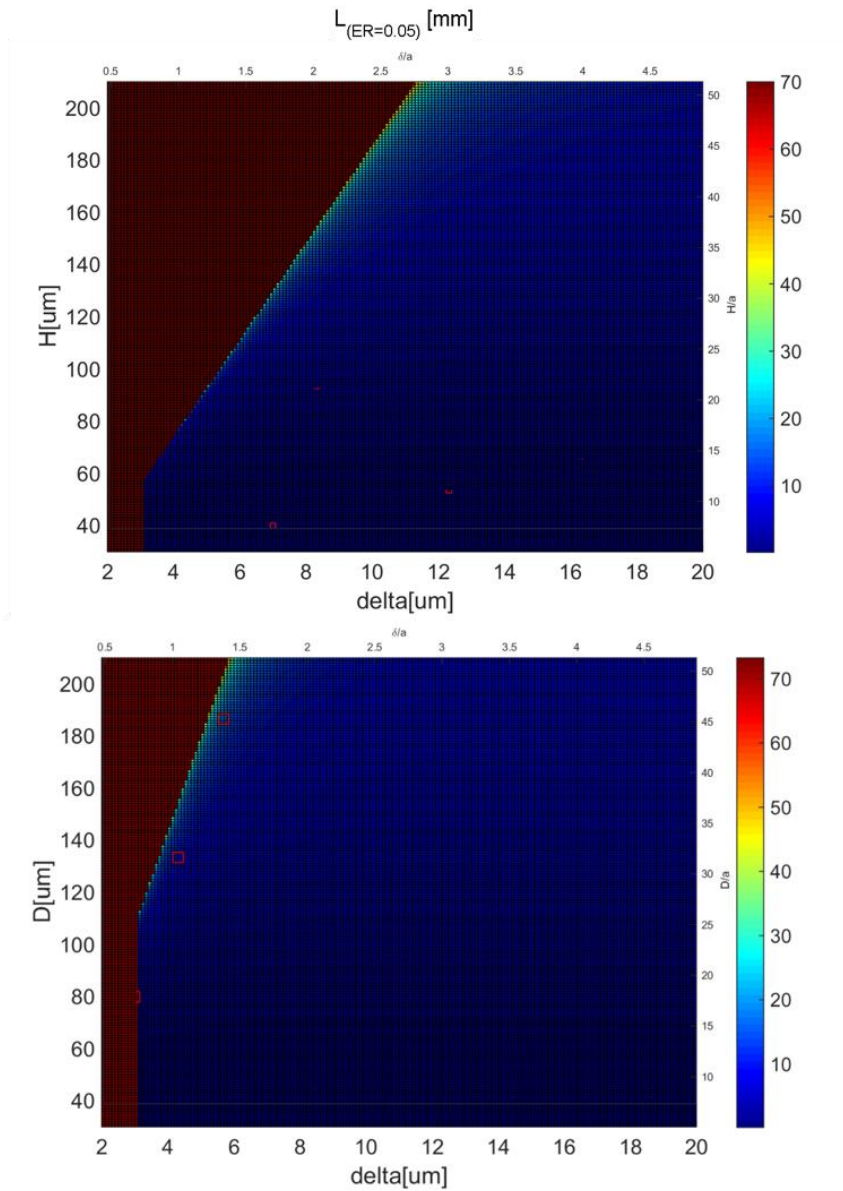


Figure 4-20. Meta-models of RBC $L_{(ER=0.05)}$ as functions of channel size and sheath stream thickness for rectangular channels (top) and circular channels (bottom)

Dimensionless scales D/a and δ/a are also shown on the right and top axes. For the case that $ER_{eq} < .05$, $L_{(ER=0.05)}$ would be infinite. In such case, $L_{(ER=0.05)}$ was set to 70mm for Figure 4-20 to aid visualization. Circular channels are of main interest for the design space exploration

of the proposed dialyzer, and rectangular channel's $L_{(ER=0.05)}$ is presented together as a reference. For rectangular channels, it should be noted that it is applicable for a channel that is wide enough to neglect the sidewall effect since the rectangular channel cases represent infinitely wide channels. This figure shows that $L_{(ER=0.05)}$ of RBC increases for large channel size and small sheath stream thickness. Since longer $L_{(ER=0.05)}$ is preferred for the design space exploration of the proposed dialyzer so that sufficient middle molecule removal can be achieved, increasing channel size and reducing sheath stream thickness will expand the design space of the feasible design space of the proposed dialyzer concerning RBC loss.

2D plots of $L_{(ER=0.05)}$ meta-models are compared with the circular and rectangular channel cases simulation results, as shown in Figure 4-21.

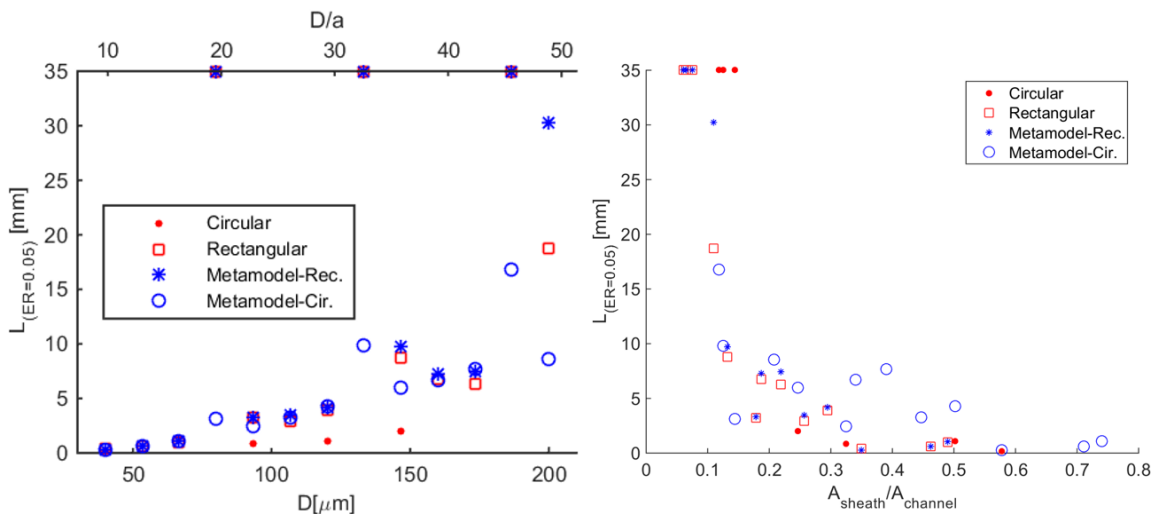


Figure 4-21. RBC $L_{(ER=0.05)}$ vs. channel size and area ratio of sheath to channel

The DNS results are in red markers, and meta-model predictions are in blue markers. For the case that $ER_{\text{eq}} < .05$, $L_{(ER=0.05)}$ was set to 35mm for Figure 4-21 to aid visualization. The meta-model prediction shows a close match for both circular and rectangular channel case

results. It shows that the meta-model created based on rectangular channel results can be used for predicting the RBC migration behavior in circular channels.

$L_{(ER=0.05)}$ of platelets are plotted with that of RBCs in Figure 4-22 in order to compare the values and choose the right length for the design space exploration.

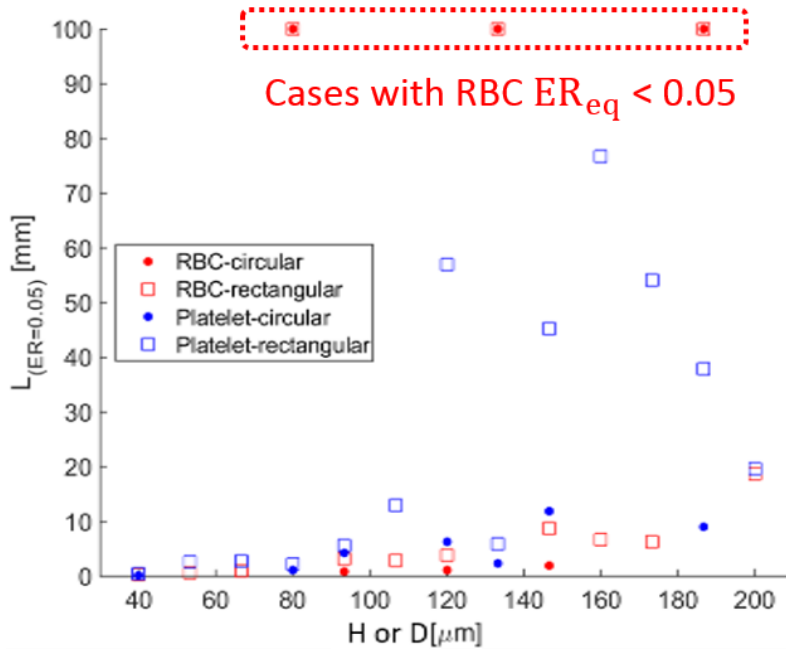


Figure 4-22. $L_{(ER=0.05)}$ vs. channel size

RBCs are in red markers and platelets are in blue markers. For the case that $ER_{eq} < .05$, $L_{(ER=0.05)}$ was set to 100mm for Figure 4-22, to aid visualization of the result. This figure shows that $L_{(ER=0.05)}$ of RBC is generally shorter than that of platelets. It is because L_{τ} of RBCs are always shorter than that of platelets because of the different length scale, as was described with Figure 4-16, due to the different particle size of RBCs and platelets. This figure shows the same trend as the right plot of Figure 4-16 showing exceptionally large platelet $L_{(ER=0.05)}$ for large channel size cases. $L_{(ER=0.05)}$ of platelet becomes shorter than that of platelets when RBC $ER_{eq} < .05$; thus, $L_{(ER=0.05)}$ of RBC would be infinite as shown with the three cases in Figure

4-22. This means that when a designer explores a design space, the designer needs to consider $L_{(ER=0.05)}$ of RBCs when ER_{eq} of RBCs is larger than 0.05, but must consider $L_{(ER=0.05)}$ of platelets when ER_{eq} of RBCs is smaller than 0.05, since the shorter length of the two should be chosen to prevent both RBC and platelet loss.

It should be noted that all cases were studied with initially uniformly suspended platelets in the blood stream region. In reality, the blood stream is injected to the micro-fluidic channel to flow with the sheath stream in direct-contact. Before the injection, the blood flowed through the channel without the sheath stream, and the platelets would have been already margined to some extent by the time the blood entered this channel. Thus, the platelet extraction ratio is expected to be higher in real situations, and it would depend on the injection channel length. However, for the design space exploration of the proposed dialyzer, the injection channel length would be in the range of only a few centimeters. Considering that the platelet's length constants are in the range of 100 cm, using the simulation results for the design space exploration of the proposed dialyzer is acceptable.

4.5 Summary

In this chapter, the effect of hematocrit, Re , channel size, sheath stream thickness, flow distance, and channel geometry on blood cell extraction ratio were studied. It was found that the realistic 40% HCT case results would be different from the 20% or 30% HCT cases; thus 40% HCT cases were studied with LB-SL method for later studies. Extraction ratio curves were found to fit to exponential curves when plotted against flow distance, and it was also confirmed that Re would not be an important parameter for the ranges studied. The RBC extraction ratio curve's length constant was found to depend on the channel size and the area ratio of sheath to

channel. RBC ER_{eq} was found to depend on the area ratio of the sheath to the channel. The platelet extraction ratio was analyzed based on the assumption of $ER_{eq} = 1$, due to the platelet margination behavior, and the length constants of platelet extraction ratio were found to be much larger than those of the RBC extraction ratio. The effect of channel geometry is considered in the area ratio of sheath to channel; thus, the meta-model of rectangular channel cases matched the results of circular channel cases as well.

$L_{(ER=0.05)}$ was found, from both the LB-SL method and the meta-model, in order to answer the first research question: What are the conditions that retain blood cells in the blood stream when it flows with sheath fluid in a micro-fluidic channel? The result showed that the RBC extraction ratio would be limited when the channel size is large and sheath stream thickness is small. For platelets, the LB-SL results showed that $L_{(ER=0.05)}$ of platelets would always be longer than that of RBCs, except for the case that $L_{(ER=0.05)}$ of RBCs is infinite due to $ER_{eq} < .05$. Thus, $L_{(ER=0.05)}$ of platelets would be of concern when ER_{eq} of RBCs is less than 0.05, and $L_{(ER=0.05)}$ of RBCs would be of concern for other cases for designing a micro-fluidic channel that limits blood cell loss. However, considering the real situation where the platelets would have already margined by the time the blood enters the micro-fluidic channel to flow with sheath fluid, this result would not reflect the real situation because the simulations were conducted with initially uniformly suspended RBCs and platelets. Thus, platelet extraction ratios are expected to be higher than the simulation results show, and the differences would increase with longer injection channel length. These findings will be utilized in Chapter 5 to identify the feasible conditions that will retain blood cells in the blood stream while providing efficient waste removal in the proposed new dialyzer design.

CHAPTER FIVE

DESIGN SPACE EXPLORATION OF A DIALYZER

This chapter explores the design space of a dialyzer in order to address the second research question: What is the feasible design space of the proposed dialyzer with improved waste removal rate while retaining blood cells? A tubule model is created in Comsol to study the waste molecule diffusion behavior in each membrane tubule. The tubule length is determined based on the results of Chapter 4 to limit blood cell loss. Then, to predict the performance of a dialyzer that is made of a number of tubules, a hemodialysis system model was used. Based on the resulting waste level, dialyzer size, and the amount of sheath and dialysate usage, important design variables and feasible design space of the proposed dialyzer are identified.

5.1 Proposed Dialyzer Design

This work proposes a new dialyzer design that could increase the waste removal rate of middle molecules and reduce bioincompatibility. The new configuration is proposed in Chapter 1. The details are explained again in this section.

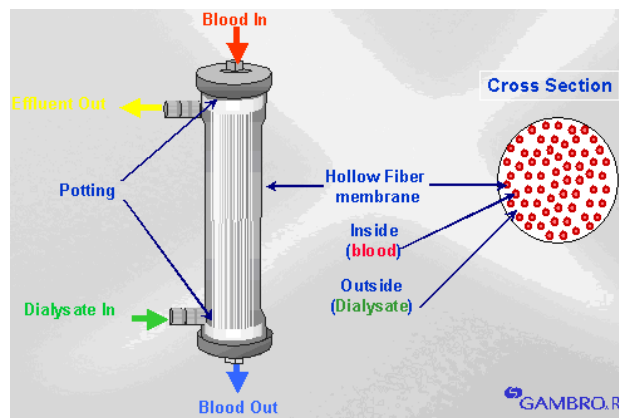


Figure 5-1. A typical dialyzer (Gambro Training Manual)

As shown in Figure 5-1, a typical dialyzer takes the shape of a long cylinder and houses porous hollow fiber tubules, with spacing between the tubules. The blood flows through each tubule while the dialysate, the cleaning fluid, flows countercurrent in the spacing between the tubules. The fiber tubules are made of a semi-permeable membrane. Due to the concentration gradient between the blood and dialysate, waste in the blood diffuses into the dialysate across the semi-permeable membrane. Then, the cleaned blood returns to the body, and used dialysate is disposed. In the new dialyzer, instead of only blood flowing through the tubule, sheath fluid is added. A close-up view of each tubule of the proposed dialyzer is shown in Figure 5-2.

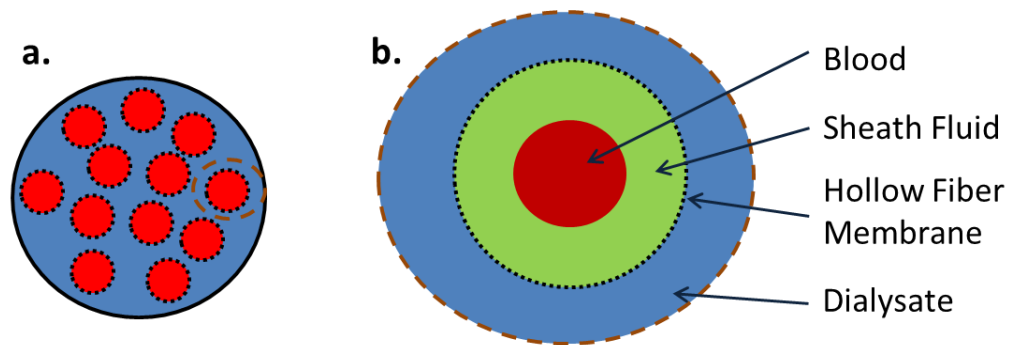


Figure 5-2. a. Cross-section of a typical dialyzer and b. close-up view of proposed configuration

The blood stream is surrounded by sheath fluid so that blood-membrane contact is completely avoided. The sheath fluid will be a plasma-like fluid so that the blood is not contaminated in case any mixing occurs. Waste diffusion happens simultaneously in two places; 1. from blood to sheath fluid and 2. from sheath fluid to dialysate. Middle molecules will easily diffuse into sheath fluid because no membrane is blocking the way. The proposed design can result in a system very similar to typical hemodialysis systems, but with improved waste filtration rate.

5.2 Consol Model for the Study of Molecule Diffusion Behavior

For the design space exploration of the proposed dialyzer design, it is important to understand diffusion behaviors of different molecules so that good proteins can be retained and waste molecules can be filtered in the blood stream. Because of their small size scale, the diffusive behaviors are studied in depth using the Consol model separate from the blood cell migration study based on LB-SL method.

Filtration rates (clearance) of different molecules for different filtration methods including kidneys are shown in Figure 5-3.

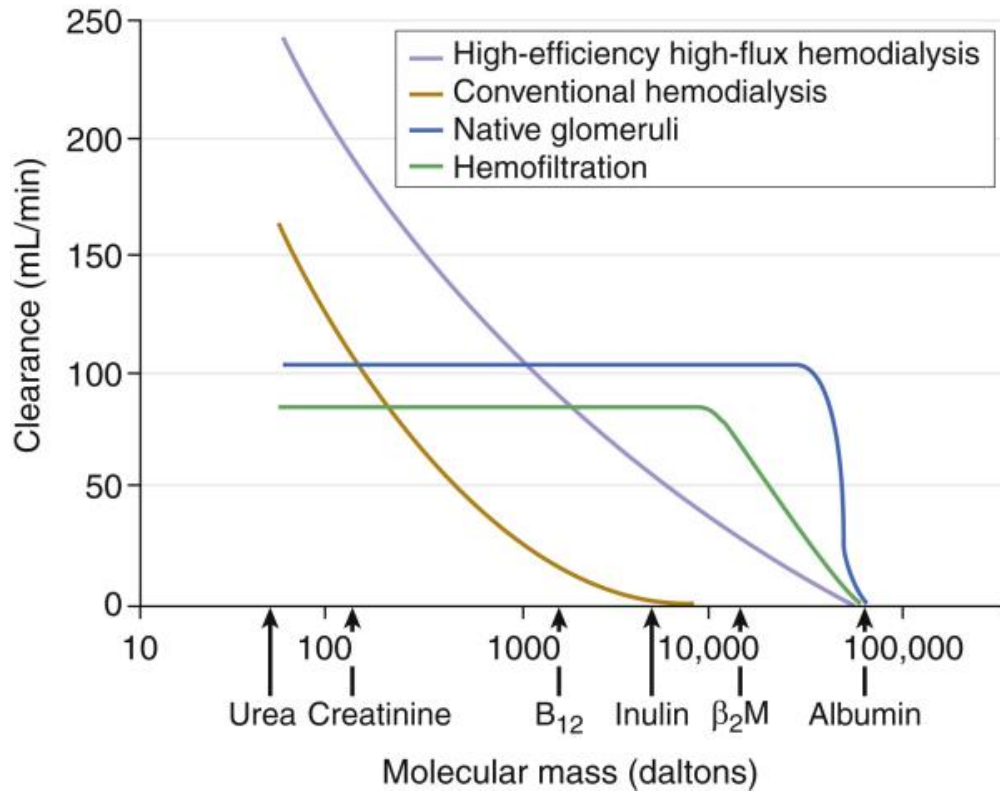


Figure 5-3. Clearance (filtration rate) vs. molecular mass for different filtration methods [97]

Albumin (67 kDa) is a good protein that should be retained in the blood stream. The kidneys (native glomeruli in Figure 5-3) filter out all waste molecules while not losing Albumin.

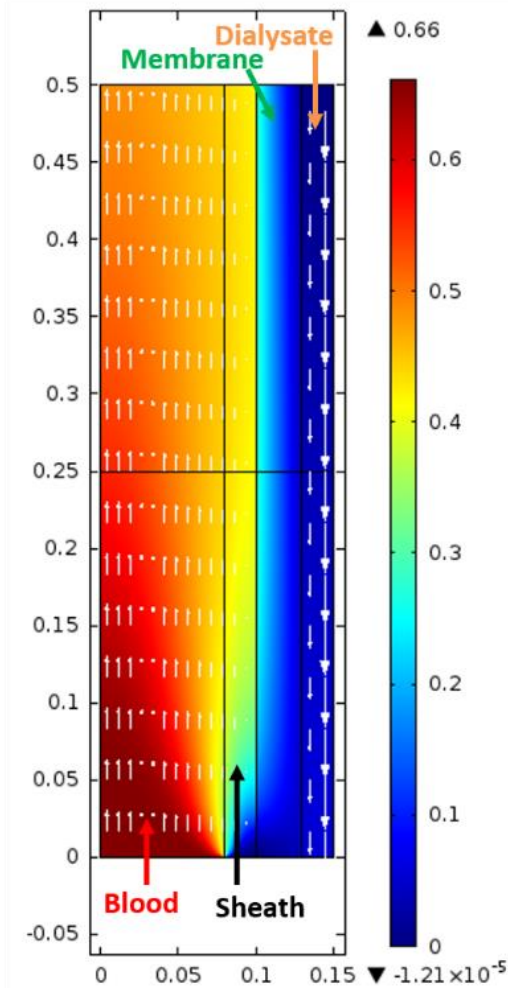
Commonly used low flux dialyzers filter out only small molecules such as urea and Creatinine. Modern high flux dialyzers perform a little better and remove some of middle molecules such as β_2 -microglobulin (11.8 kDa), but the efficiency does not reach that of kidneys. β_2 -microglobulin is one of the largest middle molecules that are not efficiently filtered out with existing dialyzers, and Albumin is one of the smallest proteins that should be retained. Natural kidneys' filtration cut-off (~45 kDa [98]) exists between the two molecules. Thus, the two molecules, Albumin and β_2 -microglobulin, are considered for the design space exploration. In addition, the diffusion behavior of urea is studied together. Although filtration of urea is not the main objective of the proposed dialyzer design, urea will be filtered together with other middle molecules, and it is valuable to understand how small waste molecules like urea are filtered using the proposed design.

5.2.1 Model Set-up

The diffusion behaviors of Albumin, β_2 -microglobulin, and urea are studied based on convection and diffusion physics for a tubule based on Dialysis module in Comsol (model ID: 258. Separation through dialysis). The calculation of molecule transport is based on only diffusion and convection. Because it is based on transport of diluted species, diffusion of different molecules are assumed to be independent of each other. Thus, the simulation results are the same whether the three molecules are studied together or separately.

The model is created in 2 dimensions, since the micro-fluidic channel is axis-symmetric. Figure 5-4 shows the model in both 2D and 3D views with concentration field and flow velocity (arrow).

(a) 2 D view



(b) 3 D view

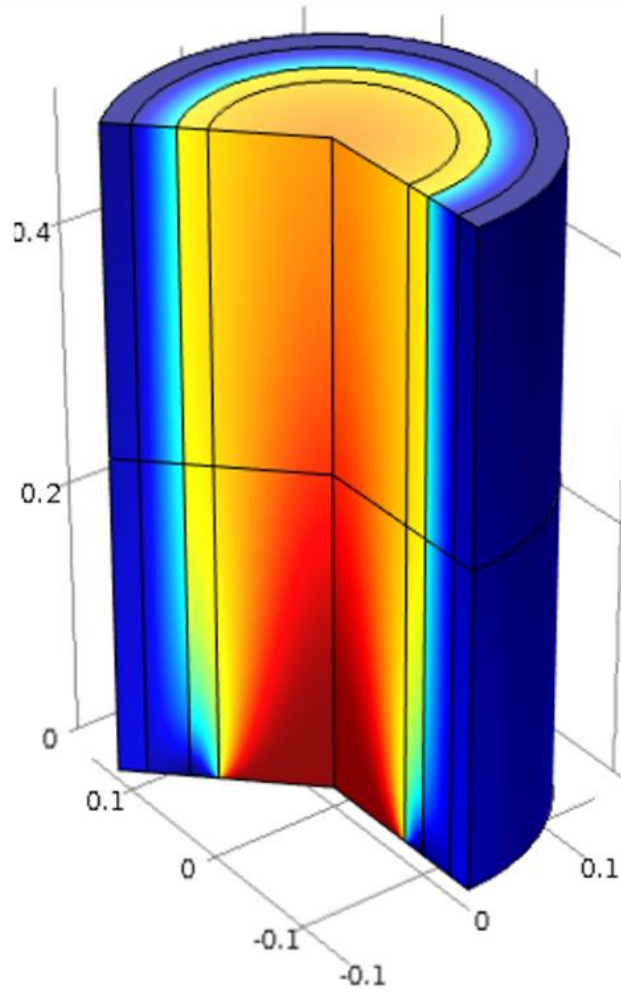


Figure 5-4. Comsol model in 2D and 3D with concentration field and flow velocity (arrow)

The model is divided into four regions in the radial direction. The four regions from the center of the tubule are blood, sheath, membrane, and dialysate. The model is divided into 2 regions in the axial direction because of the mirror geometry used for easier meshing. As shown with velocity arrows, the blood and sheath flows from the bottom inlet to the top outlet, and dialysate flows in the counter-current direction (top to bottom). It is assumed that there is no flow in the membrane, and waste molecules diffuse only based on diffusion, not convection. The blood stream in the center enters with initial concentration of Albumin, β_2 -microglobulin,

and urea. The sheath and dialysate stream enter with zero concentration. Figure 5-4 shows the molecule transport from the blood side to the sheath side and to the dialysate side as the flow continues.

The fluid fields are prescribed with fully developed laminar parabolic velocity profiles for both inside and outside the hollow fiber, and membranes are modeled to simulate discontinuity of concentration based on a membrane tubule model [99]. For the blood and sheath that flows inside the tubule, a simple Hagen-Poiseuille flow condition was assumed. For the dialysate that flows outside the tubule, a hexagonal-shaped unit cell of a tubule assembly is approximated with a dotted circle as shown in Figure 5-5.

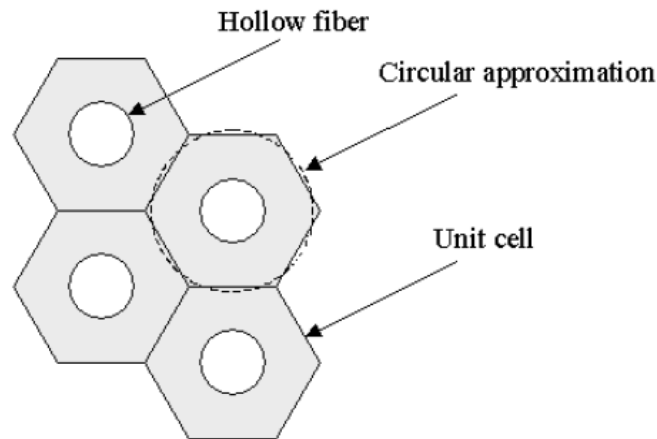


Figure 5-5. Hexagonal-shaped unit cell of the fiber assembly (Comsol Document - model ID: 258. Separation through dialysis)

This figure shows the dialysate stream region in grey with dotted circle the dialysate's position of maximum velocity in the axial direction. In addition to the circular approximation, the axial length is scaled to simplify the calculation to avoid excessive amounts of elements and nodes because of the much longer axial length of a tubule (~25 cm) compared to the diameter (~450 μm). The resulting velocity profile equations are shown below.

$$v_z^i = \frac{v_i}{scale} \left(1 - \left(\frac{r}{R_1} \right)^2 \right) \quad (5-1)$$

v_z^i is the flow velocity of the blood and the sheath stream, v_i is the maximum velocity inside the tubule, r is the radial coordinate, and R_1 is the inner radius of the tubule.

For the calculation of the dialysate fluid field, a momentum balance over a thin cylindrical shell is integrated twice due to the circular approximation [99].

$$v_z^d = \frac{v_d}{scale} \frac{(r^2 - R_2^2 - 2R_3^2 \log(r/R_2))}{(r^2 - R_2^2 - 2R_3^2 \log(R_3/R_2))} \quad (5-2)$$

v_z^d is the flow velocity of the dialysate stream, v_d is the maximum velocity of the dialysate (at the circle in Figure 5-5), R_2 is the outer radius of the tubule (membrane), and R_3 is the radial coordinate of the approximated circle.

Molecules are assumed to dissolve into the membrane and to rely only on diffusion for transport in the membrane. The interface condition is modeled with the dimensionless partition coefficient, K . The partition coefficient is defined as the ratio of the concentrations in two phases which are in equilibrium with one another [100]. It is a measure of the different solubility in the two phases, and it is often used as a coefficient that determines the boundary conditions of phase boundaries for modeling diffusion through two phases [101-103]. This model also used the partition coefficient to model the discontinuity of concentration at the boundary by setting the ratio of concentration on the membrane to liquid side as shown in the equation below.

$$K = \frac{c_{mem}}{c_{liq}} = \frac{c_b}{c_a} = \frac{c_c}{c_d} \quad (5-3)$$

c_a , c_b , c_c , and c_d are the concentrations at the interface of the membrane at the liquid side (inside tubule), membrane (inside and membrane interface), membrane (membrane and outside interface), and liquid side (outside tubule), respectively. To get continuous flux at the phase boundary, a special type of boundary based on a stiff-spring model is applied. Inward flux equations are listed in Table 5-1 for each of the membrane boundaries.

Table 5-1. Inward flux equations at the membrane boundaries

| Domain | Inward Flux at Boundary |
|-----------------------------|---|
| Sheath | $(-D_s \nabla C_s + C_s \mathbf{u}) \cdot \mathbf{n} = M(C_m - K \times C_s)$ |
| Membrane (sheath) | $(-D_m \nabla C_m) \cdot \mathbf{n} = M(K \times C_s - C_m)$ |
| Membrane (dialysate) | $(-D_m \nabla C_m) \cdot \mathbf{n} = M(K \times C_d - C_m)$ |
| Dialysate | $(-D_d \nabla C_d + C_d \mathbf{u}) \cdot \mathbf{n} = M(C_m - K \times C_d)$ |

C_s , C_m , and C_d are the concentration in each domain: sheath, membrane, and dialysate, respectively. M is a nonphysical velocity large enough to let the concentration differences in the brackets approach zero to satisfy equation (5-3).

During a typical dialysis session, water is removed from the blood stream to the dialysate side through ultra-filtration. In this study, water removal is neglected for simplification. In reality, the water removal may lead to complex streamline and enhanced migration of blood cells and molecules. The water removal effect may be cancelled if the pressure drop ratio of sheath to blood is increased to make the total flow velocity profile similar to Poiseuille flow even with the ultra-filtration. If this proposed dialyzer is used after a typical hemodialysis treatment session to remove more middle molecules, then water is already

removed, so it is not a concern. Thus, the simplified model can still guide the design space exploration without too much of complication.

5.2.2 Relevant Variables and Parameters

Relevant variables and parameters for the study of waste diffusion behavior in a dialyzer tubule are listed in Table 5-2.

Table 5-2. Relevant variables and parameters for the study of waste diffusion behavior

| | Symbol | Study Range |
|---|------------------|--------------------------------------|
| Tubule Inner Diameter | D | 40-700 μm |
| Sheath Stream Thickness | δ | 3-17.7 μm |
| Membrane Thickness | tM | 35 μm |
| Dialysate Stream Thickness | tD | 20-110 μm |
| Axial Length | L | 0.16-250 mm |
| Albumin Stagnant Diffusivity | D_{0a} | 3.53e-11 m^2/s [104] |
| β_2-microglobulin Stagnant Diffusivity | D_{0B} | 9.15e-11 m^2/s [104] |
| Urea Stagnant Diffusivity | D_{0u} | 1.69e-09 m^2/s [104] |
| Albumin Initial Concentration | C_{0a} | .0061 Mol/m^3 [98] |
| β_2-microglobulin Initial Concentration | C_{0B} | .0027 Mol/m^3 [105] |
| Urea Initial Concentration | C_{0u} | 34.9 Mol/m^3 [106] |
| Maximum Mesh Size | h_{max} | 0.2-3.2 μm |
| Scale | scale | 1-3000 |
| Diffusivity Enhancement Ratio | r_{Dp} | 2.5 |
| Blood Maximum Velocity | v_i | 5-60 mm/s |
| Dialysate Maximum Velocity | v_d | 3-11 mm/s |
| Albumin Partition Coefficient | K_a | 0.2 |
| β_2-microglobulin Partition Coefficient | K_B | 0.9 |
| Urea Partition Coefficient | K_u | 0.4 |
| Albumin Porosity Coefficient | P_a | 0.2 |
| β_2-microglobulin Porosity Coefficient | P_B | 0.9 |
| Urea Porosity Coefficient | P_u | 0.9 |
| Stiff-spring Velocity | M | 10,000 |

Channel dimensions and flow velocity are extensively studied for their effects on molecule diffusion behavior for design space exploration; they are, thus shown in ranges. Membrane

thickness is set to 35 μm for simplification based on the comparison of the model to an existing dialyzer in section 5.2.3.2. The dialysate stream thickness range is also based on an existing dialyzer with $t_D = 100\mu\text{m}$. Diffusivities are calculated based on their molecular mass as shown in equation 5-4 below [104].

$$D = 1.62 \times 10^{-4}(\text{MW})^{-.552} [\text{cm}^2/\text{s}] \quad (5-4)$$

MW represents molecular weight: Albumin 66,463 g/mol, β_2 -microglobulin 11,818 g/mol, urea 60 g/mol. The calculated diffusivities are stagnant diffusivities. Particle interactions of blood cells enhance the diffusivity of molecules, and the effect is applied by multiplying the diffusivity enhancement ratio of 2.5 [52] to the diffusivity values in the blood stream. References of the initial concentration values are presented in section 5.4.2 along with the objectives (steady state concentration level) of the design space exploration. Porosity coefficients are multiplied to the diffusivity values in the membrane to model the reduced effective diffusivity due to the porosity. More details on the specific values follow in the next section.

5.2.3 Model Validation

The model needs validation in two aspects, accuracy of results and realistic filtration property modeling of the existing dialyzer. Through the validation, the range of acceptable mesh size and coefficients of the membrane filtration property are determined.

5.2.3.1 Accuracy

Accuracy is measured by comparing clearance of waste molecules. Clearance is measured in the same units as flow rate, as was shown in Figure 5-3 on page 101. Clearance represents the rate at which waste substances are cleared from the blood, and it is calculated with equation 5-5.

$$K^d = Q_B \times \frac{C_{Bi} - C_{Bo}}{C_{Bi}} \quad (5-5)$$

K^d is the clearance, Q_B is the blood flow rate, C_{Bi} is the concentration at the blood inlet, and C_{Bo} is the concentration at the blood outlet. Clearance does not depend on the initial concentration, and it is usually provided by dialyzer manufacturers to specify performance. Thus, it will be used as a performance measure for the design space exploration; it is important to validate the accuracy of clearance for different scale and meshing.

The accuracy of the results depends on meshing, and meshing is affected by scale and maximum mesh size, h_{max} . Because meshing is applied on the scaled geometry, realistic axial mesh sizes increase together as scale increases. In addition, different diffusivities and flow velocities require different minimum mesh sizes. With increasing values of the scale and h_{max} , the computation time decreases due to decreasing numbers of elements, but accuracy will decrease. Thus, finding an acceptable mesh size, which provides accurate results with reduced computation time, is important. Table 5-3 lists the studies conducted for the validation of accuracy with different L , v_i , scale, and h_{max} .

Table 5-3. Validation cases studied for accuracy

| Study | Study Conditions | Parameter | Parameter Values |
|----------|-----------------------------------|--|--|
| A | $L = 5\text{mm}$ | scale | 1, 10, 70, 200, 400, 700 |
| B | $L = 250\text{mm}$ | scale | 200,600,1200,2000,2900,4200,5600 |
| C | $L = 5\text{mm}$, scale = 100 | $v_i = 24.8\text{mm/s}$, $h_{max} = 1$ | h_{max} .2, .4, .7, 1.1, 1.7, 2.4, 3.2 |
| D | $L = 5\text{mm}$ | scale | 10, 70, 200, 400, 700 |
| E | $L = 250\text{mm}$ | scale | 200,600,1200,2000,2900,4200,5600 |
| F | $L = 5\text{mm}$, scale = 100 | $v_i = 60\text{mm/s}$, $h_{max} = .7$ | h_{max} .2, .4, .7, 1.1, 1.7, 2.4 |

For all six cases, $D = 205 \mu\text{m}$, $\delta = 20 \mu\text{m}$, $tD = 100 \mu\text{m}$, $v_d = 10.2\text{mm/s}$, $K_a = 0.4$, $K_B = 0.7$, $K_u = 0.7$, $P_a = 0.2$, $P_B = 1$, $P_u = 1$. Other study conditions are the same as listed in Table 5-2 except for what is listed in the study conditions column in Table 5-3. Tables of results with calculation time and error of clearances are documented in Appendix A: Tables. The results showed great reduction in calculation time with the increase of scale and h_{max} . h_{max} is the most important parameter for accuracy, while v_i does not greatly affect accuracy. In order to maintain the error below 5%, $h_{\text{max}} < 0.7$ is required with scale < 400 for the short $L = 5\text{mm}$ and scale < 4200 for the short $L = 250\text{mm}$. Considering that the computation time does not greatly reduce after certain reduction amounts, $h_{\text{max}} < .7$ and scale < 3000 will be used for later simulations depending on L .

5.2.3.2 Comparison to Experimental Results of a Dialyzer

The model's filtration property is further validated by comparison with *in vivo* experimental results of a dialyzer, FX60 (Fresenius). Because this device does not include a sheath stream, the sheath flow region is calculated as the blood region by including initial concentration at the inlet of the sheath stream and using enhanced molecule diffusivity. Validation of the membrane filtration property (clearance) is the main purpose; thus, exclusion of sheath stream is acceptable. The snapshot of a validation case is shown in both 2D and 3D in Figure 5-6 with concentration field and flow velocity.

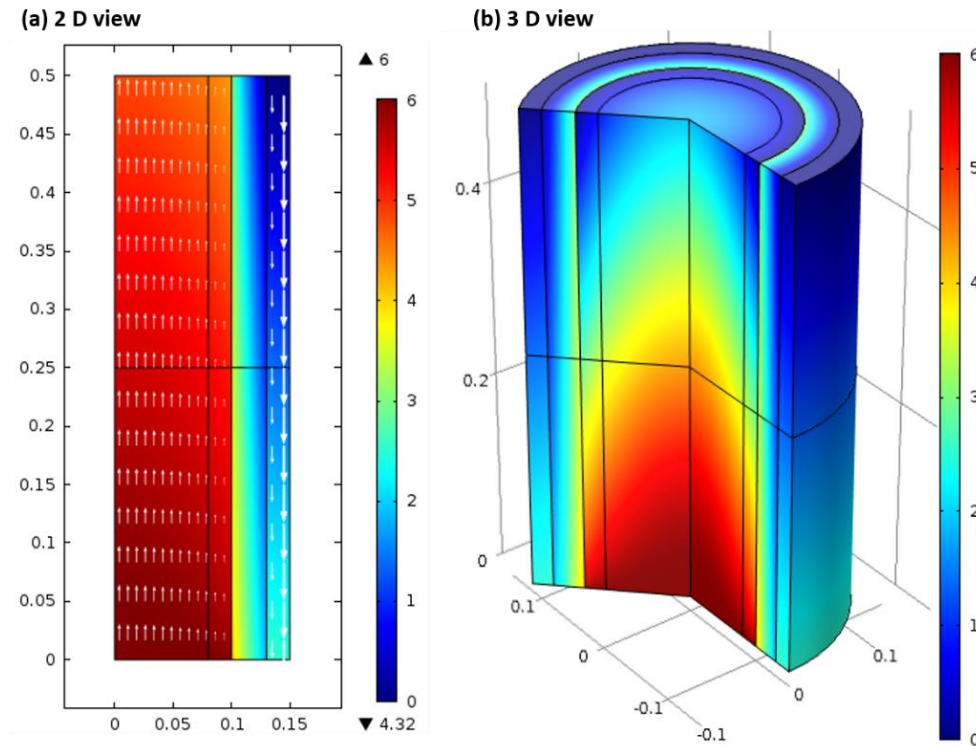


Figure 5-6. Comsol model in 2D and 3D with concentration field and flow velocity (arrow) for dialyzer validation

The particular dialyzer, FX60, was chosen because the most tubule dimensions and *in vivo* experimental results are available [107]. The membrane is modeled with partition coefficients, K_a , K_B , K_u , and porosity coefficients, P_a , P_B , P_u . The partition coefficient sets the ratio of the concentrations on the membrane to liquid side to model discontinuity at the phase boundary. The porosity coefficients are multiplied to the stagnant diffusivity of molecules to model the reduced effective diffusivity in membrane. In order to understand the effect of the coefficients on clearance, four parametric studies were conducted as listed in Table 5-4.

Table 5-4. Validation cases studied for comparison to dialyzer FX60

| Study | Study Conditions | Parameter | Parameter Values |
|-------|-------------------------|-----------------|-------------------------|
| G | $v_i = 24.8\text{mm/s}$ | K_a, K_B, K_u | 0.1,0.3,0.5,0.7,0.8 |
| H | $v_i = 37.2\text{mm/s}$ | K_a, K_B, K_u | 0.1,0.3,0.5,0.7,0.8 |
| I | $v_i = 24.8\text{mm/s}$ | P_a, P_B, P_u | 0.2, 0.4, 0.6, 0.8, 1.0 |
| J | $v_i = 37.2\text{mm/s}$ | P_a, P_B, P_u | 0.2, 0.4, 0.6, 0.8, 1.0 |

Other conditions were matched to the available *in vivo* experimental data: $L = 200\text{mm}$, scale = 2000, $h_{\text{max}} = .4$, $D = 185\ \mu\text{m}$, $tD = 100\ \mu\text{m}$, $v_d = 10.2\text{mm/s}$. $v_i = 24.8\text{mm/s}$ and $v_i = 37.2\text{mm/s}$ corresponds to the blood flow rate of $Q_B = 200\text{ml/min}$ and $Q_B = 300\text{ml/min}$ with 10,000 tubules. Other membrane properties were initially set as following: $K_a = 0.4$, $K_B = 0.7$, $K_u = 0.7$, $P_a = 0.2$, $P_B = 1$, $P_u = 1$. Other parameters were set to the same values listed in Table 5-2. The results are shown in Figure 5-7.

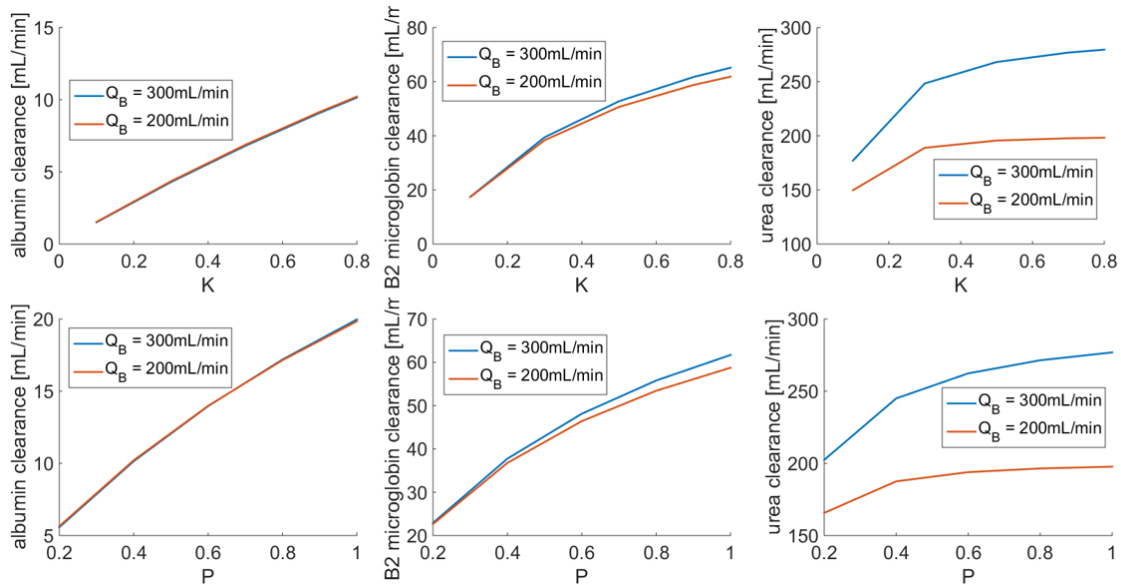


Figure 5-7. Clearance vs. partition coefficient and porosity coefficient

Clearance of each molecule increased with partition coefficient and porosity coefficient. This figure also shows that the blood flow rate greatly affects urea clearance, but does not affect clearance of larger molecules. In order to match the experimental data of FX60, $K_u = 0.4$, $P_u =$

0.9, $K_B=0.9$, $P_B = 0.9$, are set. The comparison to the *in vitro* experimental data is shown in Table 5-5.

Table 5-5. Comparisons of clearances [107]

| | Blood Flow Rate | Dialysate Flow Rate | <i>in vivo</i> Clearance | Simulation Clearance |
|------------------------------------|-----------------|---------------------|--------------------------|----------------------|
| Urea | 200 mL/min | 500 mL/min | 193 mL/min | 192 mL/min |
| | 300 mL/min | 500 mL/min | 242±19 mL/min | 256 mL/min |
| | 300 mL/min | 400 mL/min | 221±28 mL/min | 246 mL/min |
| β₂-microglobulin | 300 mL/min | 500 mL/min | 78±12 mL/min | 65 mL/min |
| | 300 mL/min | 300 mL/min | 69±13 mL/min | 61 mL/min |

This shows that the simulation results match to the experimental results for different flow rate cases within the error range of urea and β₂-microglobulin. Albumin clearance data was not available; because the Albumin molecule is larger than most pores of the membrane, most Albumin does not pass through the membrane. Thus, $K_a = 0.2$ and $P_a = 0.2$ are arbitrarily chosen to keep the clearance less than 5 mL/min. The finalized coefficients are used for later cases studied for design space exploration.

5.3 Hemodialysis System Model

The Comsol tubule model created in section 5.2 enables the calculation of each molecule’s clearance for the given tubule dimension and flow velocities. In order to determine the performance of a dialyzer based on the clearance data, a hemodialysis system model is needed because the Comsol tubule model is based on only one tubule, and typical dialyzers contain up to 15,000 tubules. In addition, exploring different treatment schedules for a given set of patient information provides a realistic prediction of how different dialyzer designs are feasible or not. In this study, an existing hemodialysis system model is used together with the

Consol tubule model to explore the design space in section 5.5. The hemodialysis system model is briefly introduced in this section with references for the values used in the study.

5.3.1 Overview

An analytical hemodialysis system model that predicts the waste level change over time was created by Olson et al [108]. The model was implemented in MATLAB Simulink, and the waste level was calculated based on the patient information, dialyzer property, treatment schedule, and flow rates of blood and dialysate. Figure 5-8 shows the predicted waste level change over time with the dark solid line for the case in which a patient gets treatment every day.

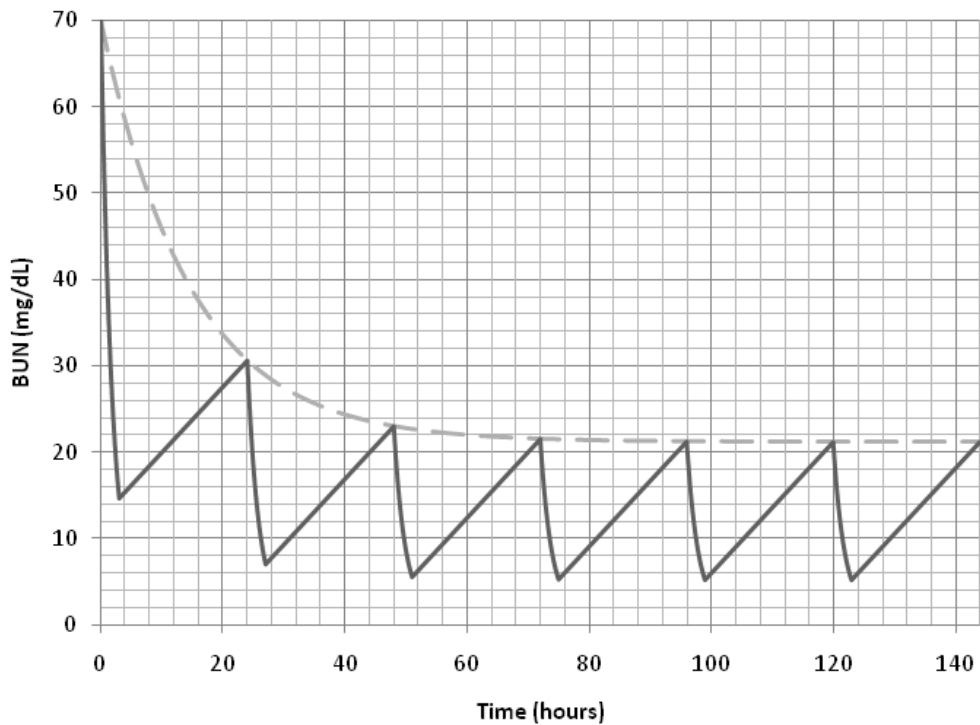


Figure 5-8. Waste level change for several cycles of treatment (solid line) and connections of maximum waste level for each cycle (dashed line – peak waste decay curve) [109]

The waste level decreases during the treatment, and it increases in between the treatments because of the waste generation. The light dashed line, peak waste decay curve, connects the peak points of each cycle, and it was found to fit to an exponential curve as shown in the equation below.

$$y = C + Aexp(-t/\tau) \quad (5-6)$$

t is time, C is the steady state waste level, and τ is the time constant that dictates how quickly the steady state is reached. Olson found that the initial waste level, C_I , does not affect the steady state waste level, C [109]; thus, $A = C_I - C$. In this study, the effect of different design variables on C of Albumin, β_2 -microglobulin, and urea are explored to find a feasible design space. The relevant variables of the hemodialysis system model are listed in Table 5-6.

Table 5-6. Relevant variables and parameters of hemodialysis system model

| | Symbol | Study Range |
|---|---------------|--------------------|
| Blood Flow Rate | Q_B | mL/min |
| Dialysate Flow rate | Q_D | mL/min |
| Dialyzer Property | K_0A | mL/min |
| Waste Generation Rate | WGR | mg/min |
| Residual Kidney Function | GFR | 0.03 |
| Total Blood Volume | V_B | 35000 mL |
| Initial Blood Molecule Concentration | C_I | mg/mL |
| Treatment Length | t_{treat} | 4, 8, 12, 16 hours |
| Treatment Cycle Length | t_{total} | 24, 39, 54 hours |

Q_B and Q_D represent the blood and dialysate flow rates of a dialyzer. K_0A represents a dialyzer property, and it has the following relation with clearance, K^d .

$$K_0A = \frac{Q_B}{1 - Q_B/Q_D} \ln \left(\frac{K^d/Q_D - 1}{K^d/Q_B - 1} \right) \quad (5-7)$$

For the design space exploration, it is calculated by converting the clearance data of the Comsol simulation based on the above equation to calculate K_0A of the tubule, and multiplying it by the number of tubules in the dialyzer.

Waste generation rates, WGR , are different for each molecule, and estimated values used for the design space exploration are presented in section 5.3.2.

Patients are diagnosed with End Stage Renal Disease (ESRD) and receive hemodialysis treatments when residual kidney function is less than 15% of normal. For the design space exploration, 3% of residual kidney function was used because removal of middle molecules is especially important for long term patients who have little residual kidney function.

V_B represents the fluid volume in the body where waste molecules can be distributed. The blood volume can be estimated as 55% of weight [110], and 35 L is a standard volume used in literature to normalize data.

Initial blood waste concentrations of Albumin, β_2 -microglobulin, and urea are presented in section 5.4.2 along with the requirements and objectives (steady state concentration levels) of the design space exploration.

t_{total} is the time interval between the start of two treatments. Currently, a typical hemodialysis schedule is about 4 hours of treatment for 3 times per week. For the design space exploration, more frequent and longer treatment options are explored as well.

5.3.2 Waste Generation Rates

An Albumin concentration of 3.7 g/dL was found to stabilize with an extracorporeal albumin loss of 4.23g/24hr/1.73m² [111]. (Surface area of 1.73m² is commonly used for

normalization of data along with 35L of plasma volume.) Albumin generation rate hugely varies depending on the patient's status including their diet, and the definitive generation is not clearly known [112]. Thus, Albumin generation rate is estimated based on the amount lost during a treatment session. If the concentration level stabilizes at a certain value, this suggests that the amount lost is the same as the amount generated. Thus, for the design space exploration, 2.9375mg/min of Albumin generation rate is used accordingly based on the following calculation.

$$\frac{4230\text{mg}}{24\text{hr}} \times \frac{1\text{hr}}{60\text{min}} = 2.9375 \text{ mg/min} \quad (5-8)$$

Typical β_2 -microglobulin generation rate is 2.4 mg/kg.day and assuming that 35 L plasma volume is 55% of weight [110], 0.106 mg/min of β_2 -microglobulin generation rate is used accordingly based on the following calculation.

$$\frac{2.4 \text{ mg}}{\text{kg} \cdot \text{day}} \times \frac{1\text{day}}{24 \times 60\text{min}} \times \frac{35\text{L}}{0.55\text{L/kg}} = 0.106\text{mg/min} \quad (5-9)$$

Pre-treatment concentrations of urea are around 34.9 mmol/L and drop to about 12.3 mmol/L after a treatment [106]. With the same assumption of 35 L plasma volume and three treatments per week, 14.3297 mg/min of urea generation rate is used for the design space exploration.

$$\begin{aligned} & \frac{(34.9\text{mmol/L} - 12.3\text{mmol/L})}{24 \times 2.3 \times 60\text{min}} \times \frac{60\text{mg}}{1\text{mmol}} \times 35\text{L} \\ & = 14.3297 \text{ mg/min} \end{aligned} \quad (5-10)$$

Considering that a typical urea generation rate is 25 g/day or 17.3611 mg/min [113], and dialysis patients are on a diet, the estimated generation rate is a reasonable value, and it also shows that the estimation method is valid.

5.4 Design Requirements and Objective of the Proposed Dialyzer

The objective of the design space exploration is to maintain less than 25 mg/L of β_2 -microglobulin concentration. Requirements of the proposed dialyzer design are listed in Table 5-7.

Table 5-7. Requirements of the proposed dialyzer design

| Requirements | R/W |
|---|-----|
| RBC loss < 5% | R |
| Platelet loss < 5% | W |
| Blood flow rate < 300 mL/min | R |
| Albumin concentration > 3.5 g/dL | R |
| Dialyzer volume < $4 \times \pi \times 2.5^2 \times 25 = 1964 \text{ cm}^3$ | R |
| Fluid (sheath and dialysate) consumption < 100 L/day | R |

Requirements and wishes are listed with R and W in the right column. More details of each requirement and objective are discussed in the following sections.

5.4.1 Blood Cell Loss

The proposed dialyzer design includes the blood stream flowing in direct contact with the sheath stream. Thus, it is important to prevent blood cell loss while allowing enough time for waste middle molecules to diffuse into the sheath fluid. The blood cell size is in the range of microns, whereas good proteins and waste molecules sizes are in the range of nanometers. Blood cell migrations are based on sheared migration, and particle interactions play an important role. Molecule diffusion is based on Brownian motion. Thus, the migration behaviors

of RBCs and platelets were studied in Chapter 4 separately for pressure driven flows through circular pipes using direct numerical simulation based on LB-SL method. The channel length in which 5% of blood cells are lost, $L_{(ER=0.05)}$, was found, and it is used in this chapter for the design space exploration. Total amount of blood cell loss will depend not only on the channel dimension but also on the duration that the loss occurs. Considering that RBC lifetime is around 120 days, and blood donation is possible every 12 weeks, losing 0.83% of blood cells per day is affordable. Considering typical hemodialysis treatment schedule that up to 12 hours of treatment is provided per week, losing 5% of blood cells for 12 hours per week is equivalent to 0.36% loss per day. Although calculating the blood cell loss for each different treatment schedule will lead to more precise design space exploration, it was simplified as considering the blood cell loss of 5% through the channel in this study to reduce the complexity of the problem.

Limiting platelet loss to less than 5% was categorized as a wish, not a requirement, because the platelet extraction ratios found in Chapter 4 cannot be generalized for real cases. This is because platelet migration behavior showed only a general trend. Thus, the design space was explored for two cases; one case in which only RBCs loss is concerned and other case in which both platelet and RBC loss are concerned.

5.4.2 Blood Flow Rate

The blood flow rate is limited by the method of blood access from the patient's body, and typical hemodialysis treatments are conducted with 300 mL/min of blood flow rate. Thus, less than 300 mL/min of blood flow rate was used as a requirement in this design space exploration.

5.4.3 Protein Loss

For the proposed dialyzer design, retaining good proteins in the blood stream while maximizing waste filtration is another crucial objective. Blood Albumin concentration for a normal person is 3.5 to 5.0 g/dL [98]. For the initial patient information, 4.0 g/dL is assumed for the design space exploration. Steady state Albumin concentration of 3.5 g/dL is used as a requirement for the design space exploration.

5.4.4 Dialyzer Size

Typical dialyzers take the shape of long cylinders, 16 to 25 cm in length and 3 to 5 cm in diameter. They house 7,000 to 15,000 porous hollow fiber tubules, and each tubule is about 200 μm in diameter. The requirement for the size of the dialyzer is set to quadruple the size of typical dialyzers because this value is still acceptably small for the improved filtration of middle molecules.

The total diameter of the Comsol tubule model used for the validation in section 5.2.3.2 was $185 + 2 \times (35 + 100) = 455 \mu\text{m}$, and the cross-sectional diameter of the whole dialyzer can be estimated as $\sqrt{10,000} \times 455 \mu\text{m} = 45.5 \text{ mm}$ based on the following relation.

$$A_{\text{dialyzer cross-section}} = \frac{\pi}{4} (D_{\text{dialyzer}})^2 = N \times \frac{\pi}{4} (D_{\text{comsol tubule}})^2 \quad (5-11)$$

Considering that typical dialyzer sizes are about 5cm in diameter, this estimation is very close to the actual size. This calculation method was used for the size estimation for the design space exploration.

5.4.5 Fluid Usage

Current hemodialysis treatments use up to 200L of dialysate for each treatment when no dialysate regeneration is used. With the proposed dialyzer design, both sheath and dialysate fluid are used as cleaning fluid and are disposed after one use. Considering that current treatments are conducted three times per week, consuming less than 100L/day of total sheath and dialysate fluid is used as a requirement for the design space exploration.

5.4.6 Waste Concentration

The β_2 -microglobulin concentration in blood for a normal person is less than 2 mg/L [114]. However, the concentration of hemodialysis patients can be much higher than 50 mg/L, and maximum of 100 mg/L was reported [3, 114]. The concentration of most of hemodialysis patients are in 20-50 mg/L range [115], and 32.2 mg/L was used as a concentration value that divides patients into a high concentration group and a low concentration group in one study [105]. For the design space exploration, maintaining β_2 -microglobulin concentration less than the 25 mg/L with the initial concentration of 32.2 mg/L is used as an objective.

Although urea filtration was not the main objective of the proposed dialyzer, it is studied together in order to understand the effect of different designs on urea filtration. The normal concentration level of urea is about 0.4 g/L (6.67 mmol/L) [114]. However, pre-treatment concentrations of patients are around 34.9 mmol/L [106]. Thus, 34.9 mmol/L (2.094 mg/mL) is used as the initial concentration for the design space exploration.

5.5 Design Model of the Proposed Dialyzer Design

Design space exploration of the proposed dialyzer design required connecting information from the three different models: the blood cell migration meta-model, the Comsol tubule

model, and the hemodialysis system model. The overview of the design variables, models, and output flows are presented in a diagram, as shown in Figure 5-9.

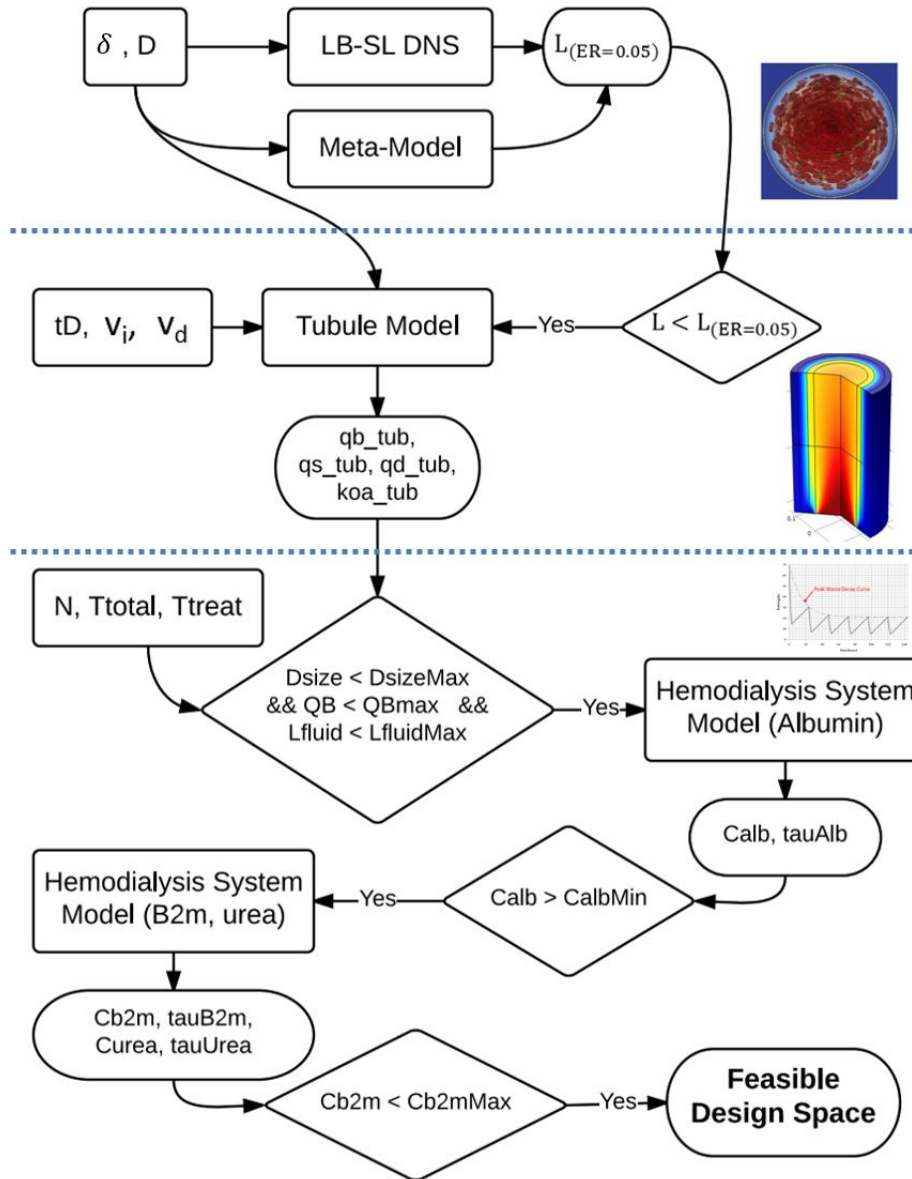


Figure 5-9. Overview of the design space exploration

The relevant variables were explained in previous sections when the three models were introduced. The input variables are briefly explained again for readability: δ -sheath stream thickness, D -tubule inner diameter, tD -dialysate stream thickness, v_i - blood maximum velocity,

v_d -dialysate maximum velocity, N-number of tubules in a dialyzer, Ttotal- treatment cycle length, Ttreat-treatment length.

The initial design space exploration was conducted for the 8 cases of circular channels that were studied in Chapter 4 (Figure 4-6). $L_{(ER=0.05)}$, the channel length over which 5% of blood cells are lost, was found from LB-SL DNS results except for case 11 in which the simulation was not able to continue. For case 11, $L_{(ER=0.05)}$ was estimated based on the exponential curve that fitted available extraction ratio in Chapter 4. $L_{(ER=0.05)}$ was used as the maximum channel length to study molecule diffusion behavior with the Comsol tubule model, and the values are listed in Table 5-8.

Table 5-8. Resulting ER curve parameters of each cases studied with circular channels

| Case No. | δ [μm] | D [μm] | $L_{(ER=0.05)}$ RBC [mm] | $L_{(ER=0.05)}$ Plt [mm] |
|----------|----------------------------|---------------------|--------------------------|--------------------------|
| 3 | 17.7 | 120.0 | 1.1113 | 6.3568 |
| 4 | 7.0 | 40.0 | 0.1608 | 0.2052 |
| 5 | 5.7 | 186.7 | 250 | 9.0548 |
| 6 | 4.3 | 133.3 | 250 | 2.3251 |
| 7 | 8.3 | 93.3 | 0.8479 | 4.2286 |
| 9 | 3.0 | 80.0 | 250 | 1.1613 |
| 10 | 9.7 | 146.7 | 2.0207 | 11.8647 |
| 11 | 11.0 | 200.0 | 8.5588 | 3.5526 |

For cases 5, 6, and 9, the ER of RBC would never reach 5%; thus, maximum tubule length of 250mm was used.

The effect of different design variables on molecule diffusion behaviors of Albumin, β_2 -microglobulin, and urea were extensively studied using for-loop with Comsol tubule model, as shown in Figure 5-10.

```

Lmax=L(ER=0.05)
for L = Lmax/2:Lmax/2:Lmax
  for tD = 20:30:110
    for vi = 20:20:60
      for vd = -3:-4:-11
        [qb_tub, qs_tub, qd_tub, koa_tub] = ComsolTubuleModel( $\delta$ , D, L, tD, vi, vd)

```

Figure 5-10. For-loop for waste diffusion study using Comsol tubule model

qb_tub, qs_tub and qd_tub are the tubule flow rates of blood, sheath, and dialysate, respectively. Clearance values for each molecule were also calculated based on the tubule blood flow rate and concentrations at the inlet and outlet, using equation 5-5 on page 109. Then, the clearance value was converted to koa_tub, K_0A of the waste molecule for a tubule, using equation 5-7 on page 115. The conversion is based on the clearance and flow rates of blood and dialysate. For the conversion, the sum of sheath and dialysate flow rate was used as dialysate flow rate in the equation. This is a valid operation because K_0A is a measure of a membrane property used in the hemodialysis system model to dictate how waste molecules are removed from the blood stream. Based on the for-loop, 72 tubule cases were studied for each of 8 cases listed in Table 5-8.

In the hemodialysis system model, N, the number of tubules, is determined based on the three requirements of the design; 1. The size of dialyzer (Dsize) should be less than the maximum allowed size of dialyzer (DsizeMax), 2. Blood flow rate of the dialyzer (QB) should be less than the maximum allowed blood flow rate of the dialyzer (QBmax), 3. Total fluid consumption of sheath and dialysate (Lfluid) should be less than the maximum allowed fluid consumption (LfluidMax). Dsize, QB, and Lfluid were calculated based on the number of tubules as shown in the following equations.

$$D_{\text{size}} = V_{\text{dialyzer}} = N L \frac{\pi}{4} (D_{\text{comsol tubule model}})^2 \quad (5-12)$$

$$Q_B = N \times q_{b_tub} \quad (5-13)$$

$$L_{\text{fluid}} = Q_D \times T_{\text{treat}} \times \frac{60 \text{min/hr}}{1000 \text{mL/L}} \times \frac{24 \text{hr}}{T_{\text{total}}} \quad (5-14)$$

The effect of different design variables on dialyzer performance (steady state waste level) was studied using for-loop with the hemodialysis system model, as shown in Figure 5-11.

```

Nmax=f(Dsize, QB, Lfluid)
for N = Nmax/10:Nmax/10:Nmax
    Qb=N×qb_tub, Qd=N×(qs_tub+qd_tub), KoA=N×tub_koa
    for Ttotal = 24:15:54
        for Ttreat = 4:4:16
            [C, tau] = HemodialysisSystemModel(Qb, Qd, KoA, Ttotal, Ttreat)

```

Figure 5-11. For-loop for dialyzer performance study using hemodialysis system model

As was mentioned, the sum of sheath and dialysate flow rates from the Comsol tubule model was multiplied by the number of tubules to calculate dialysate flow rate of dialyzer. As was shown in Figure 5-9, the hemodialysis system model was used separately for the three waste molecules. First, Calb, the steady state concentration level of Albumin, was found to check if it meets the requirement of maintaining the normal Albumin level. For the Calb calculation, minimum values of each cycle in the waste level (Figure 5-8) were chosen to fit the minimum waste decay curve to an exponential curve. This is because the requirement for the Albumin level is a minimum, not a maximum. If Calb is higher than CalbMin, the minimum required Albumin concentration in steady state, then the hemodialysis system model was run for β_2 -microglobulin and urea to calculate Cb2m and Curea, steady state concentration values of β_2 -microglobulin and urea, respectively. For the calculation of Cb2m and Curea, the peak waste

decay curve was used as was explained in section 5.3.1 because the maximum values are of concern for the waste molecules that should be filtered out. Based on the for-loop, 120 cases were explored for each of 72 tubule cases.

5.6 Design Space Exploration Results

The design space was extensively searched based on the for-loops, as was explained in section 5.5. The results of the design space exploration is presented in this section.

5.6.1 Design Space Exploration A – $D < 200 \mu\text{m}$

The design space was explored for the same cases that were studied in Chapter 4, as was listed in Table 5-8.

5.6.1.1 Requirement I – RBC loss less than 5%

The design space was explored concerning only RBC loss; thus, L_{max} was set to $L_{(\text{ER}=0.05)}$ of RBCs. The results showed that there is no feasible design. The lowest steady state concentration values of β_2 -microglobulin (Cb2m) were found for cases 5, 6, and 9; 0.1331 mg/mL, 0.124 mg/mL, and 0.1263 mg/mL, respectively. For these three cases, sheath stream thickness is small and RBC ER never reach 5% loss; thus $L_{\text{max}}=250\text{mm}$ was used. And yet, Cb2m values were 5 times higher than the target value, 0.025 mg/mL. This result shows that Cb2m, the steady state concentration values of β_2 -microglobulin, would decrease with small sheath stream thickness, but it is not low enough in the range it was studied.

5.6.1.2 Requirement II – RBC & platelet loss less 5%

The design space was explored concerning both RBC and platelet losses; thus, L_{max} was set to the shorter of RBC or platelet $L_{(\text{ER}=0.05)}$. Because platelet $L_{(\text{ER}=0.05)}$ is shorter than RBC

$L_{(ER=0.05)}$ for the three cases in which RBC ER never reaches 5% loss, only the three cases, 5, 6, and 9, were studied by setting L_{max} to $L_{(ER=0.05)}$ of platelets. Since there were no feasible design even with a long channel length concerning only RBC loss, it is expected that there would be no feasible design with the shorter channel length considering both RBC and platelet losses. However, to identify the important variables that reduce Cb2m, it was further studied.

The results showed that there is no feasible design that meets $Cb2m < 0.025$ mg/mL. The best-case scenario showed Cb2m of 0.5965 mg/mL, which is about 24 times higher than the target value. The maximum blood flow velocity, v_i , and dialyzer length, L, were found to be the important variables that affect Cb2m value. In order to visualize the results, the cases that all other requirements are met except for Cb2m with $Cb2m < 0.9$ mg/mL are plotted against v_i and L for the three cases, 5, 6, 9, in red, blue, and green, respectively as shown in Figure 5-12.

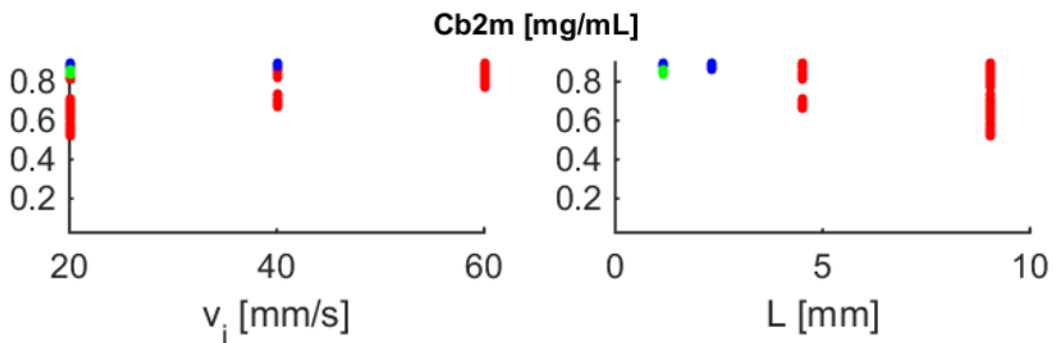


Figure 5-12. Steady state concentration values of β_2 -microglobulin vs. v_i and L for cases 5 (red), 6 (blue), 9 (green)

This shows that small v_i and long L leads to lower Cb2m values. Considering that molecule diffusion hugely depends on the duration time, this suggests that there was not enough time for β_2 -microglobulin to diffuse due to the fast flow velocity and short channel length that was studied. The smallest Cb2m value was found for case 5, which has the largest channel diameter among the three cases.

In order to understand the relationship between the steady state concentration values and dialyzer clearance values, steady state concentration values of Albumin (Calb) and β_2 -microglobulin (Cb2m) were plotted against clearances and clearance ratio of β_2 -microglobulin to Albumin for cases 5, 6, 9, in red, blue, and green, respectively as shown in Figure 5-13.

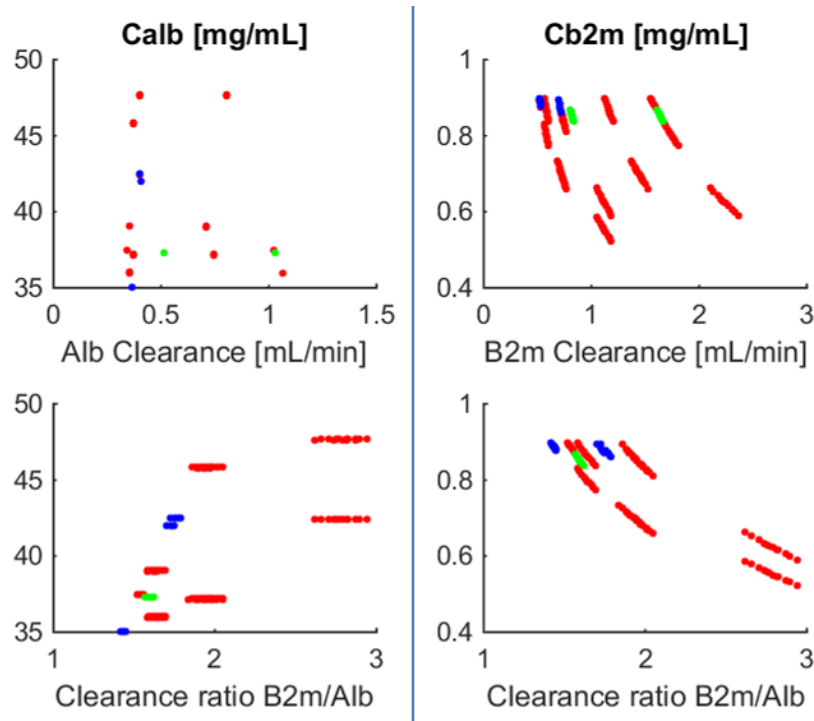


Figure 5-13. Steady state concentration values of Albumin and β_2 -microglobulin vs. clearances and clearance ratios for cases 5 (red), 6 (blue), 9 (green)

Calb and Cb2m are plotted on the left and right columns in this figure against dialyzer clearance of the molecules and clearance ratios on the top and bottom rows. The top left plot shows that Albumin clearance should be less than about 1 mL/min in order to maintain the normal level of the steady state Albumin concentration. β_2 -microglobulin clearance values were less than about 2.5 mL/min, which is a very small value even compared to conventional dialyzers with about 15 mL/min clearance values. Comparing plots on the bottom row to that of top row, low Cb2m can be achieved with large clearance ratio of β_2 -microglobulin to Albumin, so that Calb can be

maintained in the normal level. These results suggest that the clearance of β_2 -microglobulin should increase while maintaining the clearance of Albumin to less than 1 mL/min to increase the clearance ratio of β_2 -microglobulin to Albumin.

This first design space exploration suggested that a feasible design space would exist when channel diameter is large, sheath stream thickness is small, channel length is long, and flow velocity inside the tubule is slow. A combination of larger channel diameter and smaller sheath stream thickness reduces the Albumin clearance and limits Albumin loss because the area ratio of sheath to channel is small. And longer channel length and lower inner flow velocity maximizes the time for middle molecule diffusion for filtration. Larger channel diameter also allows longer channel length because $L_{(ER=0.05)}$ increases. Based on this reasoning, another set of design space explorations was conducted and is presented in the following section.

5.6.2 Design Space Exploration B – $D > 200 \mu\text{m}$

In this section, larger channel cases, with $D = 500, 600, 700 \mu\text{m}$, were explored with slower flow velocity inside the channel. The same sheath stream thickness as in case 5, $\delta = 5.7 \mu\text{m}$, was used. Because blood cell migration behavior was studied only up to $200 \mu\text{m}$ in Chapter 4, $L_{(ER=0.05)}$ was not available for the larger channels. Although it is expected to be much longer for the larger diameter cases, to be conservative, the platelet $L_{(ER=0.05)}$ value of case 5 was used; $L_{\text{max}}=9\text{mm}$.

The lower limit of v_i , 20 mm/s, was chosen based on the current hemodialysis treatment. With about $200 \mu\text{m}$ diameter tubules, it is the minimum required blood flow velocity that would avoid blood clotting. However, with larger tubules, the blood flow velocity may be lower without creating blood clotting issues. Thus, lower v_i cases were additionally searched.

The minimum Cb2m values for each case, including case 5 with $D = 186.7 \mu\text{m}$, are listed in Table 5-9, and Figure 5-14 shows the change in the minimum Cb2m over v_i .

Table 5-9. The minimum Cb2m values [mg/mL] for different cases

| v_i | 5 mm/s | 10 mm/s | 15 mm/s | 20 mm/s | 25 mm/s | 30 mm/s | 40 mm/s | 45 mm/s | 60 mm/s |
|---|-----------|------------|------------|------------|------------|------------|------------|------------|------------|
| D=186.7 μm | - | - | | 0.5226 | | | 0.6714 | | 0.7732 |
| D=500 μm | 0.1219 | 0.1760 | 0.2234 | | - | 0.3306 | | 0.4503 | |
| D=600 μm | 0.1193 | 0.1497 | 0.1898 | | - | 0.3067 | | 0.3823 | |
| D=700 μm | 0.1069 | - | 0.1864 | | 0.2412 | - | | - | |

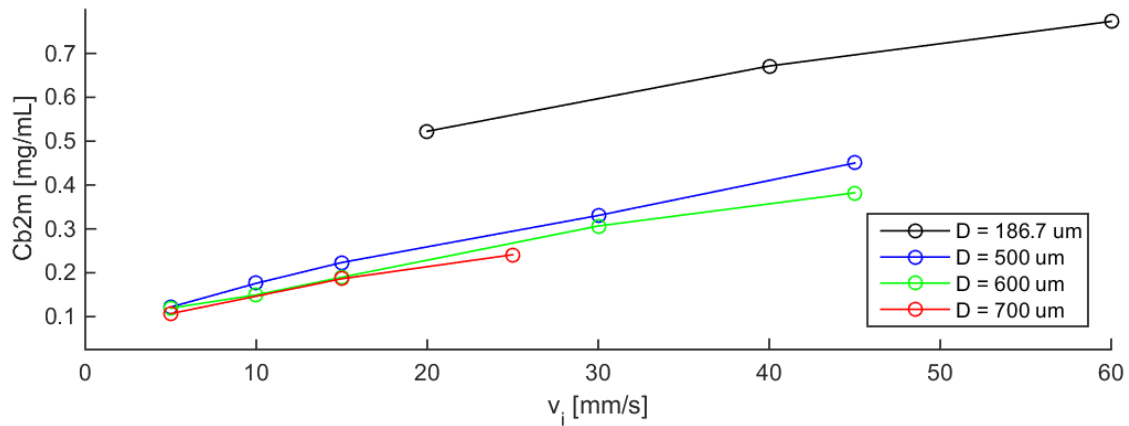


Figure 5-14. Cb2m over v_i for different channel sizes

Figure 5-14 clearly shows that Cb2m decreases with lower v_i . The larger channel also leads to lower Cb2m. However, even with the larger channel diameter and lower flow velocity inside the tubule, there was no feasible design; target value of Cb2m is 0.025 mg/mL, which is the bottom line in the plot. The best-case scenario was still 4 times higher than the target value. In order to visualize the results, the cases that all other requirements are met except for Cb2m with $\text{Cb2m} < 0.15 \text{ mg/mL}$ are plotted against the input design variables for $D = 500, 600, 700 \mu\text{m}$, in green, blue, and red, respectively, as shown in Figure 5-15.

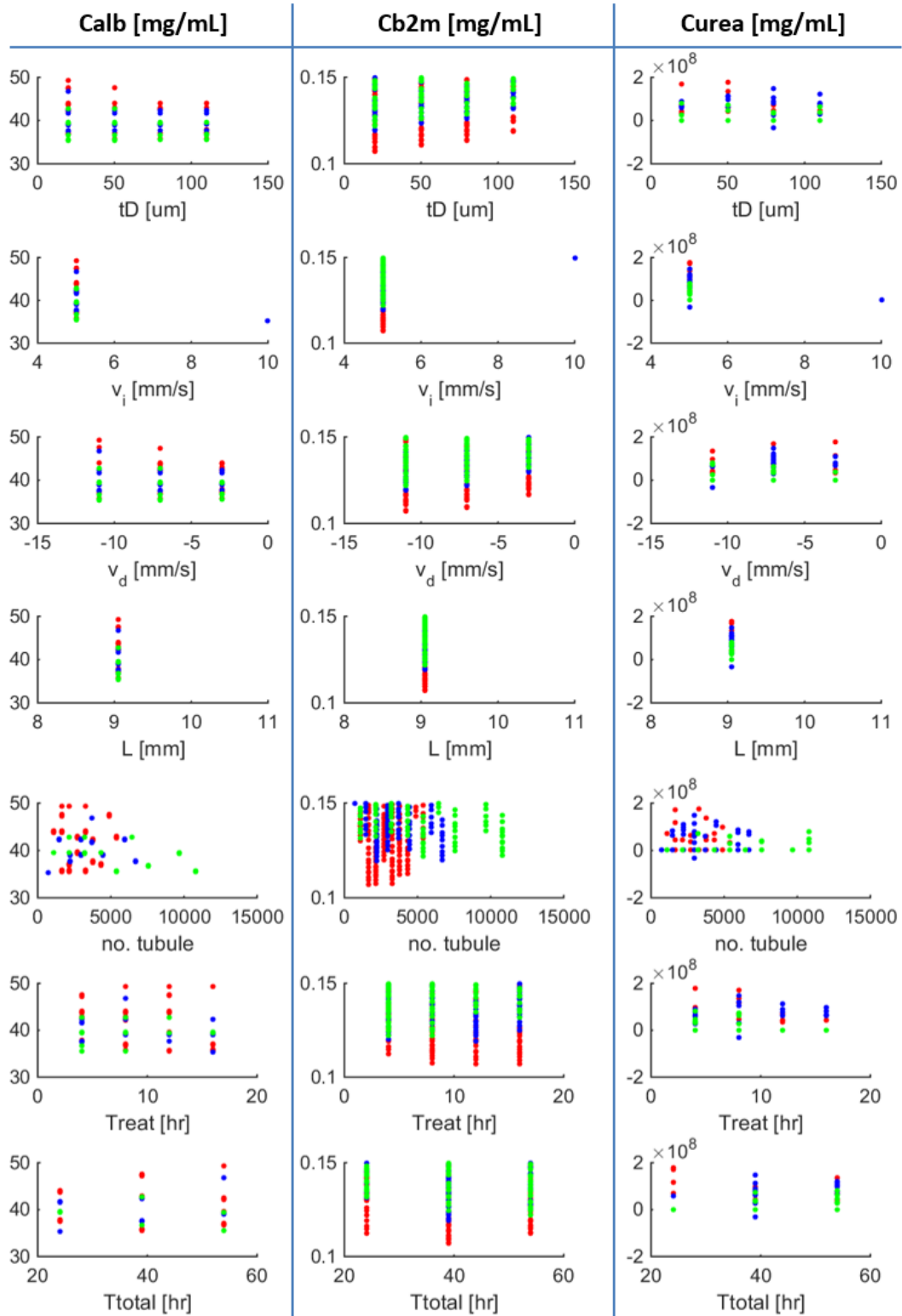


Figure 5-15. The effect of design variables on Calb, Cb2m, Curea for $D = 500 \mu\text{m}$ (green), $600 \mu\text{m}$ (blue), $700 \mu\text{m}$ (red)

This shows the steady state concentration of Albumin, β_2 -microglobulin, and urea in each column with input variables on each row. The cases that values of Calb are within the normal range, 35-50 mg/mL, are plotted as shown on the left column. Cb2m values are shown on the middle column against the design variables. Cb2m values are spread out in all tested values for tD (dialysate stream thickness), v_d (the maximum dialysate flow velocity), number of tubules, treatment time, and treatment cycle time, suggesting that Cb2m values are not hugely dependent on these variables. As was found in the design space exploration A, L should be long and v_i should be small so that enough time is provided for middle molecules to diffuse in order to reduce Cb2m. Values of Curea shown on the right column are much higher than normal range, and shows the same trend as Cb2m; long L and small v_i reduces Curea.

In order to understand the relationship between the steady state concentration values and dialyzer clearance values, steady state concentration values of Albumin (Calb) and β_2 -microglobulin (Cb2m) were plotted against clearances and clearance ratio of β_2 -microglobulin to Albumin for $D = 500, 600, 700 \mu\text{m}$, in green, blue, and red, respectively as shown in Figure 5-16.

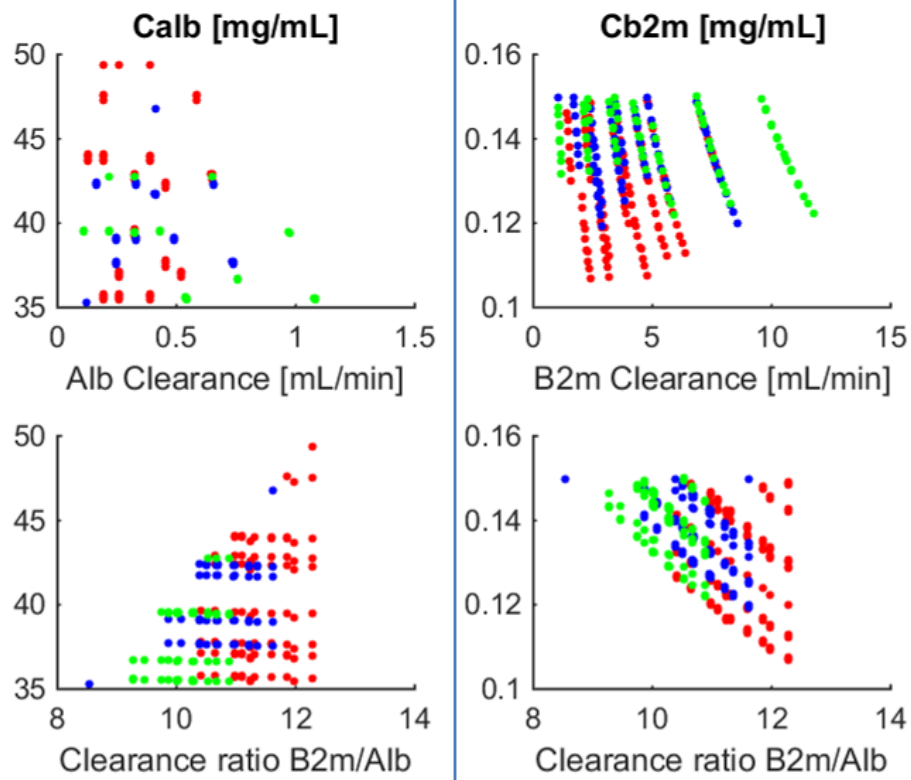


Figure 5-16. The effect of clearances and clearance ratio on Calb and Cb2m for D = 500 μm (green), 600 μm (blue), 700 μm (red)

Calb and Cb2m are plotted on the left and right columns in this figure against dialyzer clearance of the molecules and clearance ratios on the top and bottom rows. The top left plot shows that Albumin clearance should be less than about 1 mL/min in order to maintain the normal level of the steady state Albumin concentration, as was found in the design space exploration A. Clearance of β_2 -microglobulin were less than about 12.5 mL/min, which is still lower than conventional dialyzers with about 15 mL/min of clearance. Comparing plots on the bottom row to that of top row, low Cb2m can be achieved with large clearance ratio of β_2 -microglobulin to Albumin, so that Calb can be maintained in the normal level. Lower values of Cb2m in this design space exploration B with the larger channel and slower inside flow velocity was achieved

by keeping Albumin clearance to less than 1 mL/min while increasing the clearance ratio of β_2 -microglobulin to Albumin to about 12.5 compared to 3 of the design space exploration A.

In order to understand if Cb2m is related to the resulting dialyzer size and total fluid consumption, Cb2m values are plotted against dialyzer size and total fluid usage for $D = 500, 600, 700 \mu\text{m}$, in green, blue, and red, respectively as shown in Figure 5-17.

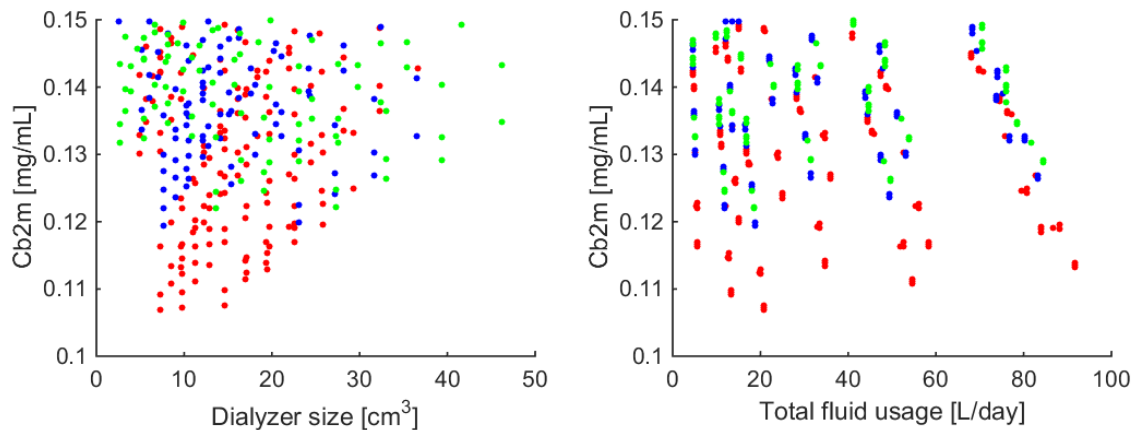


Figure 5-17. Cb2m vs. dialyzer size and total fluid usage for $D = 500 \mu\text{m}$ (green), $600 \mu\text{m}$ (blue), $700 \mu\text{m}$ (red)

The left plot shows that dialyzer sizes range up to less than 50 cm^3 , which is only about 10% of the currently used dialyzer size. And Cb2m values are not strongly related to the size of the dialyzer. Even though these are infeasible designs and Cb2m needs to be further reduced with different channel dimensions to make it feasible, considering such low relationship of Cb2m and dialyzer size, further design explorations can be conducted without enforcing the dialyzer size requirement, as it would not change the design space exploration results.

The right plot shows that increasing the fluid usage does not necessarily lead to lower Cb2m values. Small values of Cb2m are possible even with the total fluid usage of much less than 100

L/day. The effect of input variables on the total fluid usage is shown in Figure 5-18 for $D = 500$, 600 , $700 \mu\text{m}$, in green, blue, and red, respectively.

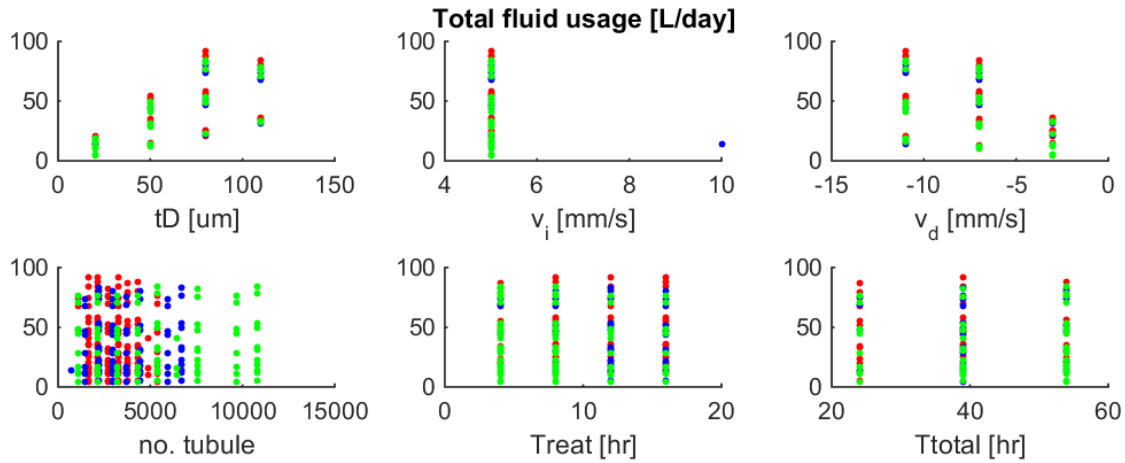


Figure 5-18. The effect of design variables on the total fluid usage for $D = 500 \mu\text{m}$ (green), $600 \mu\text{m}$ (blue), $700 \mu\text{m}$ (red)

This figure shows that smaller total fluid usage cases tend to exist with smaller dialysate thickness, tD , and slower dialysate flow velocity, v_d , but small total fluid usage cases exist for most of the input variable ranges.

The number of tubules was determined as a function of dialyzer size, total fluid usage, and blood flow rate, which is limited by the patient blood access, as was explain in section 5.5. Considering that the dialyzer size was much smaller than the requirement, and total fluid usage is not particularly dependent on input variables nor does it affect Cb_{2m} , the blood flow rate through the dialyzer was the main requirement that determined the number of tubules. This suggests that further design space exploration can be done with a fewer number of input variables since only a few variables are the important variables.

5.7 Summary and Conclusion

In this chapter, the design space was explored to identify a feasible design space for the proposed dialyzer to answer the second research question: What is the feasible design space of the proposed dialyzer with improved waste removal rate while retaining blood cells? Minimum blood cell loss was ensured by using the channel length established in Chapter 4 based on the direct numerical simulation study. Molecule diffusion behaviors were studied using a Comsol tubule model, and together with hemodialysis system models, feasible designs with minimum protein loss and sufficient removal of middle molecules were explored.

There was no feasible design in the studied range with the channel diameter (inner tubule diameter) of less than 700 μm . The best-case scenario was still 4 times higher than the target value of the steady state β_2 -microglobulin concentration with β_2 -microglobulin clearance around 12.5 mL/min. However, important variables that affect the performance of the dialyzer were identified; area ratio of sheath to the channel should be small with small sheath stream thickness ($< 6 \mu\text{m}$) and larger inner tubule diameter ($>> 700 \mu\text{m}$), and enough duration time should be provided with long dialyzer length ($> 10\text{mm}$) and low maximum blood flow velocity ($< 5\text{mm}$). Other input variables, including treatment schedule, do not greatly affect the steady state concentration levels. Dialyzer blood flow rate is an important requirement that limits the number of tubules, and dialyzer size and fluid consumption are not important requirements for the design space exploration. Maintaining the normal protein (Albumin) level is an important requirement, and Albumin clearance should be less than 1 mL/min. In order to match the performance of the state-of-the-art dialyzer in the market, the clearance ratio of β_2 -microglobulin to Albumin should be more than around 50; the best-case scenario clearance ratio was about 12 in this design space exploration.

The 2-stage serial filtration system for hemodialysis and a blood cleansing device for sepsis treatment, proposed by other researchers in the literature, initially focused on blood cell migration. This is because limiting blood cell loss was considered to be the main issue. Because their experiments showed that blood cell loss cannot be prevented in the range they studied with relatively large sheath stream thickness ($\sim 100 \mu\text{m}$), this study focused on relatively small sheath stream thickness cases ($\sim 20 \mu\text{m}$) and showed that limiting blood cell loss is possible for such cases. However, the design space exploration results suggest that sufficient middle molecule removal and limiting protein loss is as important as limiting blood cell loss.

5.8 Future Design Space Exploration Strategy

Future design space exploration strategy is discussed in this section because no feasible design was found in this study.

Further design space exploration can be conducted with a fewer design variables based on the learning from this study. Inner tubule diameter, sheath stream thickness, inner tubule flow velocity, and channel length that provide the clearance ratio of β_2 -microglobulin to Albumin higher than 50 and Albumin clearance of less than 1 mL/min with limited blood cell loss should be searched. Other variables, including the membrane thickness, dialysate stream thickness, dialysate flow velocity, treatment schedules, can be set to those similar to typical hemodialysis. This will reduce the computation time for the design space exploration without missing a feasible design.

Variations of the proposed design may be worth considering. One set of conditions that can be considered are the cases in which the sheath stream flows faster than the blood stream. This was suggested in the literature as a method to reduce blood cell loss. However, the faster

sheath flow also decreases the time for the middle molecule to be removed. Thus, it is not obvious whether such different flow rates will help find a feasible design space. Studying such fast sheath stream cases to find the conditions, that will retain protein loss with sufficient filtration of middle molecules, will show the feasibility of such variation.

Another set of conditions that can be considered are the cases in which sheath stream thickness of outlet is thinner than inlet as shown in Figure 5-19.

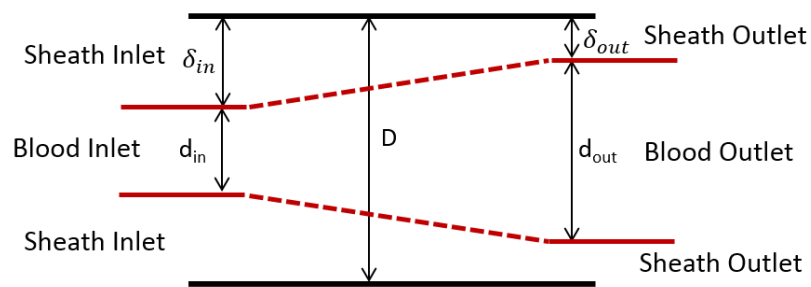


Figure 5-19. An example variation of the proposed dialyzer design

In this design, blood cell loss in the outlet would reduce, so the channel length that 5% of blood cells are lost would increase. Water removal process should follow with the use of this example dialyzer because the blood stream exiting the dialyzer will include additional sheath stream. However, with the expanded design space based on much longer channel design, a feasible design may be found.

To find the inner tubule dimensions and channel length that limits the blood cell loss, another set of blood cell migration studies is needed based on LB-SL direct numerical simulation (DNS). To find the tubule dimensions, channel length, and inner tubule flow velocity that increases the clearance ratio of β_2 -microglobulin to Albumin, another set of molecule diffusion studies is needed based on the tubule model. Considering that the molecule diffusion studies

are much cheaper than the DNS study of blood cell migration, the molecule diffusion studies should be conducted first to identify if such conditions exist that will yield the clearance ratio of 50 or higher with less than 1 mL/min clearance of Albumin. Such condition may not exist, and then there is no need to explore the blood cell migration behavior for larger channel diameter cases for this dialyzer design. Relying only on the diffusion through direct contact may not be a feasible direction for the removal of middle molecule considering that the diffusivity of β_2 -microglobulin is only 3 times that of Albumin, and exploring other methods that can selectively increase the clearance of β_2 -microglobulin might be required.

CHAPTER SIX

CLOSURE AND CONTRIBUTIONS

The broad goal of this research was to study blood cell migration in non-uniform suspension flows, and use the results to define a feasible design space for the proposed dialyzer. Chapter 3 introduced and validated the Lattice-Boltzmann and Spectrin-Link method that was used for the direct numerical simulation (DNS) study of the blood cell migration. Chapter 4 studied the effect of different design variables and flow conditions on the blood cell migration behavior using the LB-SL method. Chapter 5 explored the design space of the proposed dialyzer design and identified important design variables for improved middle molecule filtration and limited blood cell loss, protein loss, total fluid usage, and dialyzer size.

In Chapter 1, two research questions were posed for this research with a hypothesis for each question. In the first section of this chapter, each hypothesis will be addressed in the context of the work completed in this thesis. The following sections will address the contribution this research has made and specify the scope and limitation. The last section will provide the future work.

6.1 Answering the Research Questions

This research was divided into two research questions, which are now evaluated.

6.1.1 Research Question One

The first research question was addressed in Chapter 4.

RQ 1. What are the conditions that retain blood cells in the blood stream when it flows with sheath fluid in a micro-fluidic channel?

Hypothesis 1: A meta-model that predicts migration of RBCs and platelets can be created by a parametric study using LB-SL method based direct numerical simulations. Then, the meta-model can be used to specify the conditions that will retain blood cells in the blood stream.

In chapter 4, a parametric study was conducted to create a meta-model of blood cell extraction ratios (ER), the ratio of cells lost into the sheath stream. Blood cell ER evolutions over flow distance were fitted to exponential curves, and each curve was defined by L_τ and ER_{eq} . A meta-model of RBC ER was created by fitting L_τ and ER_{eq} as function of channel size and the area ratio of sheath to channel. It showed that the RBC ER would be limited with large channel size and small sheath stream thickness. Platelet ERs showed a similar trend, but no clear enough trend was found to create a meta-model. However, the study suggested which $L_{(ER=0.05)}$, the length when the extraction ratio reaches 5%, should be considered, that of RBC or platelet, for designing a micro-fluidic channel that will retain blood cells in the blood stream. $L_{(ER=0.05)}$ of RBC should be considered except for the case in which RBC ER never reaches 5% loss. $L_{(ER=0.05)}$ of platelet should be considered for other cases in which RBC ER never reaches 5% loss. This is because L_τ of platelet is much longer than that of RBC, and platelet ER_{eq} is assumed to be 1 due to platelet margination.

In conclusion, the meta-model of RBC extraction ratio was created from the parametric study. It can be used to specify the conditions that will retain RBCs in the blood stream.

General trend of platelet extraction ratio was found, and longer simulation study is required for

a clear meta-model of platelet extraction ratio. The general conditions that can retain both RBCs and platelets in the blood stream was suggested.

6.1.2 Research Question Two

The second research question was addressed in Chapter 5.

RQ 2. What is the feasible design space of the proposed dialyzer with improved waste removal rate while retaining blood cells?

Hypothesis 2: The meta-model of blood cell migration behavior, a tubule model of molecule diffusion, and a hemodialysis system model can be used together to identify the feasible design space of the proposed dialyzer by studying the effect of design variables on the blood cell loss, molecule diffusion, dialyzer size, and the amount of sheath and dialysate usage.

In Chapter 5, the Comsol tubule model of waste diffusion and the hemodialysis system model were successfully used together to explore the feasible space of the proposed dialyzer. The design space exploration was conducted to meet the requirements of limiting blood cell loss, protein loss, dialyzer size, and total fluid usage. However, the meta-model of blood cell migration behavior was not used. Instead, DNS results of the particular channel dimensions were used because no clear meta-model of blood cell ER was provided from Chapter 4.

No feasible design was found in the range it was studied. However, important design variables were identified; large channel size, small sheath stream thickness, long channel, and slow flow velocity inside the tubule are needed to reduce the steady state concentration of middle molecules while limiting the blood cell loss and protein loss.

Using the three models enabled to consider the blood cell loss, molecule diffusion, dialyzer size, and the amount of sheath and dialysate usage for the design space exploration. Dialyzer size and the fluid usage are found to be not important requirements that affect feasibility.

6.2 Contributions

The overall goal of this research was to understand the blood cell migration in non-uniform suspension flows where the blood flows with sheath in direct contact and to identify the feasibility of the proposed dialyzer based on the results. In that scope, several contributions were made.

6.2.1 Validation for RBC Diffusivity in Non-uniform Suspension Flows

The focus of the blood cell migration behavior study was to understand how many blood cells would be lost to the sheath stream. Because finding $L_{(ER=0.05)}$ was an important task for the design space exploration, and because previous LB-SL method validations were conducted only for isolated RBC in the equilibrium state, validating the LB-SL method for non-uniform suspensions in the transient phase, where the blood cell migration is still the the progress, was important. This work was one of the first to validate the method for the transient phase in non-uniform suspensions by comparing simulation results to experimental RBC diffusivity results published in the literature. In addition to the validation of blood cell spreading in the channel width direction, the Segre Silberberg effect was found in the channel depth direction. The depth-direction view was not available through the experimental study, and the simulation results suggested that the same effect might have existed in the experiment as well; thus, the

assumption of the literature that the depth-direction concentration is homogeneous may not be valid.

6.2.2 Parametric Study of Blood Cell Migration Behavior – Extraction Ratio

A parametric study of the design variables on the blood cell extraction ratios was conducted with LB-SL method based DNS. This DNS study showed that the flow velocity or Re is not an important variable to consider, but flow distance is. Analyzing ER over the flow distance showed that the channel dimension and the area ratio of sheath to channel are the main variables that affect the ER. Based on the relationship found, a meta-model of RBC was created, although platelet ERs showed only a general trend. This provided the guideline for the design space exploration and can be applied in a variety of applications for the manipulation of cells in a micro-fluidic channel. In addition, it was found that the effect of channel geometry can be considered with the area ratio of sheath to channel. It enabled to study more cases with rectangular channels for the prediction of circular channel results while saving the computational cost.

6.2.3 Dense Suspension Study with Improved RBC Properties

There are few dense suspension studies of blood cells in literature, either for experimentation or for simulation, because of the complexity of dense suspension studies. Simulation studies are not only computationally expensive, but the simulations can be very unstable and can crash due to the densely packed blood cells. This parametric study of blood cell migration behavior was conducted with the realistic hematocrit value of 40%. The addition of an automatic restart function on the LB-SL code allowed the simulation to run without excessive crashing, based on the local change of lubrication and contact parameters, which does not affect the flow behavior. In addition, improved RBC properties have been validated to

match closer to the experimental results. This was accomplished in lower resolution, which saved computational cost and enabled more simulation runs in the limited time and computational resources. The realistic hematocrit simulation study clearly showed that the blood cell migration behaviors are different compared to dilute cases. Thus, the dense suspension study of blood cell migration behavior is valuable for the design of micro-fluidic channels that involve blood flows.

6.2.4 Feasibility Study of the Proposed Dialyzer Design

Feasibility of the proposed dialyzer was studied based on direct numerical simulation results of blood cell migration, molecule diffusion modeling, and hemodialysis system modeling. No feasible design was found in the studied range suggesting that relying purely on the diffusion based on the direct contact for the removal of middle molecules is not a feasible solution with the small channel size ($\sim 700 \mu\text{m}$) due to the loss of protein. It suggested that in order to increase the middle molecule removal while maintain the protein level, clearance ratio of middle molecule to protein should be increased using large channel size, small sheath stream thickness, long tubule length, and slow blood flow velocity. Dialyzer size and total fluid usage limits were not the main requirements that limited feasible designs. However, limiting blood flow rate and blood cell loss while maintaining protein level and sufficiently removing middle molecules were the main problem. These findings guide the next step for a larger feasibility study of the proposed dialyzer and imply that exploring other method that can selectively increase the clearance of middle molecule might be required.

6.3 Scope and limitations

One major limitation of this research is that the blood cell migration behavior study was conducted in a relatively ideal condition compared to the proposed design. In the proposed dialyzer design, the blood and the sheath stream flow inside a tubule made of membrane. Through the membrane, not only waste molecules are removed, but also water is removed from the blood during the hemodialysis treatment. For the blood cell migration study, however, the water removal was neglected, and smooth channel wall was used instead of membrane. These factors can affect the flow field, which may lead to different blood cell migration behaviors. However, if the water removal is found to affect the flow field and change the blood cell migration behavior, the proposed dialyzer can be used after a patient receives the traditional treatment to remove water before receiving treatment with the proposed dialyzer. Given the complexity that comes from the proposed configuration with small channel size and sheath stream thickness, initially conducting a simplified DNS study provides the justification for further study of the complex proposed design. Even though the blood cell migration behavior was studied with simplified geometry, it allowed initial design space exploration and helped identify the feasible design space, providing direction for the next step. This understanding can also be applied for other micro-fluidic channel designs.

Another limitation of this research comes from the assumptions made for the design space exploration. Blood cell loss of 5% was chosen arbitrarily for the design space exploration. However, allowable blood cell loss would depend on the treatment schedule and the patient's blood cell generation rate. In addition, allowable blood cell loss might be different for RBCs and platelets. This is because platelets' main role is in blood clotting, and the normal range for the number of platelets is much wider than that of RBCs. The feasible design space identified in this

research based on the simple assumption of 5% allowable blood cell loss might be affected by more precise requirement for the blood cell loss. Another assumption that might affect the design space exploration results is the enhanced diffusivity of 2.5 for the molecules in the blood stream region. This value was based on an experimental result of enhanced albumin diffusivity in literature. However, the diffusivity enhancement is yet to be fully understood, and researchers reported a large range of diffusivity enhancement in suspension flow. Also, the enhancement was applied only on the blood stream region, but a small portion of blood cells lost into the sheath stream might affect the diffusivity in sheath stream as well. More precise design space exploration can be conducted once the diffusivity enhancement is better understood.

Blood cell migration behavior was studied using LB-SL method based DNS. The simulations were run in parallel with multiple cores utilizing the high performance computing system called Stampede at Texas Advanced Computing Center (TACC). In order to provide the size of the DNS studies conducted in this research, the computational costs are listed in Table 6-1.

Table 6-1. Computational cost of LB-SL method based DNS studies

| | SUs |
|---|------------|
| Chapter 3: Non-uniform suspension validation cases | 342,000 |
| Chapter 3: Preliminary runs and other validation cases | 150,000 |
| Chapter 4: Research Question 1 | 239,000 |

SUs refers to service units where 1 SU = 1 hour of computing on 1 CPU. This huge DNS study would not have been possible without parallel runs on a high performance computing system.

6.4 Future Work

The following directions for future work have been identified for realizing the proposed dialyzer design and broadening the understanding of the blood cell migration behavior and molecule diffusion behavior.

6.4.1 Design Space Exploration for Larger Domain

The design space exploration conducted in this research found no feasible design, and suggested that the larger channel cases should be studied to find a feasible design space. Since the blood cell migration behavior was studied only up to 200 μm sizes in this research, another set of LB-SL based direct numerical simulation should be conducted for the larger channel cases to find the allowable channel length with the large channel diameter. It will also add more data so that a more clear meta-model of blood cell extraction ratios can be constructed.

A molecule diffusion study based on the Comsol tubule model and hemodialysis system model should be conducted first to identify the feasible conditions that will increase the clearance ratio of middle molecule to protein so that proteins can be retained and a sufficient amount of middle molecules can be removed. It is because these studies are computationally much cheaper than the direct numerical simulation study of blood cell migration behaviors.

Variations of the proposed dialyzer designs, including faster sheath stream flow cases and smaller outlet sheath stream thickness cases should be considered to study the feasibility of the proposed dialyzer design concept of the middle molecule removal based on diffusion on direct contact. If relying purely on the diffusion is found to be not feasible even for the larger channel diameter and varied design cases, because the diffusivity of middle molecule is only

about 3 times higher than protein, other method that can selectively increase the clearance of middle molecule should also be explored.

6.4.2 Addition of Blood Cell Level Change to the Design Space Exploration Model

As was mentioned in the previous section, more precise estimation of blood cell loss can benefit the design space exploration. This can be done with a system very similar to the hemodialysis system model. From the given channel length, the ratio of blood cells lost per tubule is known. Together with the given treatment schedule and additional information regarding the patient's blood cell generation rate, the steady state level of blood cells can be estimated for RBCs and platelets, just as the how molecule concentration level was predicted with the hemodialysis system model. Then, the steady state level of blood cells can be used as a requirement for feasible designs. Such an addition will lead to a more realistic feasible design space exploration.

6.4.3 Experimental Proof of Concept

Once a larger domain is searched for larger channel diameters and faster sheath flows with the updated blood cell level requirement, and once the feasible design space is identified, experimental proof of the concept should follow. Because of the small sheath stream thicknesses and the complex configuration that requires separation of sheath and blood flow, manufacturing even one channel will be challenging. Then, manufacturing a dialyzer that consists of 1,000s of such channel will be another big challenge that should be resolved to realize the proposed dialyzer.

6.4.4 Segre Silberberg Effect for Rigid vs. Deformable RBCs

The validation cases studied with the DNS for the use of LB-SL method on non-uniform suspension flows showed the Segre Silberberg effect that the maximum concentration of RBCs being around $0.6d$, where d is the half of channel depth. This suggests that the Segre Silberberg effect might have been present in the experiments reported in the literature, and leads to the next question; what would be the effect of rigidity of blood cells on the blood cell migration behavior, particularly for the Segre Silberberg effect? This question was not address in this research because it is out of the scope. However, many experimental studies are conducted with treated rigid RBCs, and such a comparison study based on DNS can provide valuable insight on how those experimental results based on treated rigid RBCs can be used to predict the behavior for non-treated normal RBCS.

6.4.5 Particle Stress Analysis of Suspensions

In this research, the DNS results of the blood cell migration behavior in non-uniform suspension flows were analyzed for the extraction ratios over the flow distance to find the allowable channel length that limits the blood cell loss. However, normal stresses and particle phase stresses in suspensions, which are the key information needed to study rheology and understand why particle migration happens according to the suspension balance model, were also calculated at the same time. These were not analyzed in this research because it was out of the scope, but further analysis on these values will identify the forces acting on the particles. Considering that the suspension flow community has not agreed on the forces acting on the particles, the further analysis of the DNS results, which cannot be achieved through experiments, will help the suspension flow community to understand what drives the particle migration.

6.4.6 LB-SL Method Based DNS for the Molecule Diffusion Behavior Study

In this research, the blood cell migration behavior was studied using LB-SL based DNS, and the molecule diffusion behavior was studied using a Comsol tubule model. One of the reasons that those were separately studied is that the current LB-SL code does not have the capability to study molecule diffusion. Addition of such a capability will greatly aid the understanding of diffusivity enhancement and will enable more precise design space exploration of the proposed dialyzer based on this understanding.

APPENDIX A
TABLES

In section 5.2.3.1, a set of studies was conducted to validate the accuracy of the Comsol tubule model. The conditions of the six studies are listed in Table 5-3, and the calculation time and the errors of each studies are presented in the following six tables.

Appendix A-1. Calculation time and errors, Study A

| scale | 1 | 10 | 70 | 200 | 400 | 700 |
|-------------------------------------|----------|-----------|-----------|------------|------------|------------|
| Time (sec) | 788 | 128 | 26 | 15 | 11 | 10 |
| K_a^d error (%) | - | .01 | -2.1 | -1.7 | -1.3 | 1.3 |
| K_B^d error (%) | - | -0.22 | -0.92 | -0.04 | 0.16 | 2.5 |
| K_u^d error (%) | - | 0.43 | 2.1 | 4.9 | 6.9 | 12.2 |

Appendix A-2. Calculation time and errors, Study B

| scale | 200 | 600 | 1200 | 2000 | 2900 | 4200 | 5600 |
|-------------------------------------|------------|------------|-------------|-------------|-------------|-------------|-------------|
| Time (sec) | 647 | 284 | 131 | 86 | 59 | 44 | 34 |
| K_a^d error (%) | - | 0.45 | 1.1 | 1.7 | 2.4 | 3.2 | 4.1 |
| K_B^d error (%) | - | 0.30 | 0.72 | 1.2 | 1.7 | 2.5 | 3.4 |
| K_u^d error (%) | - | .05 | 0.13 | 0.22 | 0.31 | 0.41 | 0.48 |

Appendix A-3. Calculation time and errors, Study C

| h_{max} | .2 | .4 | .7 | 1.1 | 1.7 | 2.4 | 3.2 |
|-------------------------------------|-----------|-----------|-----------|------------|------------|------------|------------|
| Time (sec) | 125 | 52 | 28 | 20 | 15 | 12 | 11 |
| K_a^d error (%) | - | -1.3 | -3.4 | -6.3 | -10.5 | -14.3 | -17.6 |
| K_B^d error (%) | - | -0.76 | -2.0 | -3.7 | -6.5 | -9.5 | 13.4 |
| K_u^d error (%) | - | 0.18 | 0.20 | 0.21 | -0.02 | -0.13 | -1.2 |

Appendix A-4. Calculation time and errors, Study D

| scale | 10 | 70 | 200 | 400 | 700 |
|-------------------|-----|------|-------|-------|-------|
| Time (sec) | 122 | 28 | 18 | 14 | 12 |
| K_a^d error (%) | - | -1.6 | -2.4 | -2.0 | -1.3 |
| K_B^d error (%) | - | -1.3 | -0.86 | -0.22 | -0.56 |
| K_u^d error (%) | - | 1.2 | 3.0 | 5.0 | 6.3 |

Appendix A-5. Calculation time and errors, Study E

| scale | 200 | 600 | 1200 | 2000 | 2900 | 4200 | 5600 |
|-------------------|------|------|------|------|------|------|------|
| Time (sec) | 1204 | 443 | 200 | 154 | 85 | 55 | 42 |
| K_a^d error (%) | - | 0.28 | 0.57 | 0.95 | 1.3 | 1.9 | 2.4 |
| K_B^d error (%) | - | 0.26 | 0.64 | 1.1 | 1.5 | 2.1 | 2.6 |
| K_u^d error (%) | - | 0.36 | 0.98 | 1.9 | 2.8 | 4.0 | 5.2 |

Appendix A-6. Calculation time and errors, Study F

| h_{max} | .2 | .4 | .7 | 1.1 | 1.7 | 2.4 |
|-------------------|----|-------|-------|-------|------|------|
| Time (sec) | 92 | 36 | 31 | 25 | 16 | 13 |
| K_a^d error (%) | - | -2.1 | -5.1 | -8.3 | -12 | -16 |
| K_B^d error (%) | - | -1.2 | -3.3 | -6.1 | -10 | -14 |
| K_u^d error (%) | - | -0.07 | -0.36 | -0.83 | -1.8 | -2.7 |

WORKS CITED

- [1] M. P. C. Grooteman and M. J. Nubé, "Haemodialysis-related bioincompatibility: fundamental aspects and clinical relevance," *The Netherlands Journal of Medicine*, vol. 52, pp. 169-178, 1998.
- [2] B. Canaud, A. Assounga, P. Kerr, R. Aznar, and C. Mion, "Failure of a daily haemofiltration programme using a highly permeable membrane to return β 2-microglobulin concentrations to normal in haemodialysis patients," *Nephrology Dialysis Transplantation*, vol. 7, pp. 924-930, January 1, 1992 1992.
- [3] A. K. Cheung, M. V. Rocco, G. Yan, J. K. Leypoldt, N. W. Levin, T. Greene, *et al.*, "Serum β -2 Microglobulin Levels Predict Mortality in Dialysis Patients: Results of the HEMO Study," *Journal of the American Society of Nephrology*, vol. 17, pp. 546-555, February 1, 2006 2006.
- [4] L. M. Dember and B. L. Jaber, "UNRESOLVED ISSUES IN DIALYSIS: Dialysis-Related Amyloidosis: Late Finding or Hidden Epidemic?," *Seminars in Dialysis*, vol. 19, pp. 105-109, 2006.
- [5] E. F. Leonard, A. C. West, N. C. Shapley, and M. U. Larsen, "Dialysis without Membranes: How and Why?," *Blood Purification*, vol. 22, pp. 92-100, 2004.
- [6] W. F. Ganong, *Review of medical physiology*, 21 ed. New York: Lange Medical Books/McGraw-Hill, 2003.
- [7] J. B. Freund and M. Orescanin, "Cellular flow in a small blood vessel," *Journal of Fluid Mechanics*, vol. 671, pp. 466-490, 2011.
- [8] G. Segré and A. Silberberg, "Radial Particle Displacements in Poiseuille Flow of Suspensions," *Nature*, vol. 189, pp. 209-210, 1961.
- [9] G. Segre and A. Silberberg, "Behaviour of macroscopic rigid spheres in Poiseuille flow Part 2. Experimental results and interpretation," *Journal of Fluid Mechanics*, vol. 14, pp. 136-157, 1962.
- [10] W. S. J. Uijttewaai, E.-J. Nijhof, and R. M. Heethaar, "Lateral migration of blood cells and microspheres in two-dimensional Poiseuille flow: A laser-Doppler study," *Journal of Biomechanics*, vol. 27, pp. 35-42, 1994.
- [11] J. Moger, S. J. Matcher, C. P. Winlove, and A. Shore, "Measuring red blood cell flow dynamics in a glass capillary using Doppler optical coherence tomography and Doppler amplitude optical coherence tomography," *Journal of Biomedical Optics*, vol. 9, pp. 982-994, 2004.
- [12] C. G. Caro, T. J. Pedley, R. C. Schroter, W. A. Seed, and K. H. Parker, *The Mechanics of the Circulation*: Cambridge University Press, 2011.

- [13] H. L. Goldsmith, "Red cell motions and wall interactions in tube flow," *Federation proceedings*, vol. 30, pp. 1578-1590, 1971.
- [14] F. P. Bretherton, "The motion of rigid particles in a shear flow at low Reynolds number," *Journal of Fluid Mechanics*, vol. 14, pp. 284-304, 1962.
- [15] V. Breedveld, D. Van Den Ende, M. Bosscher, R. Jongschaap, and J. Mellema, "Measurement of the full shear-induced self-diffusion tensor of noncolloidal suspensions," *The journal of chemical physics*, vol. 116, pp. 10529-10535, 2002.
- [16] A. W. Chow, S. W. Sinton, J. H. Iwamiya, and T. S. Stephens, "Shear-induced particle migration in Couette and parallel-plate viscometers: NMR imaging and stress measurements," *Physics of Fluids (1994-present)*, vol. 6, pp. 2561-2576, 1994.
- [17] M. Frank, D. Anderson, E. R. Weeks, and J. F. Morris, "Particle migration in pressure-driven flow of a Brownian suspension," *Journal of Fluid Mechanics*, vol. 493, pp. 363-378, 2003.
- [18] S. Hudson, "Wall migration and shear-induced diffusion of fluid droplets in emulsions," *Physics of Fluids (1994-present)*, vol. 15, pp. 1106-1113, 2003.
- [19] C. J. Koh, P. Hookham, and L. G. Leal, "An experimental investigation of concentrated suspension flows in a rectangular channel," *Journal of Fluid Mechanics*, vol. 266, pp. 1-32, 1994.
- [20] M. Lyon and L. Leal, "An experimental study of the motion of concentrated suspensions in two-dimensional channel flow. Part 1. Monodisperse systems," *Journal of Fluid Mechanics*, vol. 363, pp. 25-56, 1998.
- [21] M. Lyon and L. Leal, "An experimental study of the motion of concentrated suspensions in two-dimensional channel flow. Part 2. Bidisperse systems," *Journal of Fluid Mechanics*, vol. 363, pp. 57-77, 1998.
- [22] P. A. Aarts, S. A. van den Broek, G. W. Prins, G. D. Kuiken, J. J. Sixma, and R. M. Heethaar, "Blood platelets are concentrated near the wall and red blood cells, in the center in flowing blood," *Arteriosclerosis, Thrombosis, and Vascular Biology*, vol. 8, pp. 819-24, November 1, 1988 1988.
- [23] A. S. Popel and P. C. Johnson, "Microcirculation and hemorheology," *Annual Review of Fluid Mechanics*, vol. 37, p. 43, 2005.
- [24] E. C. Eckstein, A. W. Tilles, and F. J. Millero Iii, "Conditions for the occurrence of large near-wall excesses of small particles during blood flow," *Microvascular Research*, vol. 36, pp. 31-39, 7// 1988.
- [25] A. L. Zydney and C. K. Colton, "Augmented solute transport in the shear flow of a concentrated suspension," *PCH, PhysicoChem. Hydrodyn*, vol. 10, p. 77, 1988.

- [26] H. Goldsmith and J. Marlow, "Flow behavior of erythrocytes. II. Particle motions in concentrated suspensions of ghost cells," *Journal of Colloid and Interface Science*, vol. 71, pp. 383-407, 1979.
- [27] V. T. Turitto, A. M. Benis, and E. F. Leonard, "Platelet diffusion in flowing blood," *Industrial & Engineering Chemistry Fundamentals*, vol. 11, pp. 216-223, 1972.
- [28] M. Mehrabadi, D. N. Ku, and C. K. Aidun, "A Continuum Model for Platelet Transport in Flowing Blood Based on Direct Numerical Simulations of Cellular Blood Flow," *Annals of biomedical engineering*, pp. 1-12, 2014.
- [29] J. J. Stickel and R. L. Powell, "Fluid mechanics and rheology of dense suspensions," *Annu. Rev. Fluid Mech.*, vol. 37, pp. 129-149, 2005.
- [30] D. Leighton and A. Acrivos, "Shear-induced migration of particles in concentrated suspensions," *Journal of Fluid Mechanics*, vol. 181, pp. 415-439, 1987.
- [31] P. R. Nott and J. F. Brady, "Pressure-driven flow of suspensions: simulation and theory," *Journal of Fluid Mechanics*, vol. 275, pp. 157-199, 1994.
- [32] G. K. Batchelor, "The stress system in a suspension of force-free particles," *Journal of Fluid Mechanics*, vol. 41, pp. 545-570, 1970.
- [33] D. Lhuillier, "Migration of rigid particles in non-Brownian viscous suspensions," *Physics of Fluids*, vol. 21, pp. 023302-6, 2009.
- [34] P. R. Nott, E. Guazzelli, and O. Pouliquen, "The suspension balance model revisited," *Physics of Fluids*, vol. 23, pp. 043304-13, 2011.
- [35] R. M. Miller and J. F. Morris, "Normal stress-driven migration and axial development in pressure-driven flow of concentrated suspensions," *Journal of non-newtonian fluid mechanics*, vol. 135, pp. 149-165, 2006.
- [36] J. F. Morris and F. Boulay, "Curvilinear flows of noncolloidal suspensions: The role of normal stresses," *Journal of Rheology*, vol. 43, pp. 1213-1237, 1999.
- [37] J. R. Clausen and C. K. Aidun, "Capsule dynamics and rheology in shear flow: Particle pressure and normal stress," *Physics of Fluids*, vol. 22, pp. 123302-11, 2010.
- [38] J. R. Clausen, D. A. Reasor, and C. K. Aidun, "The rheology and microstructure of concentrated non-colloidal suspensions of deformable capsules," *Journal of Fluid Mechanics*, vol. 685, pp. 202-234, 2011.
- [39] D. A. Reasor, J. R. Clausen, and C. K. Aidun, "Coupling the lattice-Boltzmann and spectrin-link methods for the direct numerical simulation of cellular blood flow," *International Journal for Numerical Methods in Fluids*, vol. 68, pp. 767-781, 2012.

- [40] X. Grandchamp, G. Coupier, A. Srivastav, C. Minetti, and T. Podgorski, "Lift and Down-Gradient Shear-Induced Diffusion in Red Blood Cell Suspensions," *Physical Review Letters*, vol. 110, p. 108101, 2013.
- [41] C. W. Yung, J. Fiering, A. J. Mueller, and D. E. Ingber, "Micromagnetic-microfluidic blood cleansing device," *Lab Chip*, vol. 9, pp. 1171-1177, 2009.
- [42] E. F. Leonard, "Technical Approaches Toward Ambulatory ESRD Therapy," *Seminars in Dialysis*, vol. 22, pp. 658-660, 2009.
- [43] E. F. Leonard, S. Cortell, and N. G. Vitale, "Membraneless dialysis--is it possible?," *Contrib Nephrol*, vol. 149, pp. 343-53, 2005.
- [44] E. F. Leonard, C. P. Aucoin, and E. E. Nanne, "Measurement of Diffusion in Flowing Complex Fluids," *Colloids Surf A Physicochem Eng Asp*, vol. 282-283, pp. 75-78, Jul 20 2006.
- [45] C. P. Aucoin, "Transverse movement of erythrocytes in microfluidic flows," Ph.D. 3374097, Columbia University, United States -- New York, 2009.
- [46] C. K. Colton, K. A. Smith, E. R. Merrill, and S. Friedman, "Diffusion of urea in flowing blood," *AIChE Journal*, vol. 17, pp. 800-808, 1971.
- [47] W. Cha and R. L. Beissinger, "Augmented Mass Transport of Macromolecules in Sheared Suspensions to Surfaces B. Bovine Serum Albumin," *Journal of Colloid and Interface Science*, vol. 178, pp. 1-9, 1996.
- [48] N.-H. L. Wang and K. H. Keller, "Augmented transport of extracellular solutes in concentrated erythrocyte suspensions in couette flow," *Journal of Colloid and Interface Science*, vol. 103, pp. 210-225, 1985.
- [49] A. Hatch, E. Garcia, and P. Yager, "Diffusion-based analysis of molecular interactions in microfluidic devices," *Proceedings of the IEEE*, vol. 92, pp. 126-139, 2004.
- [50] C. Steiner, "Mass transfer of urea through blood," *Ann Biomed Eng*, vol. 9, pp. 217-225, 1981.
- [51] M. S. Bello, R. Rezzonico, and P. G. Righetti, "Use of Taylor-Aris dispersion for measurement of a solute diffusion coefficient in thin capillaries," *Science*, vol. 266, pp. 773-6, Nov 4 1994.
- [52] E. E. Nanne, C. P. Aucoin, and E. F. Leonard, "Molecular movement of bovine albumin in flowing suspensions of bovine erythrocytes," *Chemical Engineering Science*, vol. 65, pp. 6389-6396, 2010.
- [53] Z. Wu and N.-T. Nguyen, "Hydrodynamic focusing in microchannels under consideration of diffusive dispersion: theories and experiments," *Sensors and Actuators B: Chemical*, vol. 107, pp. 965-974, 2005.

- [54] G.-B. Lee, C.-C. Chang, S.-B. Huang, and R.-J. Yang, "The hydrodynamic focusing effect inside rectangular microchannels," *Journal of Micromechanics and Microengineering*, vol. 16, p. 1024, 2006.
- [55] G. Hairer and M. J. Vellekoop, "Experiments on hydrodynamic focusing of non coaxial sheath flows," in *Sensors, 2006. 5th IEEE Conference on*, 2006, pp. 431-434.
- [56] C. G. Koh, X. Zhang, S. Liu, S. Golan, B. Yu, X. Yang, *et al.*, "Delivery of antisense oligodeoxyribonucleotide lipopolyplex nanoparticles assembled by microfluidic hydrodynamic focusing," *Journal of Controlled Release*, vol. 141, pp. 62-69, 2010.
- [57] C. Simonnet and A. Groisman, "Two-dimensional hydrodynamic focusing in a simple microfluidic device," *Applied Physics Letters*, vol. 87, p. 114104, 2005.
- [58] J. B. Knight, A. Vishwanath, J. P. Brody, and R. H. Austin, "Hydrodynamic focusing on a silicon chip: mixing nanoliters in microseconds," *Physical Review Letters*, vol. 80, pp. 3863-3866, 1998.
- [59] J. B. Freund, "Leukocyte margination in a model microvessel," *Physics of Fluids*, vol. 19, pp. 023301-13, 2007.
- [60] A. Sierou and J. F. Brady, "Shear-induced self-diffusion in non-colloidal suspensions," *Journal of Fluid Mechanics*, vol. 506, pp. 285-314, 2004.
- [61] A. Sierou and J. Brady, "Rheology and microstructure in concentrated noncolloidal suspensions," *Journal of Rheology*, vol. 46, p. 1031, 2002.
- [62] D. A. Reasor, M. Mehrabadi, D. N. Ku, and C. K. Aidun, "Determination of Critical Parameters in Platelet Margination," *Annals of Biomedical Engineering*, vol. 41, pp. 238-249, 2012.
- [63] S. Chen and G. D. Doolen, "LATTICE BOLTZMANN METHOD FOR FLUID FLOWS," *Annual Review of Fluid Mechanics*, vol. 30, pp. 329-364, 1998.
- [64] C. K. Aidun and J. R. Clausen, "Lattice-Boltzmann Method for Complex Flows," *Annual Review of Fluid Mechanics*, vol. 42, pp. 439-472, 2010.
- [65] C. K. Aidun, Y. Lu, and E. J. Ding, "Direct analysis of particulate suspensions with inertia using the discrete Boltzmann equation," *Journal of Fluid Mechanics*, vol. 373, p. 287, 1998.
- [66] R. M. MacMeccan, J. R. Clausen, G. P. Neitzel, and C. K. Aidun, "Simulating deformable particle suspensions using a coupled lattice-Boltzmann and finite-element method," *Journal of Fluid Mechanics*, vol. 618, pp. 13-39, 2009.
- [67] D. A. Fedosov, B. Caswell, and G. E. Karniadakis, "Systematic coarse-graining of spectrin-level red blood cell models," *Comput Methods Appl Mech Eng*, vol. 199, Jun 1 2010.

- [68] M. Dao, J. Li, and S. Suresh, "Molecularly based analysis of deformation of spectrin network and human erythrocyte," *Materials Science and Engineering: C*, vol. 26, pp. 1232-1244, 2006.
- [69] D. A. Reasor, "Numerical simulation of cellular blood flow," 2011.
- [70] I. Pivkin and G. Karniadakis, "Accurate Coarse-Grained Modeling of Red Blood Cells," *Physical Review Letters*, vol. 101, 2008.
- [71] J. R. Clausen and C. K. Aidun, "Capsule dynamics and rheology in shear flow: Particle pressure and normal stress," *Physics of Fluids*, vol. 22, p. 123302, 2010.
- [72] E. J. Ding and C. Aidun, "Extension of the Lattice-Boltzmann Method for Direct Simulation of Suspended Particles Near Contact," *Journal of Statistical Physics*, vol. 112, pp. 685-708, 2003/08/01 2003.
- [73] J. Li, M. Dao, C. T. Lim, and S. Suresh, "Spectrin-Level Modeling of the Cytoskeleton and Optical Tweezers Stretching of the Erythrocyte," *Biophysical Journal*, vol. 88, pp. 3707-3719, 2005.
- [74] D. A. Fedosov, B. Caswell, and G. E. Karniadakis, "A multiscale red blood cell model with accurate mechanics, rheology, and dynamics," *Biophysical Journal*, vol. 98, pp. 2215-2225, 2010.
- [75] D. A. Fedosov, B. Caswell, and G. E. Karniadakis, "Systematic coarse-graining of spectrin-level red blood cell models," *Computer Methods in Applied Mechanics and Engineering*, vol. 199, pp. 1937-1948, 2010.
- [76] X. Shi, G. Lin, J. Zou, and D. A. Fedosov, "A lattice Boltzmann fictitious domain method for modeling red blood cell deformation and multiple-cell hydrodynamic interactions in flow," *International Journal for Numerical Methods in Fluids*, 2013.
- [77] J. Li-Guo, W. Heng-An, Z. Xiao-Zhou, and W. Xiu-Xi, "Coarse-Grained Molecular Dynamics Simulation of a Red Blood Cell," *Chinese Physics Letters*, vol. 27, p. 028704, 2010.
- [78] I. V. Pivkin and G. E. Karniadakis, "Accurate Coarse-Grained Modeling of Red Blood Cells," *Physical Review Letters*, vol. 101, p. 118105, 2008.
- [79] D. A. Fedosov, B. Caswell, and G. E. Karniadakis, "Coarse-grained red blood cell model with accurate mechanical properties, rheology and dynamics," in *Engineering in Medicine and Biology Society, 2009. EMBC 2009. Annual International Conference of the IEEE*, 2009, pp. 4266-4269.
- [80] M. M. Dupin, I. Halliday, C. M. Care, L. Alboul, and L. L. Munn, "Modeling the flow of dense suspensions of deformable particles in three dimensions," *Physical Review E*, vol. 75, p. 066707, 2007.

- [81] S. K. Boey, D. H. Boal, and D. E. Discher, "Simulations of the erythrocyte cytoskeleton at large deformation. I. Microscopic models," *Biophysical Journal*, vol. 75, pp. 1573-1583, 1998.
- [82] W. C. Hwang and R. E. Waugh, "Energy of dissociation of lipid bilayer from the membrane skeleton of red blood cells," *Biophysical Journal*, vol. 72, pp. 2669-2678, 1997.
- [83] E. A. Evans and R. Skalak, "Mechanics and thermodynamics of biomembranes," 1980.
- [84] H. Byun, T. R. Hillman, J. M. Higgins, M. Diez-Silva, Z. Peng, M. Dao, *et al.*, "Optical measurement of biomechanical properties of individual erythrocytes from a sickle cell patient," *Acta biomaterialia*, vol. 8, pp. 4130-4138, 2012.
- [85] R. Hochmuth and R. Waugh, "Erythrocyte membrane elasticity and viscosity," *Annual review of physiology*, vol. 49, pp. 209-219, 1987.
- [86] D. A. Reasor, Jr., M. Mehrabadi, D. N. Ku, and C. K. Aidun, "Determination of critical parameters in platelet margination," *Ann Biomed Eng*, vol. 41, pp. 238-49, Feb 2013.
- [87] X. Shi, G. Lin, J. Zou, and D. A. Fedosov, "A lattice Boltzmann fictitious domain method for modeling red blood cell deformation and multiple-cell hydrodynamic interactions in flow," *International Journal for Numerical Methods in Fluids*, vol. 72, pp. 895-911, 2013.
- [88] K. Tsukada, E. Sekizuka, C. Oshio, and H. Minamitani, "Direct Measurement of Erythrocyte Deformability in Diabetes Mellitus with a Transparent Microchannel Capillary Model and High-Speed Video Camera System," *Microvasc Res*, vol. 61, pp. 231-239, 2001.
- [89] M. Dao, C. Lim, and S. Suresh, "Mechanics of the human red blood cell deformed by optical tweezers," *Journal of the Mechanics and Physics of Solids*, vol. 51, pp. 2259-2280, 2003.
- [90] J. Wu, B. M. Yun, A. M. Fallon, S. R. Hanson, C. K. Aidun, and A. P. Yoganathan, "Numerical investigation of the effects of channel geometry on platelet activation and blood damage," *Ann Biomed Eng*, vol. 39, pp. 897-910, Feb 2011.
- [91] B. M. Yun, C. K. Aidun, and A. P. Yoganathan, "Blood Damage Quantification in Cardiovascular Flows Through Medical Devices Using a Novel Suspension Flow Method," *Journal of Medical Devices*, vol. 7, p. 040909, 2013.
- [92] G. B. Jeffery, "The Motion of Ellipsoidal Particles Immersed in a Viscous Fluid," *Proceedings of the Royal Society A: Mathematical, Physical and Engineering Sciences*, vol. 102, pp. 161-179, 1922.
- [93] J. R. Clausen, "The effect of particle deformation on the rheology and microstructure of noncolloidal suspensions," 2010.

- [94] B. Yun, "Simulations of pulsatile flow through bileaflet mechanical heart valves using a suspension flow model: to assess blood damage," *Mechanical Engineering, Georgia Institute of Technology. Doctor of Philosophy, Atlanta, GA*, p. 464, 2014.
- [95] R. Rusconi and H. Stone, "Shear-Induced Diffusion of Platelet Particles in Microchannels," *Physical Review Letters*, vol. 101, 2008.
- [96] M. Mehrabadi, "Effects of red blood cells and shear rate on thrombus growth," Ph.D., Mechanical Engineering, Georgia Institute of Technology, 2014.
- [97] A. K. Cheung, "Clearance vs. Molecular Mass," ed. Hemodialysis and Hemofiltration, Chapter 54, Primer on Kidney Disease, 2009.
- [98] N. L. Anderson, "The Human Plasma Proteome: History, Character, and Diagnostic Prospects," *Molecular & Cellular Proteomics*, vol. 1, pp. 845-867, 2002.
- [99] R. B. Bird, W. E. Stewart, and E. N. Lightfoot, "Transport phenomena. 1960," *Madison, USA*, 1960.
- [100] A. Leo, C. Hansch, and D. Elkins, "Partition coefficients and their uses," *Chemical reviews*, vol. 71, pp. 525-616, 1971.
- [101] M. W. Verbrugge, "Methanol Diffusion in Perfluorinated Ion-Exchange Membranes," *Journal of The Electrochemical Society*, vol. 136, pp. 417-423, 1989.
- [102] J. Lamb, J. Christensen, J. Oscarson, B. Nielsen, B. Asay, and R. Izatt, "The relationship between complex stability constants and rates of cation transport through liquid membranes by macrocyclic carriers," *Journal of the American Chemical Society*, vol. 102, pp. 6820-6824, 1980.
- [103] P. S. Stewart, "Theoretical aspects of antibiotic diffusion into microbial biofilms," *Antimicrobial agents and chemotherapy*, vol. 40, pp. 2517-2522, 1996.
- [104] B. N. Preston, W. D. Comper, A. E. Hughes, I. Snook, and W. van Megen, "Diffusion of dextran at intermediate concentrations," *Journal of the Chemical Society, Faraday Transactions 1: Physical Chemistry in Condensed Phases*, vol. 78, pp. 1209-1221, 1982.
- [105] S. Okuno, E. Ishimura, K. Kohno, Y. Fujino-Katoh, Y. Maeno, T. Yamakawa, *et al.*, "Serum β 2-microglobulin level is a significant predictor of mortality in maintenance haemodialysis patients," *Nephrology Dialysis Transplantation*, vol. 24, pp. 571-577, 2009.
- [106] M. Ziółko, J. A. Pietrzyk, and J. Grabska-Chrzastowska, "Accuracy of hemodialysis modeling," *Kidney international*, vol. 57, pp. 1152-1163, 2000.
- [107] M. Külz, B. Nederlof, and H. Schneider, "In vitro and in vivo evaluation of a new dialyzer," *Nephrology Dialysis Transplantation*, vol. 17, pp. 1475-1479, 2002.

- [108] J. C. Olson, J. D. Weaver, Y. Yang, D. N. Ku, and D. W. Rosen, "Design of a Portable Renal Replacement System Through Modeling and Experiment," in *2009 Summer Bioengineering Conference*, Hyatt Regency Irvine, Irvine, California, USA, 2009.
- [109] J. C. Olson, "Design and modeling of a portable hemodialysis system," Master of Science in Mechanical Engineering, Mechanical Engineering, Georgia Institute of Technology, Atlanta, 2009.
- [110] R. Hume and E. Weyers, "Relationship between total body water and surface area in normal and obese subjects," *Journal of Clinical Pathology*, vol. 24, pp. 234-238, 1971.
- [111] G. A. Kaysen and P. Y. Schoenfeld, "Albumin homeostasis in patients undergoing continuous ambulatory peritoneal dialysis," *Kidney Int*, vol. 25, pp. 107-114, 1984.
- [112] G. A. Kaysen, J. Gambertoglio, I. Jimenez, H. Jones, and F. N. Hutchison, "Effect of dietary protein intake on albumin homeostasis in nephrotic patients," *Kidney international*, vol. 29, pp. 572-577, 1986.
- [113] D. F. Moffett, S. B. Moffett, and C. L. Schaaf, *Human physiology: foundations & frontiers*: William C Brown Pub, 1993.
- [114] R. Vanholder, R. De Smet, G. Glorieux, A. Argilés, U. Baurmeister, P. Brunet, *et al.*, "Review on uremic toxins: classification, concentration, and interindividual variability," *Kidney international*, vol. 63, pp. 1934-1943, 2003.
- [115] G. Coppolino, D. Bolignano, L. Rivoli, G. Mazza, P. Presta, and G. Fuiano, "Tumour Markers and Kidney Function: A Systematic Review," *BioMed Research International*, 2014.